Graphene coated bare metal stents as an enhanced design for the treatment of coronary artery disease

A thesis submitted to the University of Manchester for the degree of Doctor of Philosophy in the Faculty of Biology, Medicine and Health

2019

Fatemeh Jafarzadeh

School of Medical Sciences
Division of Cardiovascular Sciences

In the Name of God The
Compassionate The Merciful

Word Count =35,292

List of Figures

List of Tables

Acronyms and Abbreviations

1G-DES	1st Generation drug eluting stent
2G-DES	2nd Generation drug eluting stent
AFM	Atomic force microscopy
BA	Balloon angioplasty
BENESTENT	BElgian NEtherlands STENT study
BES	Biolimus eluting stent
BMS	Bare metal stent
CABG	Coronary artery bypass graft
CAD	Coronary artery disease
CANTOS	Canakinumab Anti-inflammatory Thrombosis Outcome Study
CD31	Cluster of differentiation 31
CHROMA	CHROMA™ CORONARY STENT SYSTEM (Biosensors Int.)
CRP	C reactive proteins
CVD	Chemical vapour deposition
CX	Left circumflex
DAPT	Dual antiplatelet therapy
DES	Drug eluting stent
DLC	Diamond-like carbon
DNA	Deoxyribonucleic acid
DPX	Distyrene plasticizer xylene
EC	Endothelial cell
ECM	Extracellular matrix
EDTA	Ethylenediaminetetraacetic acid
EES	Everolimus eluting stent
FKBP12	FK binding protein 12
FLG	Few layered graphene
GAZELLE	GAZELLE™ CORONARY STENT SYSTEM (Biosensors Int.)
GO	Graphene oxide
Gr	Graphene
HCAEC	Human coronary artery endothelial cell
IEL	Internal elastic lamina
IFN-ɣ	Interferon-gamma
IMA	Internal mammary artery
ISR	In-stent thrombosis
LAD	Left anterior descending artery
LDL	Low density lipoprotein
LMCA	Left main coronary artery
LPE	Liquid phase exfoliation

LST	Late stent thrombosis
MCP-1	Monocyte chemotactic protein-1
M-CSF	Macrophage colony-stimulating factor
MI	Myocardial infarction
MLG	Monolayered graphene
MMP	Matrix metalloproteinase
mTOR	Mammalian target of rapamycin
NI	Neointima
NMP	1-methyl-2-pyrrolidinone
NO	Nitric oxide
PBS	Phosphate buffered saline
PCAM-1	Platelet endothelial cell adhesion molecule-1
PCI	Percutaneous coronary intervention
PES	Paclitaxel eluting stent
PLLA	Poly-L-lactic acid
PS1	1-pyrenesulfonic acid sodium salt
RCA	Right main coronary artery
RCT	Randomised control trial
RES	Rridaforolimus eluting stent
RNA	Ribonucleic acid
SCEM	Scanning electron microscopy
SEM	Standard error of the mean
SES	Sirolimus eluting stent
SiC	Silicon carbide
SMC	Smooth muscle cell
SS	Stainless steel
ST	Stent thrombosis
STEMI	ST segment elevation MI
STRESS	STent REStenosis Study
SV	Saphenous vein
UV	Ultraviolet
UV-Vis	Ultraviolet-visible spectroscopy
VCAM-1	Vascular cell adhesion protein-1
VLST	Very late stent thrombosis
VSMC	Vascular smooth muscle cell
XPS	X-ray photoelectron spectroscopy
ZES	Zotarolimus eluting stent

Abstract

Introduction

Coronary artery disease is the leading cardiovascular related death worldwide. The mainstay therapeutic intervention is either coronary artery bypass grafting or endovascular approaches, inserting a metallic scaffold to maintain the opened state of the vessel. There are many scaffolds currently available and under development, with bare metal stents being first designed followed by drug eluting stents which are now commonly used. This necessitates the use of dual anti-platelet therapy to evade thrombosis. Bare metal stents pose a significant risk of in-stent restenosis followed by late stent thrombosis risk caused by the drug eluting stent. Importantly, drug eluting stents have significantly decreased the incidence of in-stent restenosis. Consequently, there remains the need to develop a complication-free stent, and thus we propose combining the structural strength of metallic stents, bare metal stents, with the surface characteristics of graphene to promote vessel healing and prevent complications. Graphene is a mono layered sheet of hexagonal structured carbon atoms, and has been hailed as the 'wonder' material across many disciplines. We aim to incorporate many of the desirable qualities of graphene and graphene oxide; strong, flexible, anti-corrosive, smooth, biocompatible, antibacterial, into a coronary stent coating in order to alleviate some of the complications of currently available stents.

Methods

Graphene was prepared by liquid phase exfoliation using a stabilising agent known as 1-pyrene sulfonic acid sodium salt while graphene oxide was prepared by Hummer's exfoliation method. The quality of the dispersions were characterised using a range of techniques, particularly Raman spectroscopy and atomic force microscopy. Dip-coating, with applied bias and spray coating techniques were tested to select the optimal method of graphene/graphene oxide coating of bare metal stents. The selected technique was then investigated further to optimise coating to achieve thin, uniform and maximal coverage of the stent. Human coronary artery endothelial cell growth was investigated *in vitro* by incubation with the coated stents for durations of one and eight days (n=3). Following this, stents coated with graphene and graphene oxide underwent *ex vivo* incubation on porcine aortic tissue for a period of 14 days in order to determine the formation of neointimal hyperplasia. Following 14 days, visualisation by scanning electron microscopy was performed as well as Miller's staining and immunohistochemistry for endothelial cells.

Results

Spray coating was selected at a spray distance of 10cm and 400µL at 0.4 $mgmL^{-1}$ concentration to spray the stents for a duration of 60-80 minutes. Enhanced human coronary artery endothelial cell growth was observed from day one to day eight, on the graphene coated stents when compared to uncoated stents and graphene oxide coated stent. Porcine coronary and aortic tissue culture demonstrated no significant difference in neointimal thickness between any of the coated/uncoated bare metal stent groups. Graphene and graphene oxide were not inferior to uncoated bare metal stents in

neointimal thickness. There were no endothelial cells present after 14 days of aortic tissue culture, even though endothelial cells were present before tissue culture.

Conclusion

Graphene coating prototype of coronary artery bare metal stents was achieved by spray coating. Graphene coating supported enhanced viability and growth of human coronary artery endothelial cells. *Ex vivo* study of neointimal hyperplasia in the porcine aortic tissue revealed no benefit of graphene coating in reducing neointimal thickness.

Declaration

I declare that no portion of the work referred to in the thesis has been submitted in support of an application for another degree or qualification of this or any other university or other institute of learning.

Copyright Statement

i. The author of this thesis (including any appendices and/or schedules to this thesis) owns certain copyright or related rights in it (the "Copyright") and s/he has given The University of Manchester certain rights to use such Copyright, including for administrative purposes.

ii. Copies of this thesis, either in full or in extracts and whether in hard or electronic copy, may be made only in accordance with the Copyright, Designs and Patents Act 1988 (as amended) and regulations issued under it or, where appropriate, in accordance with licensing agreements which the University has from time to time. This page must form part of any such copies made.

iii. The ownership of certain Copyright, patents, designs, trade marks and other intellectual property (the "Intellectual Property") and any reproductions of copyright works in the thesis, for example graphs and tables ("Reproductions"), which may be described in this thesis, may not be owned by the author and may be owned by third parties. Such Intellectual Property and Reproductions cannot and must not be made available for use without the prior written permission of the owner(s) of the relevant Intellectual Property and/or Reproductions.

iv. Further information on the conditions under which disclosure, publication and commercialisation of this thesis, the Copyright and any Intellectual Property and/or Reproductions described in it may take place is available in the University IP Policy (see http://documents.manchester.ac.uk/DocuInfo.aspx?DocID=24420), in any relevant Thesis restriction declarations deposited in the University Library, The University Library's regulations (see http://www.library.manchester.ac.uk/about/regulations/) and in The University's policy on Presentation of Theses.

Acknowledgments

First and foremost, I thank God for the countless blessings He has bestowed upon me, one of which includes this BHF sponsored PhD scholarship.

My gratitude goes to my parents who have been my rock throughout my education, particularly being there for me during the challenging times of this PhD. Without the unconditional love and support of my parents I would not have made it anywhere in my life and I have them to thank for everything I have and am forever in debt of their kindness. My thanks also to my supportive siblings, Soheila and Mehdi, for putting up with me during the stressed times and for proof reading chapters of my thesis.

I am grateful to all my supervisors; Dr Cathy Holt, Prof Cinzia Casiraghi and Dr Nadim Malik, for their invaluable support throughout this PhD project. My thanks to Prof Casiraghi for welcoming me to her group and making me feel part of her wonderful group of students. My thanks to my advisor, Dr Halina Dobrzynski, who has been a friendly face, providing me with much encouragement.

I would also like to thank everyone in the Casiraghi lab, Dr Yuyoung Shin and Dr Daryl McManus (who prepared the Graphene dispersions for this study), who have trained me and supported me in understanding the graphene chemistry of my project. Thanks to the Casiraghi lab who welcomed me into their group.

I am thankful to Prof Kostarelos for his advice in this project and also for providing the Graphene Oxide samples for this project. I would also like to thank Dr Sumia Ali for her advices in this study as well as Rebecca Cadogan for her invaluable support with tissue culture and lending a listening ear.

My thanks to Dr Nigel Hodson from the Bioimaging Facility, Dr Tobias Starborg in the EM Core Facility (Faculty of Biology, Medicine and Health), and Dr Pete Walker in the Histology Core Facility at the University of Manchester, for their training, advice and assistance in AFM imaging, SCEM imaging and histology staining throughout this project.

Finally, I graciously thank the funding support from the British Heart Foundation, everyone who has donated, fundraised and volunteered. Without the funding support, none of this work would have been possible and I thus hope that my work, even if small, contributes to the enhancement of science that hopefully leads to impacting patient cardiovascular health.

CHAPTER 1

Introduction

1.1 Coronary Artery Disease

Coronary artery disease (CAD) arises from the substantial narrowing of the arteries responsible for supplying oxygen- and nutrient-rich blood to the heart. The narrowing of these arteries is attributed to luminal artery wall lesion growth, which protrudes into the coronary artery lumen, restricting lumen diameter and resulting in hindered blood supply to the heart. This leads to mal-perfusion of the cardiac tissue that can result in myocardial infarction (MI). This indicates the urgency of intervention to re-establish perfusion by opening/widening of the narrowed coronary artery.

1.1.1 Coronary artery anatomy

The coronary arteries responsible for cardiac perfusion stem from two main coronary arteries branching from the base of the aorta: Right main coronary artery (RCA) and left main coronary artery (LMCA). The LMCA divides into the left circumflex (CX) artery and the left anterior descending artery (LAD), the predominant arteries affected by CAD (Fig.1.4A). The order by which lesion development affects the coronary arteries has been reported as follows; LAD, RCA CX and the LMCA (1).

Healthy artery comprises of three principal layers; an outer layer, adventitia, a middle layer, media, and an inner layer known as the intima (Fig. 1.1). The intimal layer surface is covered with a monolayer of endothelial cells (EC) shielding the underlying cells from blood components that when in contact, can adhere to the underlying cells, triggering thrombus formation or inflammatory responses. The endothelial cells maintain fluidity of blood via promotion of several anticoagulation pathways; protein C and protein S pathways (2). Secretion of nitric oxide (NO) by ECs has a vasodilatory effect on the vessel as well as an anti-proliferative influence on the underlying smooth muscle cells (SMC) (3). EC disruption can lead to endothelin secretion that influences atherogenesis in addition to pro-platelet adhesion via expression of platelet adhering binding sites, such as P-selectin, on the cell surface (2, 4). Hence, the vital role the endothelial layer plays in the integrity and health of vessel walls. The components of the medial layer consist of primarily smooth muscle cells, whereas the intimal layer contains a network of connective tissue and a layer of elastic fibres (5).

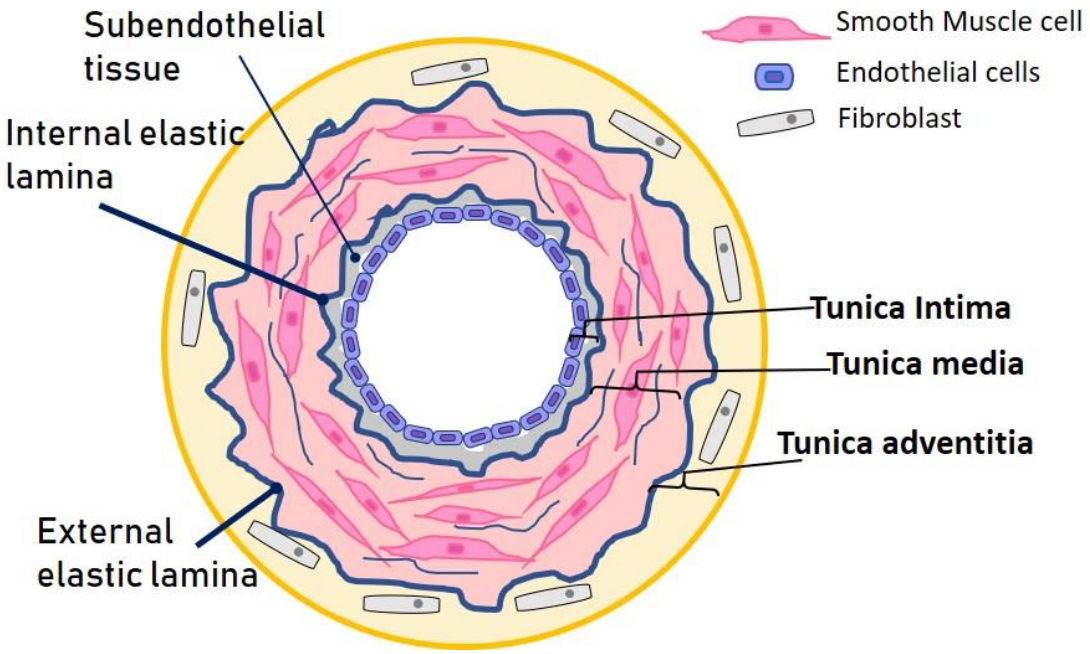

Figure 1.1: Schematic representation of an artery. Adventitial, medial and intimal layers depicted. The adventitial layer compromises of fibroblasts and connective tissue. The medial layer compromises of predominantly smooth muscle cells and elastin fibres. The intimal layer includes the subendothelial layer consisting of connective tissue followed by a monolayer of endothelial cells exposed to the artery lumen.

1.1.2 CAD Incidence

Coronary artery disease is the leading cause of cardiovascular related mortality and morbidity worldwide (Fig. 1.2) and contributes to an annual mortality of 66,000 in the UK alone (6). In spite of the many advances in the field of coronary artery intervention, CAD remains the main contributor to the 17.9 million cardiovascular related deaths worldwide (7). CAD contributes to 16% versus 10% of male and female deaths, respectively (8).

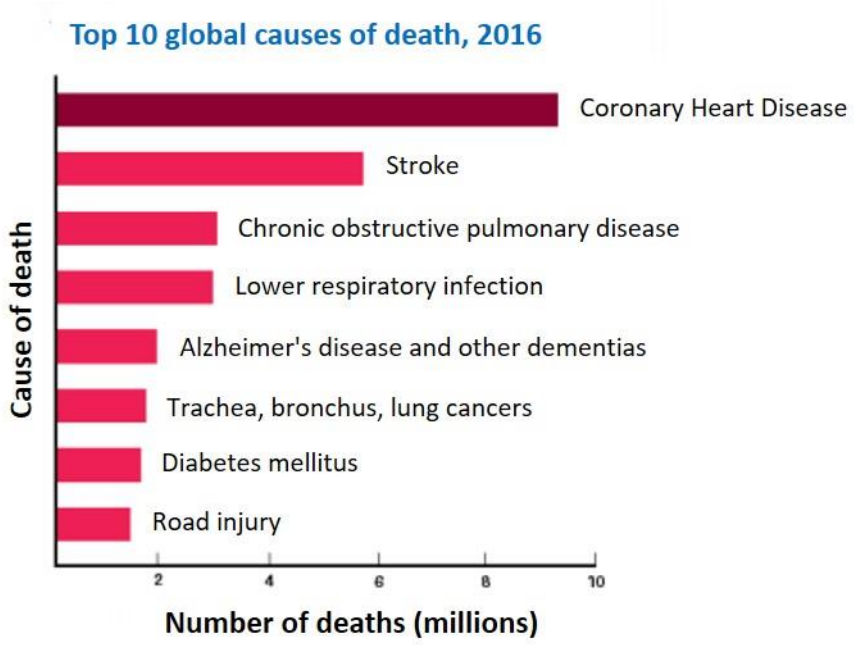

Figure 1.2: Global cause of death worldwide. Statistics of worldwide mortality and their causes in 2016 (6).

1.1.3 CAD risk factors

There are several risk factors for the development of atherosclerosis. These include hypercholesterolaemia, smoking, diabetes, hypertension, advanced age and male sex (9, 10). Hypercholesterolaemia, as one of the main risk factor of atherosclerosis, plays a major role in its development due to the elevated levels of low density lipoproteins (LDL) which accumulate within the intimal layer of the vessel, where the LDL undergo oxidation that renders them susceptible to engulfing by macrophages (detail in section 1.2.1) (11). The risk factors influence atherosclerosis and thus CAD by chronically elevated circulating harmful stimuli, such as free radicals, thereby damaging the vascular endothelium and disrupting the balance of nitric oxide that costs the endothelium its selective permeability (12).

The continued rise of CAD predisposing factors suggests a continued increase of CAD outlook. The world population is growing to advanced age and the choice of lifestyle, lack of exercise and poor eating habits, is leading to an increase risk of diabetes, hypertension, hypercholesterolaemia and obesity, all significantly contributing to the risk of developing CAD (13-15). Adding to this, is the evidence in 17% of American teenagers who have shown a pathological thickening of their coronary artery intima (16).

1.2 Pathogenesis of atherosclerosis

CAD arises from a build-up of atherosclerotic plaque, growing from the intimal layer of coronary arteries. The developing atheroma is a lipid-filled lesion on the arterial wall that grows predominantly by smooth muscle cell proliferation and inflammatory responses. Atherosclerosis was historically believed to be a lipid storing illness (17, 18). Consequently, in an attempt to alleviate circulating lipid levels and thence atherosclerosis, life style changes (exercise and dietary intake) were promoted.

The origin and progression of atherosclerosis has been widely debated, though its mechanism has now been to some extent elucidated (10). There is a complex relationship between risk factors and the inflammatory response, where a role is played by LDLs, inflammatory cells, endothelium and smooth muscle cells in initiating and developing atherosclerosis. Studies on humans as well as animals have both demonstrated the early signs of atheroma to originate from fatty streaks, also known as intimal xanthoma (19). Fatty streaks form as a consequence of chronically harmful stimuli (generated from risk factors), that lead to endothelial dysfunction, where there is a decrease in NO secretion and vasodilation as well as a move towards prothrombotic and proinflammatory state (EC dysfunction causes overproduction of pro- thrombotic and inflammatory factors) (2). Endothelium disruption means there is capability of non-selective entry via the endothelium, such as the infiltration of C reactive proteins (CRP) into the subendothelial layer; this protein is produced in the liver and believed to induce inflammation, to inhibit NO and prostacyclin production within the vessel wall (2). Fatty streaks can develop early in teenage years and progress from the infiltration of monocytes into the intimal layer, due to the loss of selective permeability of the endothelium, where they differentiate into macrophages, engulfing intimal-accumulated oxidised LDLs (19, 20). These oxidised-LDL filled macrophages, now termed foam cells reside subendothelially, being responsible for the ‘fatty’ descriptions of atherosclerosis.

1.2.1 Early atherosclerosis- fatty streak development

The initial trigger of atherosclerosis is predominantly caused by elevated blood LDL particles that penetrate the endothelium (diffuse via endothelial junctions), where the LDL constituent, apolipoprotein B, interacts with the matrix proteoglycans to accumulate within the intimal layer of arterial walls (10). Enzymatic alterations to these LDL particles occur, including oxidation, lipolysis and aggregation, that can render them susceptible to inflammatory reponses, inciting the innate immune response within the intima (10). It is

thought that lipid deposits also accumulate within the cytoplasm of the SMCs (19). Subsequent summoning of inflammatory cells, such as monocytes into the intimal layer occurs, where they differentiate into macrophages, engulfing lipid particles that lead to a lipid-rich cell, thus termed as 'foam cells' (19).

As mentioned previously, there is a substantial inflammatory component to the development and progression of atherosclerotic plaque. Some also hypothesised that this response was attributed to endothelial dysfunction or denudation that promotes leukocyte and platelet adhesion and infiltration mediated by von Willebrand factor and P selectin (2, 21, 22). Dysfunction of endothelial cells causes excessive production of Enothelin-1 (stimulate ETB receptors on monocytes), monocyte chemotactic protein-1 (MCP-1) and macrophage colony-stimulating factor (M-CSF) that all contribute to the recruitment of monocytes into the intimal layer (10). The disrupted endothelium also exhibits increased generation of macrophage activating inflammatory mediators, including interleukin 6, interleukin 8, tumour necrosis factor, prostaglandin E2 and superoxide anion (2). Moreover, dysfunction of endothelial cells produce adhesion molecules on their surface; P-selectin (potent promotor of platelet and leukocyte adhesion), E-selectin, platelet endothelial cell adhesion molecule-1 (PCAM-1, also known as CD31) and vascular cell adhesion protein-1 (VCAM-1), capturing inflammatory cells streaming past them in the blood (10, 23).

1.2.2 Intermediate lesions and advanced atheroma

The above, along with the continuation of the harmful circulating stimuli (e.g. free-radicals, LDL, low bioavailability of NO), triggers secretion of further inflammatory factors as well as triggering proliferation and migration of vascular SMCs, progressing the size of the atheroma within the intima and leading to the formation of an in intermediate lesion, known as pre-atheroma (24). As the lesion increases in size within the intimal layer, a compensatory response triggers arterial remodelling to dilate the vessel (25, 26). The relentless involvement of the immune system in this process provokes further recruitment of monocytes and lymphocytes into the lesion, expressing Interferon-gamma (IFN-ɣ) and secreting signalling proteins, enzymes (plasminogen activating and matrix metalloproteinases (MMP)) and growth factors (platelet derived growth factor), some inducing necrosis (27, 28).

The damaged endothelium causes changes to SMCs which subsequently secrete chemoattractant and chemokines, including fibroblast growth factor-2, homocysteine and angiotensin II, that lead to the migration and proliferation of the SMCs into the intima (10). Gradually, SMC extracellular matrix, immune cell and necrotic tissue accumulation ensues within the lesion, resulting in a lipid core and necrotic core that is enclosed by a fibrous cap (23). This fibrous cap forms just below the endothelium and is derived from SMCs and collagen connective network, resulting in advanced atheroma (Fig. 1.3). Eventually, the enlargement is so severe that the vessel cannot dilate anymore causing the protrusion of the atheroma into the lumen and eventually restricting the flow of blood, and consequently starving the distal tissue from oxygen and nutrients. This can finally cause myocardial ischaemia and then infarction in the acute settings and in the chronic settings where partial blockade persists, resulting in stable angina.

There are two consequences/phenotypes of atherosclerotic plaques, the lethal and acute option; plaque rupture, or the more stable alternative, plaque erosion (Fig. 1.3). The atheroma grows in size, capable of eventual rupture and then thrombosis. This is the acute state, where rupture of the atherosclerotic plaque causes an acute thrombosis event, occluding the artery completely, resulting in myocardial infarction. Thrombosis occurs as a response to contact with atherosclerotic content causing a surge of platelet and inflammatory recruitment, resulting in blockade of blood flow.

Plaque rupture

Thinning of the fibrous cap makes it susceptible to rupture. MMPs, stromolysin, gelatinases, collagenases and cathepsin, play a major role in thinning the fibrous cap by degrading the extracellular matrix (ECM) and collagen (responsible for the tensile strength of the plaque) (10, 28). Apoptosis of the collagen producing cells, SMC, is believed to add to the weakening of the plaque, due to reduced collagen secretion (28). Macrophages have been reported to reduce collagen production by either inducing SMC apoptosis, or rendering them incapable of secreting collagen (28).

Plaque rupture is a very acute process of thrombus formation, where direct contact of the thrombus with the lipid core exists. Rupture of an atherosclerotic plaque exposes its thrombogenic, tissue factor and necrotic contents, leading to a rush in thrombogenic response that leads to acute recruitment and aggregation of platelets and fibrin crosslinks, producing thrombosis at the site of rupture and blocking blood flow. About

76% of lethal MI events are attributed to rupture of the plaque which either occludes blood supply to the distal tissue completely or near-maximally (29). Vulnerable plaques are characteristic of their thin fibrous cap (poor collagen and SMC component) that envelopes the large lipid core consisting of a large immune cell and pro-coagulant material content (Fig. 1.3) (23). Macrophage accumulation within the subendothelial layer, along with the elevated expression levels of MMP1 are associated with stress and strain sensitivity (30), implicating again an inflammatory role to plaque rupture although physical disruption has been reported as the main culprit (19, 23). Highly elevated blood pressure is an example of physical disruption that may aggravate or tear the fibrous cap, causing 'rupture' (Fig. 1.3). Subsequent release of the necrotic debris and lipid/inflammatory content material into the coagulation proteins in the blood leads to a rush in coagulation processes, platelet activation and aggregation forming a large thrombus that occludes the flow of blood to the myocardium, causing oxygen starvation and MI.

Plaque erosion

Plaque erosion describes the formation of thrombus on the plaque fibrous cap surface, without contact between the thrombus and the plaque content (31). Endothelial dysfunction and erosion that result in atherosclerosis are alleged to be exacerbated by inflammation, however inflammatory processes have been described to play a reduced role in erosive plaques (32). Erosive plaques are significantly different to ruptured plaques, as is demonstrated by their contrasting inflammatory profiles (33). Unlike ruptured plaques, eroded plaques have been documented to exhibit a significantly thicker media due to larger SMC numbers as well as a more stable phenotype (32). The fibrous cap of an erosive plaque is also described to be thick and intact in contrast to ruptured plaques (34).

Raised levels of inflammatory markers like macrophages and MMP1, which are often associated with atherosclerotic plaques, are lacking in erosive plaques as well as the sparse or absence of the lipid core (32). The true process by which erosion incites cardiac events has not been well elucidated. It is believed that endothelium erosion allows contact between circulating platelets and collagen within the plaque resulting in formation of a platelet rich plaque (34). The composition of erosive plaques is dominated by extracellular matrix, collagen, glycosaminoglycan and proteoglycans (34). Literature

has described communication between circulating platelets and collagen (on fibrous cap) to activate platelet degranulation that then secretes leucocyte chemoattractant such as RANTES (also known as CCL5) and pro-inflammatory cytokines such as CD40L, further ensuing platelet activation and aggregation (34). These platelets then incite the recruitment of polymorphonuclear leukocytes that then contribute to summoning of neutrophils and granulocyte (34).

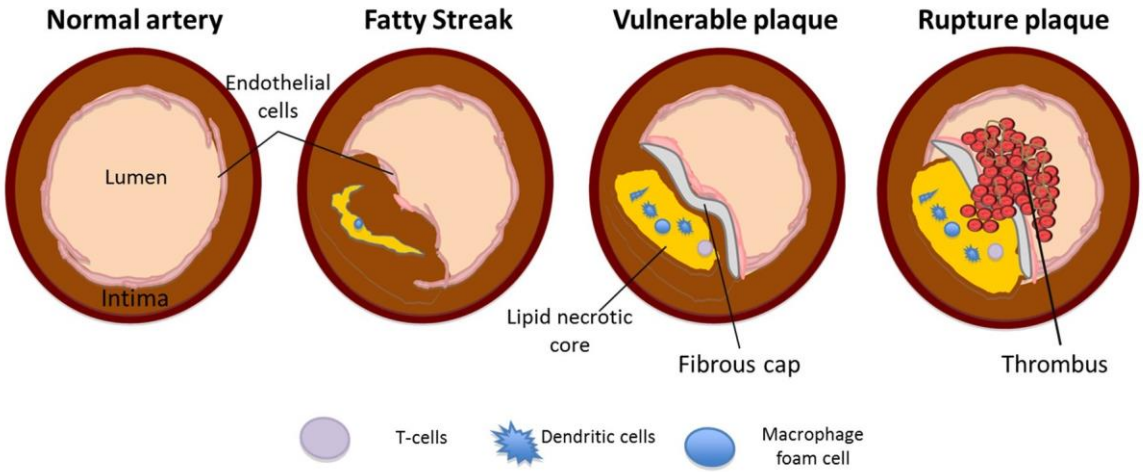

Figure 1.3: Schematic representation of atherosclerotic plaque formation. Elevated circulating lipid levels initiate the process of atherosclerosis, forming a fatty streak at first, which progresses to vulnerable plaque that may also lead to rupture. Image obtained from (35).

1.3 Coronary artery disease therapeutic strategies

There are three broad intervention strategies for CAD, with sub-treatment strategies outlined below for each:

1) Pharmacological
2) Surgical revascularisation
    a. Coronary artery bypass grafting (CABG)
3) Endovascular - Percutaneous coronary intervention (PCI)
    a. Balloon angioplasty
    b. Bare Metal Stent (BMS)
    c. 1st Generation Drug Eluting stents (1G-DES)
    d. 2nd Generation Drug Eluting stents (2G-DES)

Adjunct long-term dual anti-platelet therapy necessary

Importantly, all these interventions carry their own risk of associated complications, explaining the continued need to design new subgroup of interventions.

There remains debate in the selection of the 'best' method of treating CAD. Currently, there are several interventions for CAD; drug therapy, surgical revascularisation, as well as minimally invasive endovascular procedures i.e. angioplasty/stenting of which there are a vast number of options to choose from.

The intervention selected is personalised to the severity and extent of coronary vessel occlusion as well as the location of the occlusion (which coronary artery and site at which it exists in the artery) with considerations to the fitness and co-morbidities of the patient. Lifestyle alterations would be recommended to patients to reduce their risk factors of exacerbating their condition or to avoid additional artery narrowing, this includes; cessation of smoking, increased exercise and low-fat/healthy diet. Often pharmacological intervention is used as an adjunct to these steps.

1.3.1 Pharmacological treatment of CAD

Prophylaxis treatments that aid regression or halt progression of atherosclerosis are available, targeting predominantly circulating lipid particles. The predominant mode of prophylaxis is the use of statins. There are also pharmacological aids utilised to reduce stress on the atherosclerotic plaque as well as reducing myocardial oxygen demand. It is now well known that inflammatory response is a major contributing factor to atherosclerotic development. Thus, by logic, an anti-inflammatory pharmacological target would be a reasonable approach to tackling atherosclerosis and consequently CAD.

An approach addressing the anti-inflammatory pathway was recently trialled. This involved an inflammatory target for treating atherosclerosis particularly in patients with persistently high proinflammatory markers such as high sensitivity C reactive proteins. The Canakinumab Anti-inflammatory Thrombosis Outcome Study (CANTOS) randomised 10,061 patients with previous MI and elevated levels of high sensitivity CRPs ($\geq 2 mgL^{-1}$) to 3 doses of canakinumab or placebo groups, to assess the efficacy of canakinumab in reducing repeated vascular events (36). Canakinumab, an anti-interleukin-1β agent that results in the inhibition of the interleukin-6 (pro-inflammatory cytokine) signalling pathway as well as the multiple roles it is believed to play in the progress of atherothrombotic plaque, the drive towards coagulation activity, vascular SMC growth, and leukocyte and monocyte adhesion to ECs (36). Canakinumab demonstrated a significant reduction in interleukin-6 and high sensitivity CRP levels compared to placebo, as well as a significantly reduced incidence of recurrent vascular events in comparison to

placebo group (36). This is an important finding, affirming the strong inflammatory component to acute coronary events as well as an importantly novel therapeutic direction for CAD. However, alarmingly an increased incidence of fatal infection as well as sepsis was also observed in the treatment group than the placebo group, suggesting further investigation and analysis is necessary prior to introducing to the wider CAD patient population (36). Additionally, supplementary analysis of the CANTOS trial would be beneficial in order to determine possible effects of canakinumab in relation to the incidence of recurrent ST segment elevation MI (STEMI) and non-STEMI. Perhaps in the immediate sense, there is potential to introduce this as a therapeutic strategy only in the patient group at high risk of repeated acute coronary events with simultaneous consideration to patients' infection risk profiles. This trial has confirmed the advantage of further investigating inflammatory targets as an intervention to CAD.

Nevertheless, current medical intervention focuses on treating the risk factors that exacerbate CAD; hypercholesterolaemia, hypertension. This includes the use of statins to treat hypercholesterolaemia and to lower circulating lipid levels, angiotensin-converting enzyme inhibitor or beta-blockers to lower blood pressure and thereby attenuating stress on arterial walls, as well as calcium antagonists or nitrates to lessen myocardial oxygen demand and elevate myocardial oxygen supply (37).

1.3.2 Coronary artery bypass graft (CABG)

A surgical intervention to re-establish cardiac perfusion was first introduced in humans in 1961 (38). Prior to this, Carrel attempted the first surgical intervention of cardiovascular tissue in dogs and later successful intervention of the coronary artery also in dogs by Murray and colleagues in 1954 (39, 40). This was the first step in direct intervention to treat CAD that is still regularly performed and its superiority over PCI (with stent) continuously debated (41, 42). CABG involves the use of expendable vessels to bypass the location of vascular occlusion and thus allow perfusion of the area of myocardium distal to the obstruction via the new grafted vessel. The vessel used for the bypass is often a healthy saphenous vein (SV) or the internal mammary artery (IMA). Use of the SV involves initial isolation followed by anastomosis to a larger vessel such as the aorta and to the coronary artery distally to the occluded site (Fig. 1.4A). To use the IMA, a free end of the internal mammary artery is sutured to the affected coronary artery, therefore bypassing the region of occlusion/atherosclerosis (Fig. 1.4A). The outcome data of this procedure

are promising, though IMA is a preferred line of intervention against CAD compared to SV. This is attributed to the enhanced long term (10 year) patency associated with IMA (85%) versus SV (61%) (43). The raised failure rate of SV versus IMA is confirmed in other studies and is thought to be attributed to the resistance of the IMA to atheroma development (44).

On the other hand, CABG is a very invasive approach to revascularisation and at times not suitable for acute intervention or frail patients, consequently an alternative to this was sought. Hence, the introduction of a minimally invasive approach to revascularise the coronary arteries, PCI or also known as balloon angioplasty.

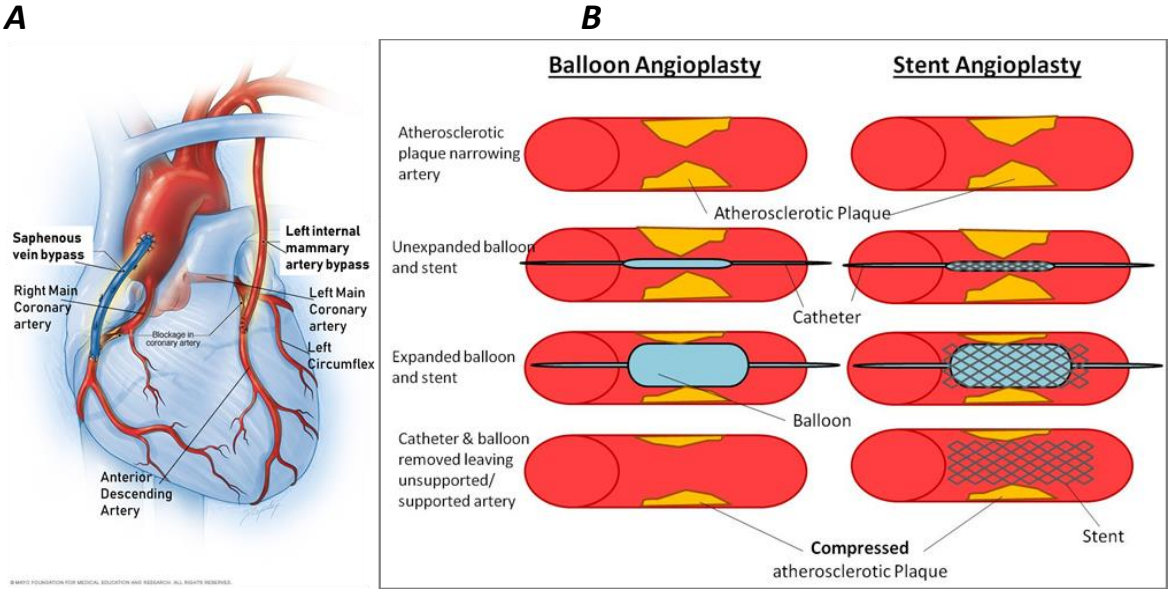

Figure 1.4: Intervention strategies for treatment of coronary artery disease. A: Illustration of Coronary artery bypass grafting, graft from saphenous vein connecting aorta to coronary artery distal to site of occlusion vessel and one end of the mammary graft rerouted to coronary artery vessel, again distal to the site of occlusion. Annotated from (45) accessed on 18/12/18). **B:** Percutaneous coronary intervention without or with stent scaffold (35).

1.3.3 Percutaneous coronary intervention

1.3.3.1 Balloon Angioplasty

Coronary artery angioplasty was first performed by Grüntzig in 1977 and rapidly became the preferred method of revascularisation, particularly as an acute intervention (46). This involved the use of a balloon-like apparatus that when inflated within the coronary artery widens the stenosed location of the artery by compression of the atherosclerotic plaque (Fig. 1.4B). As with any intervention, complications can arise, and the dominant limitation of this approach was the 20-40% associated risk of restenosis within hours to weeks, in

addition to its risk of sudden arterial collapse (47). These significant and major flaws declined the initial appeal of angioplasty (48).

The primary reason for arterial collapse (also known as arterial recoil) and restenosis, is the added stretch injury imposed on the already fragile arterial wall (49). Weakened arterial wall and damage to elastin fibres means that after balloon deflation, it can no longer support the open state leading to collapse. Balloon inflation can also cause endothelial disruption, medial layer dissection and internal elastic lamina fracture (Fig. 1.1) (49). SMC proliferation and migration into the intimal layer leads to intimal hyperplasia and arterial remodelling that protrudes into the arterial lumen causing intra-luminal bulging that results in arterial restenosis (50). To address the unsupported and weakened arterial wall, stent placement in conjunction to angioplasty emerged as a more effective method to scaffold the arterial walls in the open state post angioplasty.

1.3.3.2 Angioplasty with bare metal stents

The accompanied scaffold with the balloon angioplasty is known as a stent, and the predominant material make-up of stents are metals, particularly stainless steel, although there continues to be a shift towards cobalt chromium even though both demonstrate similar target vessel revascularisation incidence (51). The move away from stainless steel is predominantly attributed to risk of hypersensitivity of the nickel within the medical grade stainless steel, and nitinol stents (nickel/titanium alloy) (52). Some in literature have claimed an association between the nickel in the stent scaffold and restenosis (52).

Bare metal stents (BMS) were first introduced as a therapeutic strategy in 1987 (53). These stents are designed in a metal mesh like structure to support the vessel walls and avert arterial collapse (Fig. 1.4B). The BENESTENT (BElgian NEtherlands STENT study) and STRESS (STent REStenosis Study) trials presented a success rate of 96% and a restenosis risk of 32% for BMS, whereas angioplasty alone demonstrates a success rate of 90% and a restenosis incidence of 42%, rendering the BMS as the routine and preferred treatment intervention (47, 54) until more advanced designs developed. Importantly though, the recent BMS offer a greater efficacy with an improved haemodynamic design; thinner and stronger struts (55).

Meta-analyses have been conducted to compare and review results from several randomised control trials (RCT) investigating efficacy of balloon angioplasty in comparison to BMS (56). Some advantages of BMS over angioplasty alone were identified, while there

was no change in incidence of mortality or thrombosis (56, 57). Even though there were improvements associated with BMS; lower occurrences of recoil/re-occlusion and reduced rate in clinical events, there were also reported incidence of intervention related complications; myocardial tissue damage and repeat revascularisation (57).

The mechanism of restenosis is described below in section 1.4.2. Neointimal hyperplasia is the cause of restenosis and is believed to originate from the endothelial cell denudation caused when deploying the stent. It is the healing response to this that leads to neointimal hyperplasia, and consequently in-stent restenosis, and yet when compared to angioplasty alone, still demonstrates an ameliorated morbidity incidence (58-60).

Elucidating the mechanism of restenosis and thrombosis was a vital step to determine intervention targets, enabling design of pharmacologically active implants. The dominant complication of BMS was the continued incidence of restenosis that encompass the stent resulting to in-stent restenosis. When endothelial cell growth on the stent struts occur, this enables smooth streaming of the blood past the stent struts as well as suppressing adhesion of platelets by the anti-thrombotic characteristic of the re-established endothelium (61). Neointimal hyperplasia re-narrows the vessel lumen diameter to a significant degree. To address this complication and improve this incidence pharmacologically active stents targeting SMC proliferation was designed and termed drug eluting stents (DES).

1.3.3.3 Drug eluting stents

The aforementioned complications heralded the design of DES, a complication-improved stent. These include the same metal scaffolds as BMS but with polymer and drug coatings. BMS are associated with six months restenosis incidence of about 30%, whereas DES ameliorate the risk by more than half, but they do not reduce restenosis entirely (62, 63). DES often are similar in design and substrate but have incorporated anti-proliferative drugs on polymer coatings. The drugs are released gradually around the site of implantation, and the duration depends on the type of stent ranging from 30 days to 12 weeks to release approximately 80% of the drug (64). The first DES introduced were sirolimus eluting stent (SES) and paclitaxel eluting stent (PES), known as the 1st generation DES (65, 66).

1st Generation Drug eluting stents (1G-DES)

Sirolimus also known as rapamycin is an immunosuppressive and anti-proliferative drug. It acts on the cytosolic protein, FK binding protein 12 (FKBP12) to suppress the protein regulator termed mammalian target of rapamycin (mTOR), inhibiting protein synthesis for cell growth and the G1 phase of the cell cycle, consequently suppressing cycle progression and proliferation (67-69). An additional influence of Sirolimus is to repress cytokine-incited T cell proliferation as well as reducing cell matrix generation (69). Its abovementioned targets and action make sirolimus an advantageous drug for decreasing neointimal hyperplasia and thus in-stent restenosis.

Similarly, another drug predominantly acting on the cell cycle is Paclitaxel. Paclitaxel acts on the cell cycle by stabilising microtubules, which in effect halts cell cycle progression from G2 to M phase as well as G0 to G1 (70). Centrosome and spindle microtubule arrangement is crucial in mitosis, and disruption in this allows paclitaxel to hinder cell cycle progression and SMC proliferation and migration, thereby suppressing in-stent restenosis due to neointimal hyperplasia (71, 72).

Landmark randomised control trials were conducted to assess the efficacy of the sirolimus and paclitaxel eluting drugs. These included the first in man trials, RAVEL, SIRIUS, and the Paclitaxel eluting stent trials TAXUS (65, 66, 73, 74). The revascularisation and restenosis outcomes of these RCTs were promising and thus heralded the routine use of DES from here on. A meta-analysis exploring the efficacy of the BMS and DES in patients with ST segment elevation infarction (STEMI) and hence undergoing primary percutaneous coronary intervention, validated the efficacy of DES, demonstrating lower rates of revascularisation with DES but the realisation of a new morbidity, known as late stent thrombosis (LST) or very late stent thrombosis (VLST) and very late re-infarction, which was shown to be significantly higher in the DES group after 2 years (75). This is a serious and life-threatening complication that occurs some months/years after stent implantation. No significant difference between the groups in rate of mortality, reinfarction or early stent thrombosis was found (75). In contrast, a prospective multicentre primary PCI registry PREMIER (Prospective Registry Evaluating Myocardial Infarction: Events and Recovery) presented a higher mortality frequency in the DES upon withdrawal of dual anti-platelet therapy within six months of stent deployment (76).

One of the main sources of late stent thrombosis is attributed to delayed re-endothelialisation of the vessel luminal surface. BMS have been reported to show complete endothelium recovery six months post implantation, whereas DES re-endothelialisation remains incomplete even after 40 months (77). This delayed endothelium recovery is attributed to the cell cycle inhibition effect of the drugs on DES. This de-endothelialised luminal surface then becomes prone to continuous fibrin deposition and platelet adherence, encouraging thrombus formation (64, 77, 78). Some patients can also develop local hypersensitivity to the stent materials; polymer, drug or metal substrate causing an inflammatory response, although this is disputed since the drugs themselves also have immunosuppressive effect (78, 79).

The safety and efficacy of 1G-DES in the long-term settings remains under doubt. This is associated with the incidence of late stent thrombosis and the necessary and aggressive long-term anti-platelet therapy as well as the very serious and fatal concern of local thrombosis (73, 80-82). In addition to the previously mentioned concerns, there are also bleeding complications associated with the long-term anti-platelet therapy incorporated with DES implantation, particularly hazardous when CAD/non-CAD related procedures are required, necessitating the temporary discontinuation of the anti-platelet therapy (83, 84). This is a persistent predicament that clinicians often face; the balance between bleeding or thrombosis risk, with both exhibiting potentially fatal outcomes (85, 86).

2nd Generation Drug eluting stents (2G-DES)

In the pursuit of a more effective DES with superior long-term safety outcomes, the second generation DES (2G-DES) were designed and thence have now become the mainstay coronary intervention implants. These employ a thinner strut design, a more biocompatible polymer with a less toxic anti-proliferative drug (87). Everolimus eluting stents (EES) are designed on a cobalt-chromium alloy substrate (88). The 2G-DES include the everolimus eluting, zotarolimus-eluting (ZES), and ridaforolimus-eluting (RES) stents. Their efficacy outcomes are rather similar to 1G-DES but with improved long-term complication incidence of stent thrombosis, restenosis and thus MI (87). The first in man trial, SPIRIT, comparing the 2G-DES, EES with the 1G-DES, PES, demonstrated the superiority of EES over PES, both in terms of late lumen loss and major adverse cardiovascular events (89-91).

Everolimus is an analogue of sirolimus, which acts on the FKBP12 cytoplasmic protein, forming a complex that influences the regulatory protein mTOR, thereby inhibiting proteins p70 s6 kinase and 4E-BP1 preventing initiation of protein synthesis as well as supressing cell cycle progression at G1 to S phase (69, 91). EES acts on the same pathway as sirolimus though affecting other cells than T-lymphocytes (69). It is noteworthy that EES has demonstrated accelerated re-endothelialisation as compared to SES, PES and ZES in a rabbit iliac artery model after 14 days and it is also known as the best in class DES (92, 93).

1.3.3.4 Adjunct Dual anti-platelet therapy (DAPT)

The routine and dominant drugs prescribed to patients after DES implantation are; aspirin and $P2Y_{12}$ adenosine diphosphate receptor blockers; clopidogrel, prasugrel, or ticagrelor (94). The use of these drugs are crucial long-term, 6-12 months though some patients require longer periods of up to 48 months with the purpose of preventing thrombus formation (94).

In summary, although most of the previously mentioned therapeutic strategies are effective in treating CAD in the first instance, later complications demand re-intervention (Fig. 1.5 and Table 1.1) or add significant additional risks, necessitating the design for a more effective and complication-free stent.

Table 1.1: Summary of advantages and disadvantages of coronary artery disease interventions. Coronary artery bypass graft (CABG), Bare metal stent (BMS), Drug eluting stent (DES).

	Advantages	Disadvantages
CABG	- Lower incidence of repeated coronary intervention (either by CABG/PCI) (95)	- Very invasive procedure and unsuitable for some comorbidities
Balloon Angioplasty	- Transient lumen widening	- High risk of restenosis and recoil - High incidence of repeated coronary intervention (either by CABG/PCI)
BMS	- Somewhat eradicated arterial recoil/collapse - Maintains opened-state of vessel - Complete re-endothelialisation within six months (77) - Suitable for those due to undergo invasive procedure in the near future	- High incidence of restenosis and in-stent restenosis
DES	- Significantly reduced restenosis and in-stent restenosis - Less invasive and suitable for some patients with morbidities	- Poor re-endothelisation, even after several months - Incidence of late and very late stent thrombosis - Long-term (>2 years) anti-platelet therapy - Unsuitable for those soon to undergo major surgical procedure or with high risk of bleeding complications

1.4 Pathophysiology of stent related complications

The predominant shortcoming of PCI is the significant stent associated complications. Complications often develop as a response to vessel wall injury caused when inserting and deploying coronary artery balloon and stent. The type and severity of injury depends on whether angioplasty alone is performed or whether it incorporates an added stent scaffold. Balloon angioplasty poses stretch and vessel wall fracture injury, while incorporation of a stent can also cause more focal injury with stent struts indenting into the vessel wall as well as posing long term vessel wall strain (49, 96). Moreover, the permanence of the stent, as a foreign material, in contact with the vessel wall may also induce a systemic or local responses (97). The mechanism is not yet completely elucidated but known details are outlined below (Fig 1.5).

1.4.1 Elastic recoil of coronary artery post angioplasty

Elastic recoil results from a collapse of the artery within minutes to hours after balloon angioplasty. Reports of an approximate 34% loss of the luminal diameter within a quarter of an hour have been made, with recoil contributing to 50% of the luminal area loss (98). Restenosis, elastic recoil and negative remodelling have all contributed to the incidence of revascularisation in balloon angioplasty, while the latter two have almost been eradicated with stenting.

1.4.2 Restenosis of coronary artery after angioplasty without/with stent

This is a complication of balloon angioplasty where the damage induced by balloon inflation on the intimal and medial layers of the vessels results in recurrent stenosis of the vessel. The process of restenosis can include both negative remodelling (vessel constriction reducing lumen diameter) and neointimal hyperplasia (attributes to injury caused to the atherosclerotic plaque). Restenosis initiates with elastic recoil in response to balloon inflation (within hours of PCI), followed by negative remodelling arising from collagen and ECM production/accumulation as well as thickening of the adventitia with a final formation of neointima, developed from SMC proliferation and migration (99). This process can take up to six months and includes a myriad of responses including inflammatory, thrombus formation and SMC proliferation (98).

Restenosis incidence did significantly improve from 40% in balloon angioplasty to 25% with the introduction of a metal scaffold, as well as only 7% requiring total lesion revascularisation within six months (100), though presenting a novel challenge of in-stent restenosis to address (47, 54).

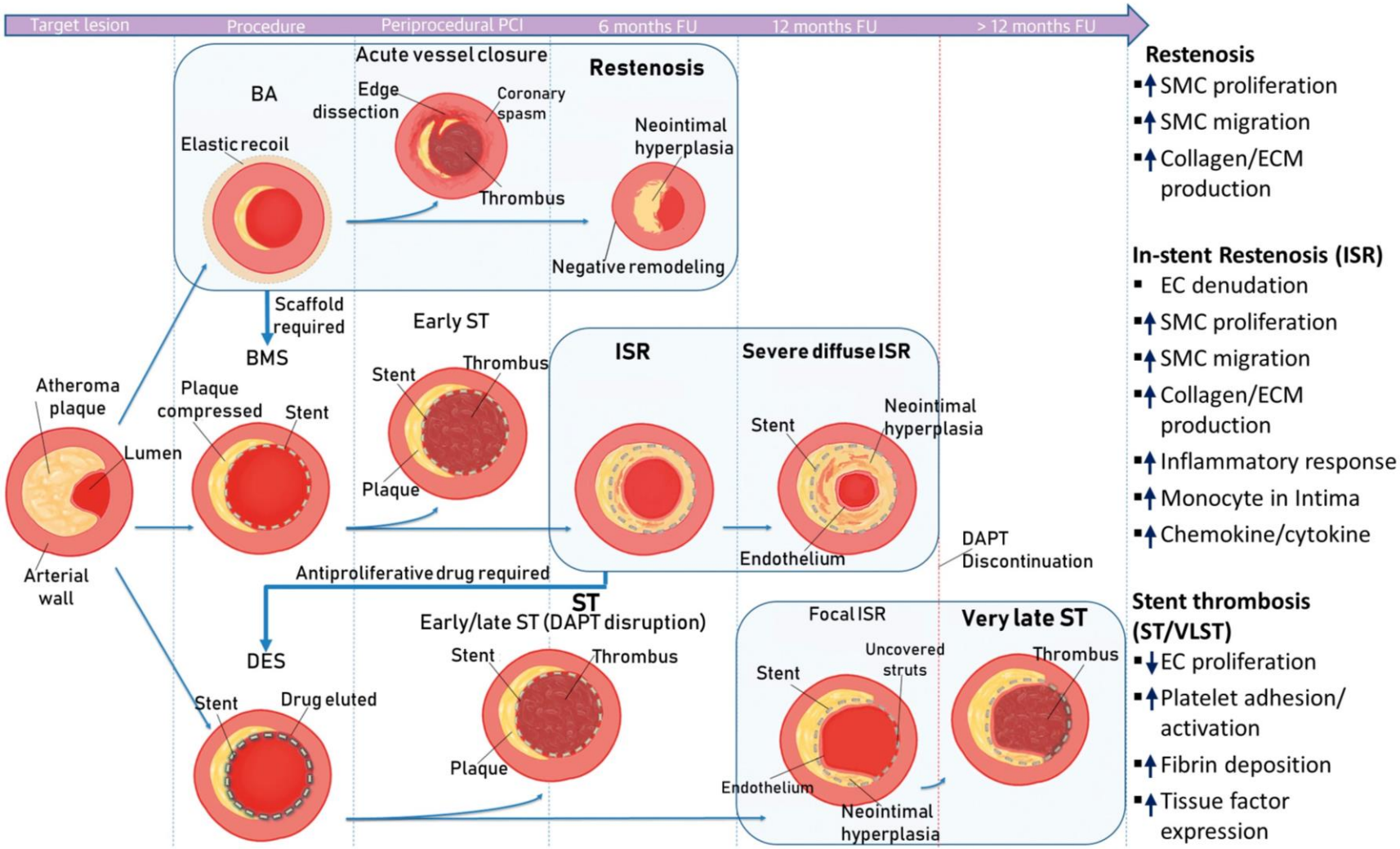

Figure 1.5: Schematic summary and representation of stent related complications. BA-Balloon angioplasty; BMS- Bare medical stent; DES- Drug eluting stent; ISR- In-stent restenosis; ST- Stent thrombosis; VLST- Very late stent thrombosis; DAPT- Dual antiplatelet therapy; EC- Endothelial cell; SMC- Smooth muscle cell; ECM- Extracellular matrix. Adapted and annotated from (55).

1.4.3 In-stent restenosis after deploying stent

In-stent restenosis (ISR) is a complication of stenting and is predominantly caused by neointimal hyperplasia originating from trauma inflicted by the stent. ISR describes the reduction of the lumen diameter by >50% at the site of stent deployment, and commonly arises within six months of BMS deployment, while the peak of DES is later at 8-12 months (49, 101). Origins of in-stent restenosis are multifactorial; hypersensitivity to the stent material, denudation of the endothelial layer, inflammatory response attributed to blood component communication with subendothelial layer (55, 101, 102). ISR occurs in 20-40% of cases (103, 104).

During implantation of the stent, endothelial cell denudation occurs, this along with the response to the metal components draws inflammatory responses such as monocytes into the intima, releasing chemokines and cytokines that stimulate SMC migration and proliferation, adding to the thickness of the intima (Fig. 1.5) (101). Loss of endothelial cells implies loss of the anti-thrombogenic influence of endothelial cells that also contribute to potential exposure of the metal struts to subendothelial content, recruiting a further inflammatory response. The SMCs also stimulate secretion of extracellular matrix into the intima, resulting in further thickening of intima that concludes to arterial obstruction. (105).

1.4.4 Late stent thrombosis after deploying drug eluting stent

Late stent thrombosis is predominantly a complication of drug eluting stents. It is a multifactorial complication, influenced by: type of lesion; technical positioning of the stents; patient co-morbidities, compliance to drug therapy; and stent related materials (106).

Late stent thrombosis develops locally and is a result of the absence of endothelialisation even months after stent implantation. This is attributed to the potent anti-proliferative drugs eluted from the stents that are targeting neointimal hyperplasia by inhibiting SMC mitosis, but also have an off-target effect on endothelial cell mitosis also (55, 81). This delayed endovascular healing increases the susceptibility of the vessel to platelet adhesion, activation and aggregation as well as relentless fibrin deposition that concludes in acute and life-threatening thrombus formation, with an incidence of 0.6 % - 5% (64, 107). There are two options to tackling this local complication, either by systemic pharmacological therapy (dual anti-platelet therapy) or by reducing stent

thrombogenicity (improving stent design). One of the main risks of stent thrombosis, is cessation of dual anti-platelet therapy for fear of excess bleeding, for instance if undergoing a medical procedure with risk of bleeding, which can greatly accelerate risk of stent thrombosis. One of the reasons for stent thrombosis, particularly in 1G-DES, such as sirolimus and paclitaxel are the increased tissue factor expressions that set-up a pro-thrombogenic environment (107).

1.5 CAD intervention comparison

1.5.1 CABG vs PCI

Approximately a third of those treated via PCI also require repeated intervention (either by PCI or CABG) within three years, hence adding further to its morbidity and mortality risks (108). The ASCERT trial which utilised retrospective data from the American College of Cardiology Foundation and the Society of Thoracic Surgeons to compare effectiveness of CABG and PCI, revealed no difference in rates of mortality between the two groups in the one year after procedure, though CABG mortality rate after 4 years was demonstrated to be lower to PCI; adjusted average of 0.2525 life years gained in CABG patients relative to PCI over the observation period (109, 110). However, the ASCERT trial did have important limitations, the severity of the CAD was not considered and the PCI group consisted of varying implants; DES (78% of PCI group), BMS (16%) and unstented (6%) intervention (109). On the other hand, the SYNTAX trial where CAD severity was considered, there was no significant difference in outcome between the CABG and paclitaxel eluting stent within a group of patients suffering from relatively mild CAD, whereas in the patient groups with intermediate severity, increased MI and revascularisation incidence was observed in the PES group vs the CABG group and in the most severe group, almost all clinical endpoints were shown to be significantly enhanced in the CABG compared to the PES group (111). These are 5 years follow up data suggesting the superiority of CABG to PES (111).

Another study analysing New York's cardiac registry, demonstrated a significantly higher in-hospital mortality in the CABG group versus the PCI group (specific stent unknown) 1.75% vs. 0.68% respectively (108). However this study as well as many others have presented long-term (1-8 years follow-up) mortality incidence of CABG to be significantly less than PCI, validating the merits of CABG over PCI in patients undergoing repair of two or more coronary vessels (108, 112).

In contrast to the above, a meta-analysis by Bravata *et al.* reported non-significance in the mortality rate after 10 years of either PCI or CABG, however documented a raised risk of stroke among CABG patients (41). Yet again, there remains essential benefits of CABG over PCI, a follow-up of 10 years emphasised an improved efficacy of CABG at relieving angina in addition to substantially lower occurrence of re-intervention with CABG in comparison to PCI (20.3% vs 76.8%, respectively) (41, 95, 113). Surprisingly however, CABG procedures are on the decline, potentially associated to the invasive nature of the procedure or it may be that most CAD cases are first identified by cardiologists that possibly undersell the benefits of CABG over PCI (114).

The financial implications of each procedure should also be considered. CABG is considered a more expensive intervention, with a reported one-year overall cost of £8905 vs £6296 in PCI (115). This is mainly attributed to the cost of long hospital stay associated with CABG, ward cost of £3915 compared to £1435 with PCI (115). This is also reflected in the USA with higher lifetime costs associated with CABG $196,256 versus PCI $187,532 (110, 115). One year medication cost was documented to be cheaper in the CABG group £455 compared to the £804 in the PCI group (115).

1.5.2 Bare metal stent vs Drug eluting stent

A study involving a sample size of just over 10,000, revealed in-stent restenosis incidence of 30.1% and 13.4% for BMS and DES, respectively (63). Similarly, comparing ISR within the DES group, ISR occurrence was 14.6% in 1G-DES and 12.2% in the 2G-DES (63).

According to a multicentre RCT, in-stent restenosis arising from BMS has been reported different in morphology and clinical presentation when compared to ISR arising from DES; describing second time (repeated) revascularisation by EES to target BMS related ISR to be lower in second time morbidity and mortality when compared to DES related ISR (116). Even though DES have been known as an enhanced stent to BMS, particularly when comparing the incidence of morbidity and mortality outcomes, they demonstrate a worse morbidity/mortality upon the development of ISR that necessitate second time revascularisation; i.e. should ISR arise from DES implantation, a worse morbidity/mortality is demonstrated in repeated vascularisation in comparison to repeated revascularisation to target ISR caused by BMS implantation (116).

In summary, superiority of either PCI or CABG continues to be controversial. Due to some of the reported similarity of mortality and morbidity incidence between CABG and PCI,

understandably there is a preference of patients to undergo PCI as a means to avoid the overwhelming and frightening prospect of open-heart surgery. However, in comparison, numerous RCTs documented the better long-term mortality of CABG over PCI (42, 111, 117).

1.6. Coronary stents currently under development/investigation

1.6.1 Bioabsorbable metal alloy stents

This is a developing technology where the metal scaffold itself dissolves/corrodes gradually within a few months in the vessel. There are several corrodible stents under investigation; these include stents composed of metal alloys including Fe-, Mg- and Zn-based metal stents. The first in man trial of magnesium alloy bioabsorbable stents on 63 patients revealed high restenosis occurrence within 4 months of implantation, mainly attributed to the fast alloy degradation (118). Fe based metal stents were also investigated by implantation to rabbit aorta demonstrating absence of thrombosis, neointimal hyperplasia or inflammatory response within 6-18 months of stent implantation; however significant safety risks were identified (even though authors did not acknowledge these as safety concerns), damage and destroying of internal elastic lamina and the medial layer of the vessel (119). Overall and to this time, biodegradable metal stents have not presented superior efficacy over current angioplasty methods in lower limbs, though contrasting animal results have been reported by the many studies and investigations are still ongoing on these types of stents (120-122).

1.6.2 Biodegradable/bioabsorbable drug eluting stents

To carry the pharmacologically active materials on the stents, the majority of DES utilise a biodegradable as well as a non-erodible polymer coating on a metal scaffold. Exploring the DES available, the predominant scaffold for 1G-DES were 316L medical grade stainless steel, while for the 2G-DES it was the cobalt-chromium alloy (69).

The main concerning complication of DES is late stent thrombosis. This is attributed predominantly to the delayed re-endothelialisation of the vessel that then exposes the scaffold to the subendothelial layer, triggering inflammatory response and platelet activation against the 'foreign material'. To address this, biodegradable drug eluting stents were introduced, as these provide an earlier and complete pharmacological elution in addition to complete bioabsorption of the mechanical scaffold (123).

The first fully biodegradable stent to be deployed in the human coronary artery, Gaki-Tamai PLLA, revealed promising results in a sample size of 50 patients, demonstrating a 4% stent thrombosis incidence during a 10 year period (124). It is noteworthy however that the two events of stent thrombosis were unrelated to the stent implant, with the first patient being attributed to inadequate heparinisation and the second patient resulting from the treatment of a separate lesion by SES deployment at another site (125). This design did not, however, advance further due to concerns raised from the clinical trial; low-risk patients were selected for study participation and the technique of stent expansion was by heat activation, adding to concerns of vessel injury (126).

Advances in this field are ongoing with several clinical trials recently conducted to determine the efficacy of bioabsorbable stents over the mainstay stents currently used (118, 127). One of the most promising bioabsorbable stent investigated was in the ABSORB trials. Recent data presenting the long-term outcome of the everolimus eluting bioabsorbable stent over the commonly used EES cobalt-chromium concluded the non-superiority of the bioabsorbable stent but also reporting a 11% target-lesion revascularisation incidence in the bioabsorbable stent versus the 5.6% in the metallic scaffold EES stent after 4 years, leading the scientific community to lose enthusiasm in the advance of bioabsorbable stents (127). However, there is the argument that the real advantage of these bioabsorbable stents would be highlighted in the very long-term duration, i.e. >5 years post stent implantation.

1.6.3 Biodegradable polymer stents

This is similar to biodegradable stents described above, though with polymer degradation (complete drug elution and carrier polymer) only leaving behind the metallic scaffold. In 2008, BioMatrix was the first biodegradable stent developed. It incorporates a biolimus A9 drug on a biodegradable polymer, that is coated onto a bare metal stent. Once the drug has been released from the polymer, the polymer breaks down within 6-9 months leaving behind the BMS scaffold (128). Biolimus A9 is also a sirolimus analogue that is highly lipophilic to allow for faster tissue absorption and also acting on the mTOR pathway, in a similar way to everolimus and sirolimus. The LEADER trial was the first RCT exploring the efficacy of the biodegradable biolimus A9 eluting stents (BES) versus the durable SES. The 5 year follow-up results described a non-inferiority of BES in comparison to SES, there was however a non-significant lower incidence of definite late stent

thrombosis observed in BES group compared to SES (2.6% vs. 4.5%, respectively) (129).

A recent RCT evaluating the efficacy of the biodegradable SES and durable EES, BIOSCIENCE trial, reported no difference in the frequency of stent thrombosis during the 5 years of follow-up, but significantly raised incidence of all-cause mortality in the biodegradable SES than in the durable EES (14.1%, 10.3% respectively), the variance mostly attributed to non-cardiac mortality (93).

As the inferiority of the bioabsorbable EES versus durable metallic EES (ABSORB III, IV trials) is released, target vessel MI (8.6% vs. 5.9%, respectively) and definite stent thrombosis rates of 2.3% vs 0.7%, respectively at 3 years (130) , some are not convinced that biodegradable DES are the future of coronary artery intervention.

In summary, long-term results indicate bio-absorbable or degradable polymer biolimus eluting stents to be non-inferior to the standard metallic backbone DES. The long-term data have been disappointing and there remains the need for a more advanced and complication-free stent.

1.6.4 Polymer-free stents

As an upgrade to the bioMatrix stent, the polymer free BioFreedom stent was designed. BioFreedom stent is a polymer-free stent with a biolimus A9 coating that has been demonstrated to reduce neointimal thickness and inflammation in swine animal models (131). LEADERS FREE trial presenting their 2-Year outcome of the BioFreedom polymer-free stent versus the GAZELLE BMS in high-bleeding risk patients (short-term dual anti-platelet therapy with aspirin and clopidogrel), this showed a revascularisation incidence of 6.8% vs 12.0% and stent thrombotic events of 8.2% vs 10.6%, respectively (132). This suggests the superiority of the polymer-free biolimus A9 coated stent over the GAZELLE BMS. On the other hand news reports have documented the inferior efficacy of the polymer-free DES with higher risk of target lesion revascularisation when compared to the bioabsorbable DES (SORT-OUT IX trial) (133). However in patients with lower tolerance to dual anti-platelet therapy the polymer-free stent is to be considered as an alternative (133). Further and larger trials in this field are required, however the initial results show some benefits in high bleeding risk patients in regard to avoiding long-term dual anti-platelet therapy, though lower efficacy compared to bioabsorbable DES indicates that it probably will be inferior to EES, as these are more effective in reducing comorbidities when comparing to bioabsorbable DES.

1.6.5 Gene eluting stents

There are now establishing investigations exploring the benefits of incorporating agents that alter genes or regulatory proteins to target stent related complications like restenosis/late stent thrombosis.

Gene eluting stents include plasmid, microRNA or siRNA coating on the stent to target, for instance, SMC proliferation directly or influence growth factor/cytokines that regulate SMC proliferation (134). There have been a few animal studies exploring potential application of this as a coronary artery stenting technology. The first stent based gene delivery technology was described by Klugherz and colleagues, where the diseased site was exposed to local proliferation defective adenoviruses, tethered to stents via antigen-antibody affinity (135). This was studied in culture and in porcine coronary arteries demonstrating no sign of thrombosis but a poor site-specific transfection efficiency (135).

In an investigation conducted in Rabbits, plasmids incorporated with specific growth factor or cytokine genes to target SMC proliferation were administered, restenosis was prevented although there still remains technical challenges prior to trialling this in humans/clinical settings (136). Animal investigations have confirmed iRNA technology to be promising in treating in-stent restenosis, although there is much further animal and in-man trials necessary to explore safety and efficacy (136-138).

1.6.6 Diamond-like carbon coatings

Diamond-like carbon (DLC) is a man-made material that has been described to be biocompatible (139). DLC's non-thrombogenicity has been confirmed by albumin/fibrinogen adsorption ratio that has led to its potential application in the biomedical settings (140). One of the dominant issues relevant to DLC is its poor adhesion to its substrate, raising concerns in terms of coating wear when deploying the stent as well as when under shear stress caused by blood streaming past (141). Also, scalability of the material is very expensive and rather difficult as high purity material would be required for biomedical purposes.

DLC coating on stainless steel coronary stent was investigated for its efficacy and complication reducing effect, identifying no significant effect within the 347 patients investigation (142). The first in man trial investigating the safety and efficacy of DLC coated cobalt-chromium stents in 40 patients with single vessel disease, revealed a restenosis incidence of 12.5% and repeat revascularisation in 15% (143). This trial was the

first evidence of feasibility and safety of these stents, although a thorough evaluation with a larger sample size is necessary (143). Continuing from this, a Japanese team compared the DLC coated cobalt-chromium stents to conventional BMS, reporting non-inferiority of this stent compared to conventional BMS (n=100) (144).

1.7 Ideal stent characteristics

The ideal stent should consist of two important characteristics: structural and surface characteristics. The structural characteristics would need to be robust scaffolds, able to withstand high stress/strain environments of coronary arteries as well as exhibiting the optimum strut design/shape that promotes optimum and smooth haemodynamic blood flow. The surface properties of a stent should exhibit low frictional wear to prevent resistance within the artery lumen, anti-thrombogenicity to avoid thrombosis and biocompatibility to evade inflammatory responses and a surface capable of allowing cellular viability /growth.

Since both the structural and surface characteristics are vital for stent design, there currently doesn't exist one material to combine both these characteristics; surface characteristics can be incorporated into already commercialised scaffolds that are known for their use in mainstay CAD therapy. These include BMS scaffolds that are also the substrate scaffolds for DES: Stainless steel, nitinol, cobalt chromium.

1.7.1 Structural characteristics

1.7.1.1 Stainless steel

Medical grade stainless steel, also known as 316L stainless steel, is predominantly used in medical implants, including orthopaedic implants. Its safety is widely known, although some reports of possible allergic reaction towards the nickel component (8.3-35%) within the alloy has been observed (145-147). Nickel as well as cobalt are allergens (147, 148). However, recently a novel and nickel-free stainless steel substitute has been developed for medical use (149). Metal ion release because of wear and corrosion have potential harmful effects which recruit inflammatory components and also have stent/ implant related complications, both due to nickel and chromium (149). However, there is a nickel component in all of the currently used coronary artery stent scaffolds including nitinol and cobalt chromium.

1.7.1.2 Nitinol

Nitinol includes a titanium and nickel alloy and is less frequently used, when comparing to stainless steel and cobalt chromium stent scaffolds. Like medical grade stainless steel, nitinol stents also have a nickel composition (45%), although reported to have the lowest nickel release and possibly superior to stainless steel though not clinically evident (146, 147, 150).

1.7.1.3 Cobalt chromium

Inflammatory response to cobalt even though less frequently reported, is also a possibility. In addition to also encompassing nickel (<0.5%), although at lower proportion than stainless steel and Nitinol (147, 148). Cobalt chromium is expensive and less frequently used although its incorporation into medical implants is now increasing (149, 151).

In summary, the metallic coronary stents currently available have not shown to be different in their clinical performance, even though animal studies have reported their superiority over each other e.g., nitinol over stainless steel (151). Stainless steel 316L continues to be used as is considered cheaper than the other alloys coronary stents.

1.7.2 Surface characteristics

As discussed above, in addition to structural characteristics, surface characteristics too are crucial influencers of coronary artery stent performance and are possibly the main contributors to stent related complications. One of the main methods to incorporate the ideal surface characteristics onto the structurally robust metallic stent is by coating the stent with a material capable of exhibiting all the relevant surface properties: anti-corrosive, smooth, flexible, low frictional wear, anti-thrombogenic and biocompatible. All these properties have been attributed to the 'wonder material' called graphene.

1.8 Graphene and its properties

Graphene (Gr) is a 2-dimensional (2d) crystal, i.e. a crystal whose lateral extension is well larger than its thickness. Indeed, graphene is just one atom thick layer of graphite, i.e. a carbon monolayer with atoms structured in a hexagonal arrangement (Fig. 1.6a). Attempts to isolate graphene monolayers were made for many years, however it was only in 2004 that Geim and Novoselov managed to extract a single layer of graphene by micro-mechanical exfoliation of graphite (more commonly known as "the scotch-tape method") (152, 153).

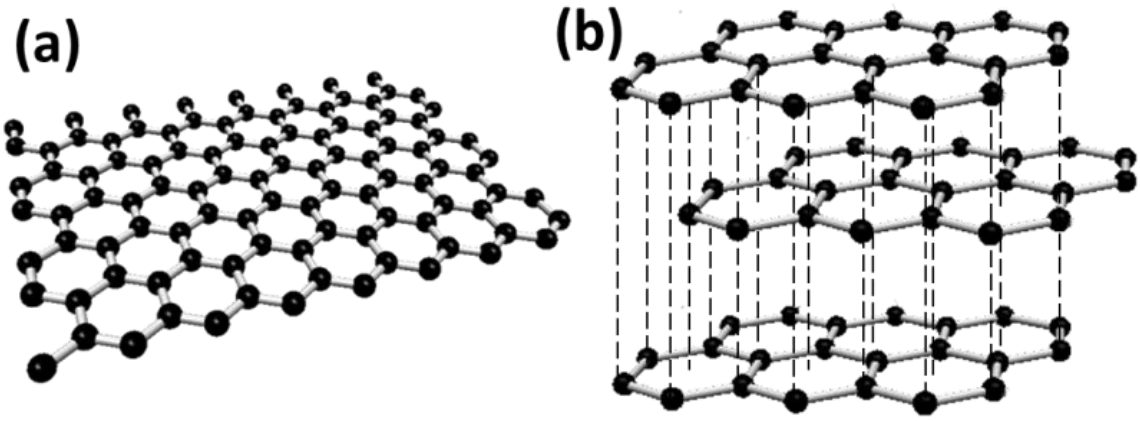

Figure 1.6: Structural comparison of graphene and graphite. a: Graphene and **b:** Graphite crystal structure. Graphene is a single layer of graphite (154).

Graphene is structurally similar to graphite: Graphite consists of several layers of graphene stacked on top of each other (Fig. 1.6b) (155), whereas the atomic arrangement of the carbon atoms in the plane remain the same (Fig. 1.6a). Despite the similar structure, the properties of graphene are very different from those of graphite: it is well known that the electronic and optical properties of a material are strongly influenced by its size and dimensionality (156). Graphene has unique properties, which are not observed in any other materials. The following are some of the outstanding and unique properties that make graphene such an interesting and exciting material:

- Strongest material ever measured (157)
- Low density, light material ideal for many engineering properties (158)
- Large surface to volume ratio, ideal for coating (158)
- Its atomic thickness makes graphene “flexible”, i.e. it can be bent and rolled (159)
- Impermeable to every gas, which promotes its anti-corrosive properties (160)

Due to its 2d nature, graphene is very sensitive to the environment and this property can be exploited to functionalise graphene (161). Functionalisation of graphene can enable a significant change in the properties of the material; the surface properties can be altered from super hydrophobic to super hydrophilic depending on the type of functionalisation (162, 163). One of the most used forms of functionalised graphene is graphene oxide (GO), which is widely used for biological applications and will be discussed in the following section. These, along with some of the other characteristics of graphene render it an ideal material for coating; smooth, anti-corrosive, flexible and strong.

Blood contains high electrolyte levels, causing higher rate of corrosion of metallic coronary stents (164). This highlights the importance of establishing an anti-corrosive surface for coronary stents. The properties of graphene to act as a protective membrane against corrosion has an important application in protecting against metal leaching of the metallic coronary stent that may induce an inflammatory response (148, 160).

The biologically inert quality of graphene is essential, as it has the potential to evade reactivity of the graphene-biomaterial to the tissue and fluids exposed to it. Since the biomaterials would be exposed to high shear strength and reactivity from surrounding tissue, it is important for any biomaterial to possess excellent anti-corrosive, anti-wear, and frictional qualities, characteristics exhibited by graphene (160, 165).

1.9 Graphene Oxide and its properties

Graphene oxide is a derivative of graphene. Oxidised graphene consists of epoxy and hydroxyl groups on the basal plane, as well as hydroxyl and carboxyl groups on the edge of the graphene sheet, rendering the material more hydrophilic (Fig. 1.7) as compared to graphene. As the structure of graphene is disrupted by the presence of the functional groups, GO has very different properties, compared to graphene. For example, graphene is metallic (i.e. it conducts electricity very well), while GO is an insulator (i.e. it does not conduct electricity, similar to diamond). The presence of the C-O groups makes GO also dispersible in water, while graphene is insoluble in water. Some of the appealing properties of GO are:

- Anti-bacterial characteristics (166)
- Amphiphilic , consists of hydrophilic and hydrophobic region on the flake (167)
- Improved wettability and surface activity of GO coated surfaces (167)
- Wide use for biomedical applications (168, 169).

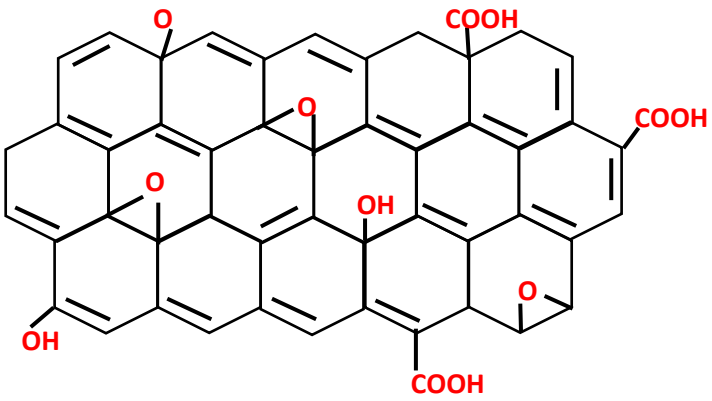

Figure 1.7: Structure of graphene oxide. Typically, the basal plane is decorated with epoxy and hydroxyl groups and the edges with carboxyl and hydroxyl groups.

1.10 Synthesis of graphene

By definition, graphene is a single layer of graphene. However, this material can be fabricated by different methods (Fig. 1.8), providing different types of graphene, in term of size, defects, thickness etc. Consequently, there is a family of graphene-based materials, characterised by varying number of layers, type and amount of defects and functional groups (158).

The highest quality material (necessary for electronic devices) is produced by micro-mechanical exfoliation; the first technique used to isolate graphene. However, this method is time consuming and not compatible with industrial needs. Therefore, novel methods have been developed for graphene production: Liquid phase exfoliation (LPE) (170); Chemical vapour deposition (CVD) (171, 172); Growth on SiC (173); and molecular assembly (174) (Fig. 1.8).

There are two main categories to manufacture graphene-based materials; the top-down approach and the bottom-up approach. The top-down approach consists of production of single layer graphene flakes from the large bulk graphite material, so from large material to very small material, whereas the bottom-up method is the reverse and describes the production of graphene from small nanosized entities e.g. self-assembly of aromatic molecules. Examples of top-down approach include LPE, mechanical exfoliation ('scotch tape' method) and bottom-up examples include CVD and growth on SiC (175).

The graphene and graphene oxide used in this work are both prepared by LPE. This involves the breakdown from the bulk material, graphite or graphite oxide, into the single or few layered graphene or graphene oxide, respectively.

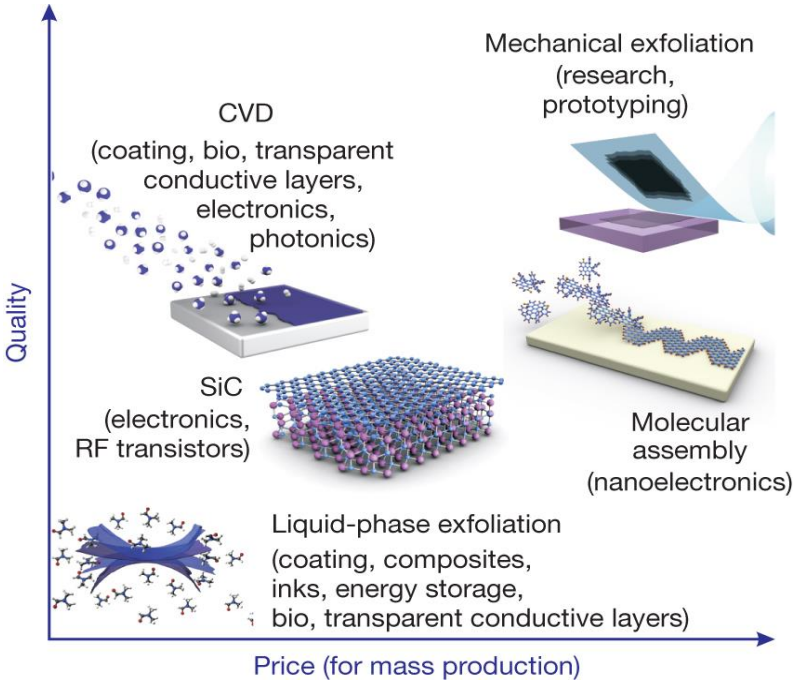

Figure 1.8: Graphene production methods. There are several methods of mass-production, yielding a range of flake size, quality and price for any particular application (158).

Table 1.2: Graphene manufacture techniques and their resulting graphene features.

Graphene production methods	Graphene layers	Quality	Yield	Cost	Ref
Liquid phase exfoliation	Single and few (< 10 layers)	Medium	Medium	Low	(176, 177)
Micromechanical exfoliation	Single and few (<10 layers)	High	Low	Low	(178)
Chemical vapour deposition	Single	High	Low	Medium-High	(179, 180)
Growth on SiC	Single	High	Low	High	(181)

The LPE method also offers a cost-effective, good quality and relatively high yield approach of achieving graphene flakes in solution (Table 1.2). Furthermore, this technique allows preparation of graphene coating onto a substrate by using simple methods such as drop casting, spray and dip-coating (158). In addition, the properties of graphene flakes in dispersions are tuneable, so they can be easily functionalised or can be mixed with polymers to change their properties. Table 1.2 provides a comparison of LPE

with alternative techniques. Since LPE is the graphene production method of choice, the next paragraph provides a short background on LPE.

1.10.1 Liquid phase exfoliation

Liquid phase exfoliation (LPE) is based on the exfoliation of graphite in a solvent (170). In the case of graphene, the starting material is graphite, which is sonicated in a bath sonicator for several days. As graphite is not soluble in water, the sonication is performed in an organic solvent, typically 1-methyl-2-pyrrolidinone (NMP). The energy released in the sonication is used to break the van der Waals forces between the graphene sheets, allowing exfoliation (182). Finally, centrifugation is used to remove the residual graphite. NMP has been shown to be an excellent solvent for LPE, i.e. enables exfoliation to be maximised, achieving the highest yield of graphene dispersed (170), as well as giving pristine graphene, i.e. free from functional groups. However, NMP is toxic and therefore cannot be used in this project. Nevertheless, the group of Prof. Casiraghi have developed a method, which allows the use of water as solvent, if a specific exfoliating agent is used (183). In this project the specific exfoliating agent used is a small aromatic molecule, in particular 1-pyrenesulfonic acid sodium salt (PS1). Graphene dispersions produced with this method typically contain <10 layer nanosheets and they are stable for several months (183). It is noteworthy that LPE cannot exfoliate all material, so there is a distribution of graphene flakes with different size and thickness, depending on the experimental conditions used for LPE. Therefore, it is very important to characterise the graphene dispersion, in order to check the size and thickness distribution, which can finally affect the properties of the graphene coating (Section 1.11).

An alternative way to produce graphene in water consists of functionalising graphite so the material turns from hydrophobic to hydrophilic. This is typically achieved by introducing oxygen-based groups, giving rise to GO. Brodie and Staudenmaier first introduced the method of preparing graphite oxide from graphite in the 19th century and the method was modified in 1957 by Hummer and Offerman (184-186). Graphene oxide production is typically performed using Hummer's method of adding strong acids and oxidising agents to graphite, however with the added multiple centrifugation and purification steps to maximally remove by-products and contaminants (168, 187). The graphite oxide produced in this way can be easily exfoliated in water, producing GO

dispersions. In contrast to the previous method, the dispersion contains 100% single layer GO (188, 189).

1.11 Rationale for studying graphene coated coronary artery stents.

The benefits and disadvantages of each CAD intervention has been summarised in Table 1.1. This reveals the ever-present associated complications from each intervention and the continued requirement for improved CAD therapeutic strategies. A complication-free coronary artery stent may be achieved by the design of a stent that incorporates the properties of an 'ideal material stent'.

The ideal coronary artery stent should demonstrate non-thrombogenicity, non-inflammatory and biocompatible properties that also aid undisturbed blood flow (smooth surface) and promote vascular healing (134). The predominant complication of stents is the stent surface that may raise the risk to restenosis and thrombosis. These complications could be overcome by modifying stent surface characteristics by coating with a material such as graphene. This may then have the potential of entirely eliminating or significantly lowering the risk of in-stent restenosis and late stent thrombosis as well as removing the necessity of long-term dual anti-platelet therapy; therefore, significantly reducing the cost of endovascular CAD intervention.

1.11.1 Bio-compatibility of graphene and previous use as a biomedical coating

Graphene bio-compatibility has been studied in a range of studies, but not as a coating and more frequently as the graphene derivative, GO. Cell survival, specifically myeloma RPMI 8226 cells, has been reported to be compromised by addition of GO flakes into *in-vitro* culture, a dose-dependent low cytotoxicity was noted and believed to be closely associated to oxidative stress that is implicated and further being studied for its possible application in the treatment of cancer (190, 191).

On the other hand, others in the literature have confirmed the safety of graphene and graphene oxide as a material of low toxicity and capable of sustaining cell adhesion and growth (192-195). To determine graphene coating as a potential in orthopaedic implants, Aryaei *et al.* investigated the adhesion and proliferation of osteoblast cells on these coatings and found an enhanced adhesion and proliferation of these osteoblast cells on the graphene coating.

Podila and colleagues were the only group to specifically investigate the potential of graphene as a coating on coronary artery stents until a very recent publication by Wawrzyńska *et al.* (196, 197), published during the current study. Both achieved coating by CVD, with Podila coating nitinol substrate and Wawrzyńska coating medical grade stainless steel discs (196, 197). This was followed by *in-vitro* tests to determine initial bio- and haemo- compatibility. Graphene coating was observed to support improved EC and SMC adhesion as well as proliferation, in addition to validating its durability in withstanding wear and tear (196, 197). Charge transfer between the exposed material and fibrinogen is necessary for platelet activation and can lead to coagulation cascade induction. Spectroscopic measurements revealed no transfer of charge between graphene and fibrinogen, implicating the capability of the graphene coating to inhibit platelet activation on its surface, thus suggesting reduced or the lack of surface thrombogenicity, a characteristic of an ideal medical implant (196). This also has potential merit in tackling late stent thrombosis observed in DES. The aforementioned studies demonstrate the compatibility of graphene as a coating to support cell viability, adhesion and proliferation and suggest it as an ideal material for coating biomedical implants (194, 196-198).

As a coating, graphene has not been associated with toxicity; however, additional investigations are necessary to assure safety, haemo- / bio- compatibility of graphene as well as its efficacy as a coronary artery stent. The efficacy and safety requires validation in the large animal prior to translating into humans.

The study conducted by Podila and colleagues achieved stent coating by CVD, which may pose difficulty in up-scaling the process. Additionally, the substrate used was a nitinol BMS, and the trial was not evaluated for its efficacy as coronary stent, as well as tissue response, i.e. *ex vivo* or *in-vivo* performance.

1.11.2 Why Graphene as a coronary stent coating?

Graphene exhibits many of the characteristics associated to an ideal medical implant coating. It is a monolayer sheet that exhibits an atomically smooth surface, crucial for smooth and unhindered stream of blood flow past the coronary stent, a property believed to impact thrombosis. Graphene has also been reported to exhibit antibacterial qualities (199), an appealing and useful property for a medical implant. Since graphene has been reported to be impermeable to gases, including even Helium, studies have

proved graphene coating to significantly improve corrosion at non-medical settings (165, 200). This may translate to the inhibition of metal leaching from the implant, that may thus lead to reduced inflammatory response and smoother implant surface (168, 201). Coating describes the coverage of the substrate material with another, more biocompatible material to achieve more desirous results, particularly in terms of coronary artery restenosis, a complaint of bare metal stent implants.

Reports of its ability to support endothelial cell adhesion and growth have added to its appeal as a coronary artery stent coating (196, 197). Since the coronary stent would be exposed to shear stress, it is important that the coating is well-adherent and not at risk of tearing off and traveling downstream of the stent locale. Nonetheless, this highlights the importance of assuring the safety of the stent adherent material. Moreover, its relatively inert quality unless in very potent environments, make it a likely safe material to use *in-vivo.*

1.12 Aim of this project

All previous literature exploring the applicability of graphene as a coronary artery stent coating have been undertaken via the CVD graphene preparation and coating methods followed by *in-vitro* investigations. We propose the use of the more scalable graphene manufacture, LPE, to establish a coating method followed by both *in-vitro* and *ex-vivo* investigations to determine biological implications in relation to cell adhesion/ proliferation and neointimal formation, respectively.

This study aims to explore the efficacy of a graphene and graphene oxide coated stent in enhancing coronary artery endothelial cell adhesion and proliferation as well as its efficacy in suppressing neointimal hyperplasia that is indicative of restenosis. However, first the stent has to be coated and the approach for this needs to be identified and optimised. LPE graphene coating of coronary artery stents will be investigated and both *in-vitro* and porcine *ex-vivo* performance of the stents explored, this has not yet been reported in literature. The more currently popular BMS, stainless steel (GAZELLE) and cobalt-chromium (CHROMA) coronary artery stents, will be utilised as a substrate to prepare a Gr/GO coating protocol. However, due to its lower price and its dominance within the BMS field, stainless steel scaffold will be the predominant stent use for coating and the main investigations. Where the cobalt-chromium acts as an additional uncoated control.

Hypothesis:

Graphene coating of coronary artery stents provides a novel, biocompatible (nontoxic to cells) and enhanced design with significantly reduced neointimal thickness associated with currently available stents.

Project objectives:

1. To formulate stable and biocompatible graphene and graphene oxide dispersions.
2. To develop a protocol to uniformly and thinly coat BMS (GAZELLE) with maximal coverage of graphene and GO.
3. To determine biocompatibility of Gr/GO coated GAZELLE stents through studying human coronary artery endothelial cell adhesion and growth by *in vitro* investigation
4. To determine whether formation of neointimal hyperplasia is reduced *ex-vivo* in porcine coronary artery and aortic tissue cultured with Gr/GO coated stents.

Summary of literature study

It is evident that CAD is a significant contributor to worldwide mortality. Even though the interventional strategies of CABG, or stent implantation are effective in bypassing or widening the stenosed vessel, each treatment strategy poses a complication of vein graft failure or restenosis, in-stent restenosis, very late sent thrombosis that necessitate repeat re-vascularisation. The most effective intervention until the present day is DES which also require adjunct dual anti-platelet therapy. In an attempt to design a complication-free stent, we propose the incorporation of graphene onto bare metal stents. Graphene has been heralded the 'wonder material', as it exhibits biomedical implant ideal properties: Durable, strong, impermeable, flexible, bio- and haemo-compatible. It has potential to be the future of medical implants, particularly coronary artery stenting.

CHAPTER 2

Materials & Methods

2.1 Graphene/ Graphene Oxide preparation and characterisation

2.1.1 Graphene preparation

Graphene dispersions were prepared by liquid phase exfoliation. The traditional LPE method (170) is based on the use of organic solvents that are not suitable for biomedical application. Therefore, a modified version of LPE was used in this project, which is based on the use of an exfoliating agent soluble in water (183). These along with powdered graphite make up the sonication mix, which undergoes bath sonication and then centrifugation to remove un-exfoliated graphite. The graphene dispersions used in this study were prepared by Dr Daryl McManus of Prof Casiraghi's lab, at the University of Manchester. To stabilise the graphite into mono and few layered graphene sheets in water, the stabiliser 1-pyrene sulfonic acid sodium salt (PS1) was used. Pyrene displays hydrophobic characteristics that interact with the hydrophobic graphene surface, while the sulfonic group allows the agent to be soluble in water, thus allowing graphene flake distribution in water (183).

In order to prepare a 10 mL sonication mix, 3 $mgmL^{-1}$ graphite (Graphexel Ltd.) was dissolved in 10 mL distilled filtered H_2O along with 10 mg PS1 (SIGMA), acting as an exfoliator and stabiliser for graphene (to prevent restacking of graphene sheets) (182, 183). In order to break the graphene layers apart, this mixture was placed in a sonicator bath (Hilsonic) for 72 hours followed by centrifugation at 295g (SIGMA1-14K) for 20 minutes preserving the top layer; discarding sedimented and un-exfoliated graphite, and a further series of centrifugation steps at 106 g (20 minutes) to eliminate the rest of the PS1 in solution (Fig. 2.1). The end result is a grey-black dispersion that is reported to be stable for months (183).

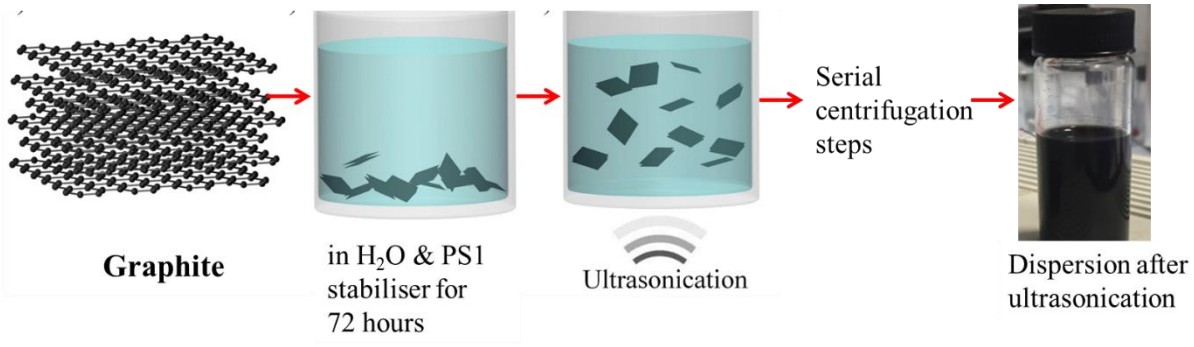

Figure 2.1: Schematic presentation of graphene dispersion production at the Casiraghi group laboratory. Adapted from (202).

2.1.2 Graphene Oxide preparation

The graphene oxide mixture used in the main investigations was prepared and provided by Prof Kostas Kostarelos's lab at the University of Manchester. The prepared graphene oxide was obtained by the modified Hummer's method described by Ali-Boucetta at Kostarelos lab (Fig. 2.2) (168).

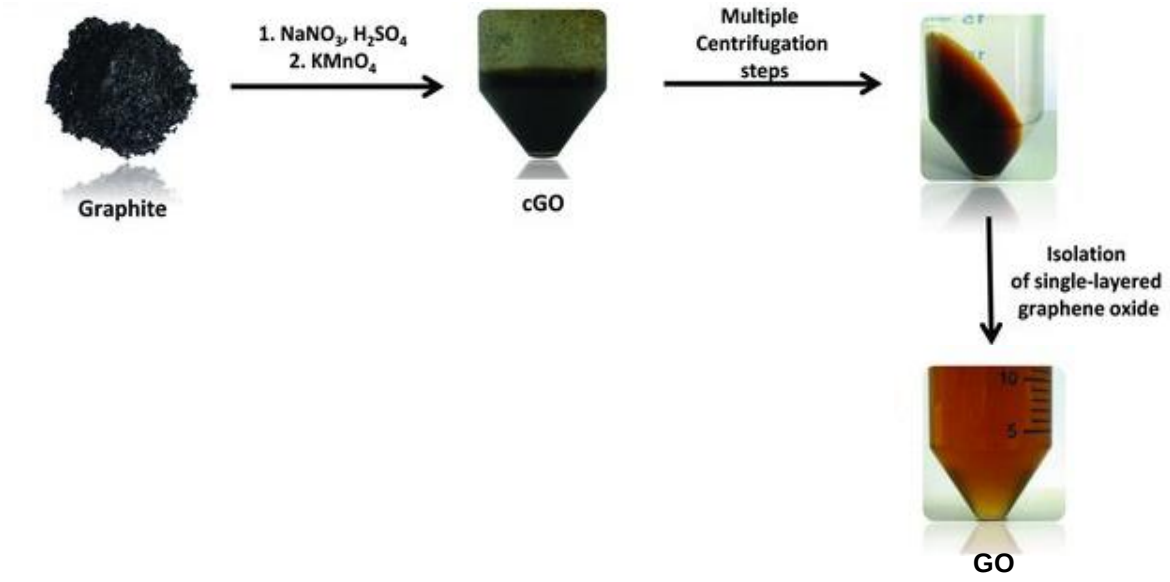

Figure 2.2: Schematic representation of the preparation of graphene oxide dispersions by the purified process and prepared by Prof Kostarelos's group. Adapted from (168)

2.1.3 Characterisation

2.1.3.1 UV-Vis Spectroscopy

The concentration of the resulting graphene or graphene oxide sample is measured by UV-Vis spectroscopy. To determine the concentration of LPE graphene, the absorbance of the 1:300 diluted graphene dispersion, prepared as described in section 2.1.1, was

measured using the Agilent Technologies Cary 5000 UV-VIS-NIR Spectrophotometer. The absorbance of distilled filtered water and the diluted graphene dispersion at 660nm was determined and subtracted from each other. Subsequently, the absorbance coefficient of 2460 $Lg^{-1}m^{-1}$, for graphene, input into the formula to calculate concentration using the Lambert-Beer law (203).

$$A = \alpha c\mathrm{l}$$

Where A is the optical absorbance of light, α is the molar absorption coefficient, which for graphene equates to 2460 $Lg^{-1}m^{-1}$, when measured at 660 nm (170), c is the sample concentration and L is the distance travelled by the light travels, i.e. the size of the cuvette (0.01m).

2.1.3.2 Raman Spectroscopy

The samples were prepared by drop-casting of the diluted graphene dispersions (~0.05 $mgmL^{-1}$) onto a smooth and flat silicon wafer chips. The substrate typically used is silicon wafer covered with a SiO_2 layer (IDB Technologies Ltd.), which is first cleaned by 15 minute sonication in acetone solution, followed by another 15 minute sonication in propan-2-ol. After drop casting, the silicon substrate is left overnight at room temperature to allow solvent evaporation, allowing the flakes to be analysed.

Raman spectroscopy measurements were performed using the WIRE 3.4 (Renishaw,2002) software connected to a Renishaw Invia Raman spectrometer, equipped with a 514.5 nm excitation laser and 1.0-2.0 mW laser power. Measurements were performed using a 100x NA0.85 objective lens and 2400 grooves/mm grating. 50 random flakes were analysed and recorded for each sample. The spectra were fitted using a home-made programme in MATLAB R2015a (Appendix I): the fit allows to qualitatively determine the thickness distribution in the samples (Section 3.1.2). Lorentzian distribution was fitted onto the spectra and coefficient of determination (R^2) value determined on the MATLAB software. The 2D shape and R^2 value enabled identification of graphene flake layer thickness.

Raman spectroscopy can also be used to collect a point by point sequential measurements at a selected interval distance (0.5 μm) within a selected area of interest. This mode of Raman spectroscopy is known as Raman mapping which allows for examination of an area of interest and for the objectives of this project, it is an ideal tool to inspect substrate surface coating coverage.

2.1.3.3 Atomic Force Microscopy (AFM)

Samples for AFM measurements were prepared following the same sample preparation protocol used for Raman spectroscopy. The MultiMode 8 Bruker Atomic force microscope was utilised to examine lateral size and thickness distribution of the graphene flakes. Tapping air mode option at a scan size of 10 μm and 2560 samples per line at a speed of 1.5 Hz was selected. Nanoscope VI controller, Nanoscope v614r1 control software (Veeco, Cambridge, UK) and a silicon tapping tip (NSG01, NTI-Europe, Apeldoorn, The Netherlands) of 10 nm curvature radius, mounted on a tapping mode silicon cantilever with a typical resonance frequency 283–374 kHz and a force constant of 12–103 N/m (Bruker OTESPA, UK). NanoScope Analysis was utilised to measure height (corresponding to thickness of flakes) and length of the flakes. Number of layers of each flake was estimated by dividing measured height of each flake by the graphene interlayer distance (0.347 nm in pristine graphene) (178). Similar method was also conducted for GO characterisation by Prof Kostarelos's group (~0.8nm in a single layer of GO) (204). Note however that this type of protocol is only qualitative: as an exfoliating agent is used in water to prepare graphene dispersions, the thickness of a single layer is likely to be higher than the nominal thickness of graphene. Thus, AFM does not provide reliable values for graphene thickness measurements, and here it is mainly used to get information on the lateral size of the flakes.

2.2 Selection and Optimisation of Coating Deposition Technique

2.2.1 Stainless steel disc coating with LPE graphene based dispersion

Once graphene and graphene oxide LPE dispersions were prepared and characterised, the next step was to establish a coating technique of the LPE graphene based materials onto medical grade (316L) stainless steel substrates. Initial testing was undertaken on 316L medical grade stainless steel discs prior to optimisation for use on the end product, stainless steel coronary artery stents.

2.2.1.1 Preparing 316L stainless steel discs for coating

Medical grade 316L stainless steel was utilised as a substrate for graphene coating and cell experimentation, as this is the material of coronary artery bare metal stents. The 316L stainless steel (SS) substrates were specifically manufactured to fit into the wells of 24-well plates, necessary for cell culture experiments. Discs were manufactured at 14 mm diameter, 0.474 mm thickness by punching holes into 316L SS sheets (Smiths Metal

Centres Ltd, UK). This resulted in smooth edged discs that fit into the bottom of each well of 24-well cell culture plates (Corning® Costar®, NY, USA). However, due to unknown finish of the stainless steel sheets used on the discs and on stents, which can influence hydrophilic nature of the substrate, discs were only used to determine coating technique to use.

The discs were cleaned in a SONIC 3D professional ultrasonic cleaner (James products Europe, Power 120 w and wavelength 40 KHz) in two steps. First, discs were submerged in 100% acetone (Fischer Chemical, UK) and sonicated for 15 mins to degrease the discs followed by another 15 minutes sonication in propan-2-ol (Fisher Chemical) to remove ionic contamination. The cleaning step was finalised by rinsing discs in distilled H_2O and allowed to air-dry (1-2 days). Next, discs were double wrapped in aluminium foil to heat sterilise at 180˚C for 30 minutes.

2.2.1.2 Gr/GO dip-coating of 316L stainless steel discs

The initial aim was to determine if adequate coverage of stainless steel discs was established with simple dip-coating methods. The discs were dipped into 0.33 $mgmL^{-1}$ of Graphene, 0.5 $mgmL^{-1}$ of graphene oxide dispersions for 5 seconds – 25 hours. Annealing of Gr/GO onto the stainless steel disc was achieved by evaporating solvent with dipped disc on a hotplate; initially at 70 °C for 15 mins followed by overnight evaporation at 40°C. Since adequate coating was not achieved via this simple procedure, the method was improved via the application of a voltage bias.

2.2.1.3 Graphene dip-coating of discs with simultaneously applied bias voltage

Pre-cleaned stainless steel 316L discs were prepared as described in section 2.2.1.1 and attached onto a positively charged crocodile clip and partially dipped into a negatively charged 0.3 $mgmL^{-1}$ graphene dispersion (Fig. 2.3). The discs were partially immersed into the graphene dispersion and the power source at first set using a 9V button battery. Following from this, the power source was set at 50V-200V and 1-15mA. To determine the optimal settings for producing relatively uniform graphene coating, three factors were investigated: Voltage, dipping duration and dipping frequency.

To test effect of varying voltage, 316L SS discs were partially immersed in 0.3 $mgmL^{-1}$ graphene dispersion for 20 seconds when 50V, 100V and 200V was reached. To explore influence of time or duration once partially immersed, discs were removed 20, 40 and 60

seconds after 50V was reached. Finally, in order to determine if frequent dipping improved coating, one disc was partially dipped one time for 20 seconds duration, starting the timer once 50V was reached, and another disc partially dipped four times with each dipping lasting 5 seconds (5 seconds from the time 50V was reached on the power source). Immediately after the above-mentioned coating strategies, discs were transferred onto a hotplate set at 70°C for 15 mins followed by overnight evaporation at 40°C to enable annealing of coating materials and substrate.

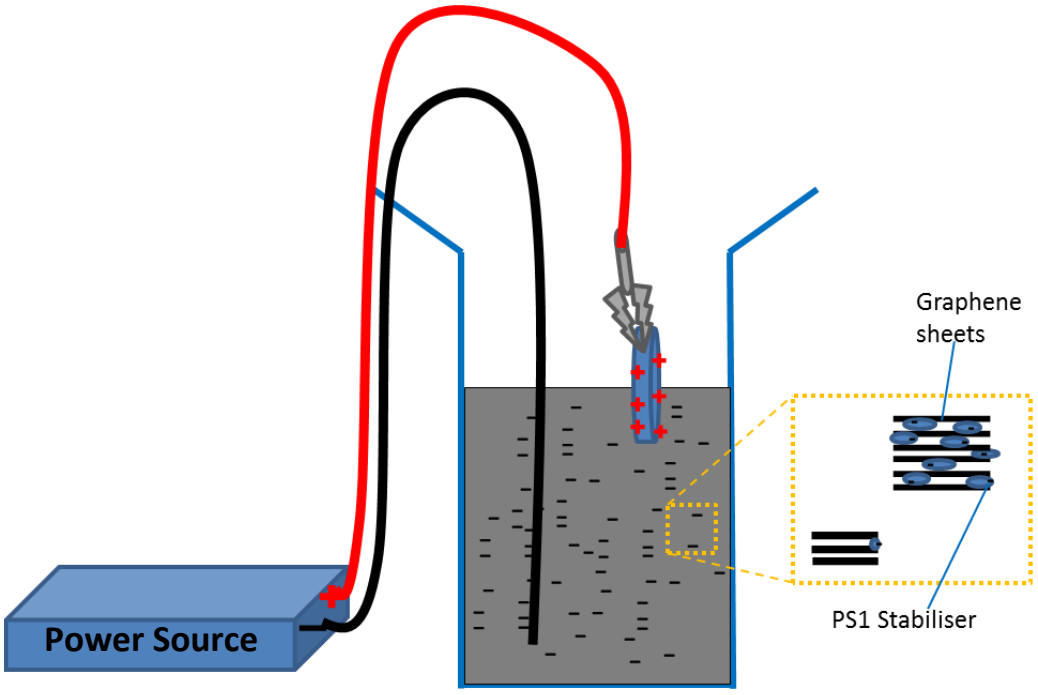

Figure 2.3: **Schematic representation of dip-coating of stainless steel discs with graphene using simultaneous bias voltage set-up.** The negatively charged 1-pyrenesulfonic acid sodium salt (PS1) as a stabiliser of graphene illustrated as wedged between the graphene sheets allows adhesion/ attraction of graphene sheets onto the positively charged stainless steel discs, enabling improved coating. Only voltage was adjusted between 50 V- 200V using power source, while current varied automatically depending on resistance and voltage set. Current at the voltage settings above ranged between 1-15 mA.

2.2.1.4 Graphene spray-coating of 316L stainless steel discs

Spray coating was introduced as a method to achieve thin and uniform coating. Figure 2.4 illustrates the set-up for spray coating. Stainless steel discs are positioned on the 75°C set hotplate, directly under a spray gun (distance of 20 cm). An initial attempt involved spraying 100 µl of 0.4 $mgmL^{-1}$ graphene dispersion onto the 316L stainless steel disc. This

was repeated another four times onto the same stainless steel disc, but with 90˚ rotation in the x-axis to spray from different orientation resulting in layers of spray coating. Simultaneous heating of the disc allowed for simultaneous annealing of the graphene onto the disc. Thickness of the graphene coating is controlled by spray time, concentration and volume of dispersion sprayed, in this case once all of the 4 x 100 µL dispersion of 0.4 mgmL^{-1} graphene/GO was sprayed (205).

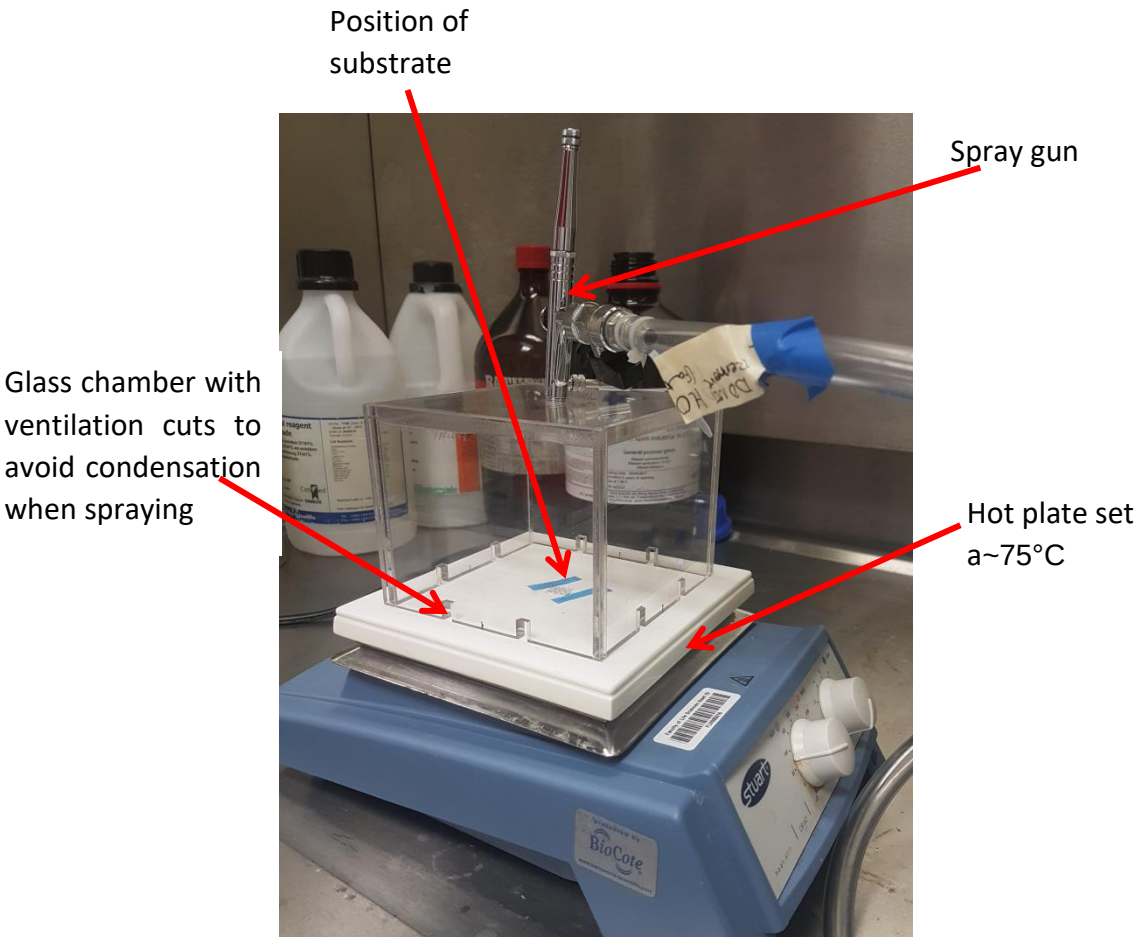

Figure 2.4: Spay coating apparatus used for coating stainless steel stents. Spray gun releases a total of 400 µl of 0.4 mgmL^{-1} Gr/GO dispersion onto approx. 12mm x 12mm stent surface. Immediate annealing achieved with simultaneous heating of the stent at ~75°C (hotplate).

Coverage of coating was examined under the upright Nikon Eclipse LV100 microscope and images acquired using the attached Nikon TV lens 0.55x Ds camera.

2.2.2 Coating GAZELLE stainless steel bare metal stents

Once the technique that produced the most uniform, thin coating with maximal substrate coverage was selected, it required testing on the project related main substrate, stainless steel GAZELLE coronary artery stents.

2.2.2.1 Preparing stent surface for coating

Gazelle stainless steel stents (size 3.0mm x 24mm) donated by Biosensors International were expanded by coronary balloon inflation followed by longitudinal cutting of the stent and flattening using fine forceps. Subsequently, the opened and flattened GAZELLE coronary artery stent, was cut in half to achieve two equally sized stent segments for spray coating. Next, the stent segment surfaces were cleared from surface contaminants/ impurities (natural contaminants such as hydrocarbons) by plasma cleaning under Argon (206). This was performed using the Pico PCCE low-pressure plasma system (Diener electronic GmbH + Co. KG) and set at 10% power, pressure controlled 0.1mbar pressure for a duration of 2 minutes.

2.2.2.2 Graphene spray-coating of 316L stainless steel stents

Figure 2.4 illustrates the set-up for spray coating. GAZELLE stainless steel stents were positioned on the ~75°C set hotplate, directly under a spray gun at a distance of 10 cm and coated within a glass chamber (Fig. 2.4). Short spray intervals and drying time were undertaken with 90° hotplate/stent rotation (x-axis) every 100 µL of 0.4 $mgmL^{-1}$ Gr/GO dispersion sprayed. A total of 400 µL dispersion was sprayed onto the stent for a total duration of 70-80 minutes before leaving on the hotplate for another 10-15 minutes to anneal coating onto stents. In order to mimic exactly the same conditions on the uncoated control stent segments, control stent segments underwent the same conditions of coating but using 400 µL of distilled water (dH_2O) for spraying. Throughout this project, dH_2O sprayed stents will be referred as 'uncoated' stents. Simultaneous heating of the stent allowed for simultaneous annealing of the graphene onto the stent. Thickness of the graphene coating was controlled by dispersion concentration, volume and spray duration, in this case once all of dispersion was sprayed within a timed duration. Coverage of coating was examined by Raman spectroscopy mapping.

Optimal coating methods were investigated by changing the following parameters:

1. WITH versus WITHOUT Plasma cleaning using argon gas prior to coating.
2. 10 cm versus 20 cm spraying distance (glass chamber designed at height of either 10 cm or 20 cm).

2.2.3 Examination of the Graphene or Graphene Oxide coating

2.2.3.1 Raman mapping to examine coating coverage

The coverage of graphene and graphene oxide coating on the stent was examined by Raman spectroscopy mapping. As with Raman spectroscopy to characterise the graphene flake (detailed description at 2.2.2), the coating involves using the same settings to evaluate a selected segment of stent area, μm^2, to determine Raman spectra at each 0.5 µm interval. To illustrate the presence of graphene or graphene oxide, the mapped area was analysed using the WIRE 3.4 software (Renishaw) and three points of the mapped area selected to present the respective Raman spectra results using the OriginPro 8.5.1 SR2 software (USA).

As explained in section 2.2.2, a desired area of the coated disc or GAZELLE stent was selected for Raman mapping analysis. This involved a Raman spectrum point by point by defining a step size of 0.5 µm. The software then fits and analyses all spectra by intensity to baseline, generating a map of the Raman fit parameters. In this case, we selected the 2D peak intensity as fingerprint of the presence of graphene, i.e. if the intensity of the peak located at 2700 cm^{-1} was zero, then no graphene was deposited. For graphene oxide, the G peak intensity was selected and analysed by signal to baseline between 1558.0 - 1617.0 cm^{-1}, since the 2D peak in GO is very weak. Essentially, the objective of the Raman spectroscopy mapping is to identify areas, if any, covered with graphene, which are associated to non-zero value on the map colour bar (Fig 2.5).

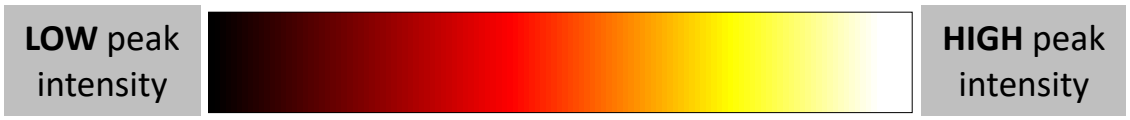

Figure 2.5: Raman spectroscopy mapping peak intensity illustration. Signal to Baseline 2D peak (graphene) G peak (graphene oxide) intensity. At BLACK colour, it represents the absence of coating while with increasing brightness the intensity (on Raman spectrum) of coating increases.

2.2.3.1.1 Calculating percentage coating coverage

Coating coverage was assessed by calculating percentage graphene or graphene oxide coverage. Each mapping point in the mapped region was analysed for Gr/GO corresponding fingerprint peaks (see above). The number of points containing the Gr/GO signature peaks was calculated over the total number of points mapped. This was demonstrated as percentage coverage.

2.2.3.2 Adherence of graphene/graphene oxide coating

To determine how well the coating remains on the stent, Raman mapping was performed after seven days of rigorous agitation on shaker immersed in cell media. The effluent media too was investigated by Raman spectroscopy by drop-casting onto a clean SiO_2 wafer to determine if any Gr/GO was washed off the stent into the effluent media.

Similarly, the coated stents incubated with porcine aortic tissue in media for a duration of 14 days (see chapter 6) were also examined by Raman spectroscopy to investigate if any coating had been removed.

2.2.3.3 Stent sterilisation by ultraviolet radiation

Stents whether Gr/GO coated or uncoated were positioned 14 cm directly under 5x 8Watts 254nm ultraviolet lamps for duration of 4 minutes, to sterilise the stents for tissue culture. The effect of UV sterilisation on the integrity of the graphene and the graphene oxide coated stents was investigated, again by Raman spectroscopy mapping using 50x NA0.85 objective lens and 2400 grooves/mm grating and laser at 514nm wavelength.

2.2.3.4 Scanning Electron Microscopy (SCEM)

Stents coated with graphene and graphene oxide were gold sputter coated with a thin gold layer to make them conductive for visualisation under SCEM (Quorum Technologies, SC7620, Sputter Coater). The Quanta 250 FEG scanning electron microscope (Quanta 250 FEG) was operated in vacuum at 5.0 kV and 20.0 kV to view coating of the stent.

2.3 Human coronary artery endothelial cell culture on Gr/GO coated GAZELLE coronary artery stents

In order to determine coronary artery cell adhesion and proliferation on stainless steel GAZELLE coronary artery stents, flat-opened stent segments were spray coated using either LPE graphene (400 µL of 0.4 $mgmL^{-1}$), graphene oxide (400 µL of 0.4 $mgmL^{-1}$), or dH_2O (400 µL as control), see detailed description on section 2.2.2. Human coronary artery endothelial cells (HCAEC) were selected due to their relevance to this study and their direct contact to coronary artery stents.

2.3.1 Endothelial cell culture

Aseptic technique was used to conduct all cell culture handling under a Class II laminar flow cabinet. Proliferating human coronary artery endothelial cells (HCAEC-p, C-1222, PromoCell) arrived within a T25 flask (25 cm^3) at passage number 2 and were incubated at

37°C and 5% CO_2 until 70-80% cell confluency was reached. Human coronary artery endothelial cells were obtained with informed consent from donor legal agent and ethical approval according to the human tissue act (details of consent/approval can be found at www.promocell.com/about-us/ethical-standards/). The cell donor demographic: Female, Caucasian and 40 years of age. HCAECs (PromoCell GmbH, Heidelberg, Germany) were maintained in endothelial cell growth medium MV (microvascular vessel) supplemented with Supplement Mix (Basal Medium) (PromoCell, Heidelberg Germany) and incubated at 37°C and 5% CO_2 until 70-80% confluency was reached. Next, the cells were split until passage 4, following which cells were either cryofreezed (section 2.3.1.3) for later use or used for proliferation experiment outlined below.

2.3.1.1 Endothelial Cell passaging

Once adequate confluency was reached, using aseptic technique, the media was removed and 0.1mL/cm^2 Hepes BSS (PromoCell GmbH) added and swirled (~30 secs) to wash the adherent HCAEC and to remove the remaining metabolic waste from the surface of the cells. Subsequently to removal of the Hepes BSS solution, cells were detached by incubation in 0.1mL/cm^2 Trypsin/EDTA (0.04%Trypsin/0.03%EDTA, PromoCell GmbH) at 37°C and 5% CO_2 for 3 minutes followed by gentle tapping to the sides of the flask to aid complete cell detachment. Cells were visualised under phase contrast microscope (OLYMPUS CKX41) to confirm cell detachment. Next, trypsin was neutralised with trypsin neutralising solution (TNS) (0.05% Trypsin Inhibitor, 0.1% BSA, PromoCell GmbH). This cell suspension mix was then transferred into a 50 mL falcon tube, balanced for centrifugation at 220g for 4 minutes in order to pellet the cells. The clear supernatant was removed, and cell pellet re-suspended in 1 mL endothelial cell growth medium MV supplemented with Supplement Mix (PromoCell, Heidelberg, Germany).

One third of the cell suspension was added to one T75 (75 cm^3) flask encompassing 18mL of pre-warmed (37 ˚C) supplemented endothelial cell growth medium MV to achieve cells at passage number 3. The above cell passaging was repeated to achieve cells at passage 4, ready for cryopreservation.

2.3.1.2 Cell count of detached endothelial cells

To determine number of live cells in the cell-suspension collected, 10µL of the cell suspension was pipetted onto a Neubauer glass haemocytometer, and cells within four small squares of the haemocytometer grid were counted under the phase contrast

microscope. Number of cells per mL of cell suspension was calculated by multiplying the average cell count per small square by 10^4.

2.3.1.3 Human coronary artery endothelial cell cryofreezing

Once cells were detached and centrifuged to achieve a cell pellet (section 2.3.1.1) it was re-suspended in cryo-SFM (PromoCell) at a density of 1-2x10^6 cells/mL. Subsequently, these were aliquoted in 1.5 mL volume into labelled cryovials and immediately transferred into Mr. Frosty Nalgene container encompassing isopropanol/ propan-2-ol and incubated overnight at -80˚C. This assured cells were cooled at a rate of 1˚C per minute, which is optimal for cell preservation. The next day, cryovials were transported for incubation in liquid nitrogen for long term storage.

2.3.2 Human coronary artery cell seeding onto coated/uncoated stents

Prior to culturing of the cells on the Gr/GO coated and uncoated GAZELLE stainless steel stents, both sides of the stent segments were sterilised as described above in section 2.2.3.3, and subsequently positioned flat at the base of the sterile and pre-resin embedded, 48-well tissue culture plate wells (Corning® Costar®, NY, USA). Each set experiment, required two 48-well plates, one 48-well plate for 1 day culture and one 48-well plate for 8 days culture, each compromising of three graphene coated, three graphene oxide coated and three 'uncoated' (dH_2O spray coated) GAZELLE stainless steel stents.

2.3.2.1 48-well tissue culture plate preparation

Under aseptic conditions, 10g of Sylgard 184 silicone elastomer (Dow Corning®) was mixed with 1g Sylgard 184 elastomer curing agent (Dow Corning®), followed by pouring into each well of the 48-well plate. Subsequently, the plates were incubated flat in an oven (40-50˚C) overnight, to minimise bubbles in the mix, followed by incubation at room temperature for another day, to allow resin to set completely. Once set, plates were UV sterilised, positioned 14 cm directly under 5x 8 Watts, 254nm ultraviolet lamps for duration of 4 minutes.

2.3.2.2 Experimental- human coronary artery endothelial cell seeding

Into each well with the positioned stents, 5000 HCAECs were seeded with 1mL supplemented endothelial cell growth medium MV (PromoCell) and incubated at 37°C and 5% CO_2 for 1 day and 8 days (media changed every other day) (Fig. 2.6). Day of cell

seeding was classed as day 0. After the required incubation period, cells were fixed and stained one day post cell seeding and 8 days post seeding, as described below. To observe the structure of the cells, cytoskeleton or specifically F-actin of the cells were stained using phalloidin and to enable cell counting, DNA was stained using 33342 Hoechst stains as described in section 2.3.2.4.

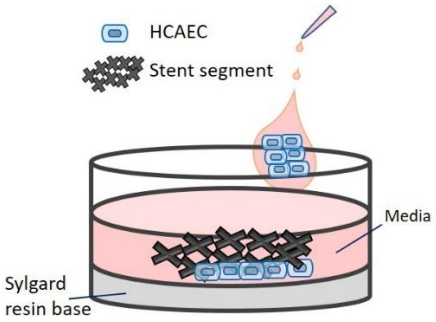

Figure 2.6: Schematic representation of the HCAEC culture set-up in each well.

2.3.2.3 Endothelial cell fixation post-culture

To avoid actin degradation, cells were fixed with freshly prepared 4% methanol-free formaldehyde solution (Thermo Scientific Pierce). At day 1 and day 8, each well was washed three times with chilled phosphate buffered saline (PBS) before and after incubating with 4% methanol-free formaldehyde for 15 minutes.

2.3.2.4 DNA and actin-f staining of endothelial cells

Post fixing, cells were permeabilised with 0.5% Triton X-100 (Sigma-Aldrich) for 5 minutes, followed by 3 x PBS washing steps. At this point, the stents were transferred into a dark, humidified chamber for the staining protocol. Non-specific binding was then blocked using 5% non-fat dry milk in PBS for 30 minutes followed by one wash step before adding pre-prepared 1:40 Phalloidin actin-f stain (PromoKine) and 1:2000 Hoechst 33342 DNA stain (life Technologies) mixed in 1% non-fat dry milk and PBS. Stents were incubated with the staining solution for 20 mins (Phalloidin), 35 minutes (Hoechst) in the dark, humidified chamber at room temperature. Subsequently, the stents were washed 2-3 times with PBS and viewed under fluorescent microscope (LEICA, DM5000 B).

2.3.2.5 Imaging & Counting of HCAEC on Gr/GO coated and uncoated GAZELLE coronary artery stent segments

Fluorescent images were viewed under a LEICA DM5000 B microscope and images acquired using the LEICA DFC 30000 G camera. The whole area of each stent was imaged by numerous visual field image acquisitions, in order to assure precise stent area measurement and cell counting. For each visual field, manual cell count (count of cell nucleus represented as blue spots on imaged stents) was undertaken in addition to stent area measurements (mm^2) by drawing around the stents on ImageJ (http://imagej.nih.gov/ij/). This was then utilised to calculate cell count per mm^2 area of stent.

2.3.2.6 Data Analysis

Data were expressed as mean ± standard error of the mean (SEM). Each triplicate experiment was undertaken three times, using cells from a single/same donor. Statistical analysis was performed to compare each group at Day 1 and Day 8 post-seeding: uncoated vs Gr coated; uncoated vs GO coated; Gr coated vs GO coated. Tukey's multiple comparisons test was performed on each group comparison using the PRISM GraphPad software. Statistical significance was illustrated as $p<0.05$ (*).

2.4 Ex Vivo Porcine Organ Culture to determine neointimal formation

2.4.1 Ex-vivo organ culture of porcine coronary artery and aorta

In order to determine neointimal formation prior to *in-vivo* work, organ culture of both the coronary artery and the aortas of commercial farm pigs (details in section 2.4.1.2) were undertaken. Hearts were collected approximately 15-20 minutes post-electrocution and aorta 20-40 minutes post electrocution. The duration from collection to culture ranged between 3.5-5 hours for coronary artery isolation and 2-4 hours for aortas.

2.4.1.1 Organ culture dish preparation

Sylgard 184 Silicone Elastomer was mixed with 10% (v/v) Sylgard 184 Silicone Elastomer Curing Agent (DOW Corning) and stirred thoroughly. The base of glass petri dishes was scored. Glass dishes of 50 mm and 75 mm diameter where half-filled with the mixture. To remove air bubbles, dishes were incubated in oven (40-50˚C) and allowed to set overnight. This base embedding allowed vascular tissue to be pinned onto the dish surface as well as the pinning of the stent onto the luminal surface of the aortic tissue.

2.4.1.2 Porcine animals used for organ culture

C.S Morphets & Sons Ltd. Abattoirs (Widnes) was used to collect porcine aortas (n=10) and hearts for coronary artery (n=4) isolations. The following were the demographic of the donor pigs.

Breed: Large White x Piétrain

Average age: 22-24 weeks

Approximate weight: 110 Kg

Sex: Mix of male and female

2.4.1.3 Organ transport solution

Organs were collected in cool (container stored on ice) 10mM PBS (constitutes 137 mM NaCl and 2.7 mM KCl) supplemented with Penicillin- Streptomycin at 200Units/mL, 200µg/mL, respectively (SIGMA Aldrich, P4333), Glutamine at 4mM (SIGMA, G7513) and Amphotericin at 5µg/mL (Gibco® Life Technologies, 15290-026). Heart and aorta were transported into University premises for isolation of coronary arteries and aortae.

2.4.1.4 Coronary artery isolation from porcine hearts

All organ culture steps were conducted within pre-UV sterilised Class II laminar flow cabinet. The left descending anterior coronary artery was harvested and the adventitia removed (Fig. 2.7). The coronary artery was cut longitudinally and pinned out onto a Sylgard filled glass petri dish with the lumen facing up and fresh/cold PBS transport solution added (Fig. 2.7). The coronary artery was cut into 6 segments for each experiment as is outlined in Table 2.1.

The experimental set-up for coronary artery organ culture is outlined in table 2.1. This study includes an additional stent, the CHROMA stent (Biosensors Int.), which is a newer bare metal stent supplied by Biosensors international and is a cobalt -chromium design. This was added to the later stages of the project as a contemporary BMS. The CHROMA and GAZELLE control stents were also coated with water as an additional control.

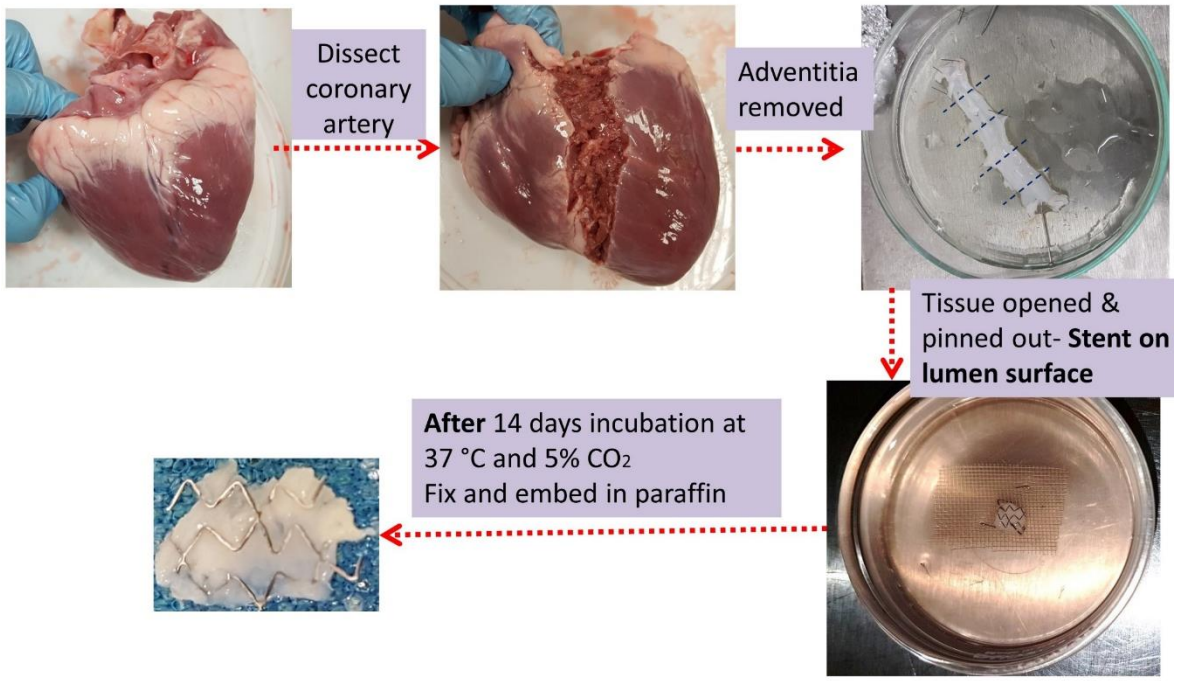

Figure 2.7: Step by step outline of porcine coronary artery isolation, stent deposition and organ culture.

Table 2.1: The experimental set-up for coronary artery organ culture.

Experimental group	**Description**
CoA- Day 0	Coronary artery segment fixed after isolation
CoA- Day 14	Coronary artery segment fixed after 14 days of tissue culture without stent
CoA- GAZELLE	Coronary artery segment fixed after 14 days of tissue co-culture with dH_2O spray coated GAZELLE stent segments
CoA- CHROMA	Coronary artery segment fixed after 14 days of tissue co-culture with dH_2O spray coated CHROMA stent segments
CoA- Graphene	Coronary artery segment fixed after 14 days of tissue co-culture with Graphene spray coated GAZELLE stent segments
CoA- Graphene Oxide	Coronary artery segment fixed after 14 days of tissue co-culture with Graphene Oxide spray coated GAZELLE stent segments

2.4.1.5 Isolation of porcine aorta

All organ culture steps were conducted within a pre-UV sterilised Class II laminar flow cabinet. All steps are outlined in figure 2.8. Adventitia around the aorta was removed using heat sterilised surgical tools. Prior to inducing balloon injury to the luminal wall of the thoracic aorta, the proximal end was cut away for fixing, as uninjured control day 0. Luminal wall injury was induced to the thoracic wall of the aorta using a 22mm balloon

inflatable catheter, inflated for a duration of 7 minutes. Following deflation of the aorta, aorta was opened longitudinally and cut into 7 segments (Table 2.2).

The experimental set-up for aorta organ culture is outlined in table 2.2. This investigation includes yet another additional stent, called everolimus eluting stent (Boston Scientific, PROMUS PREMIER^{TM}). EES is currently a commonly used stent with outstanding complication incidence (section 1.3.3.3) and was utilised in this study as a comparison of a stent likely to prevent neointimal hyperplasia.

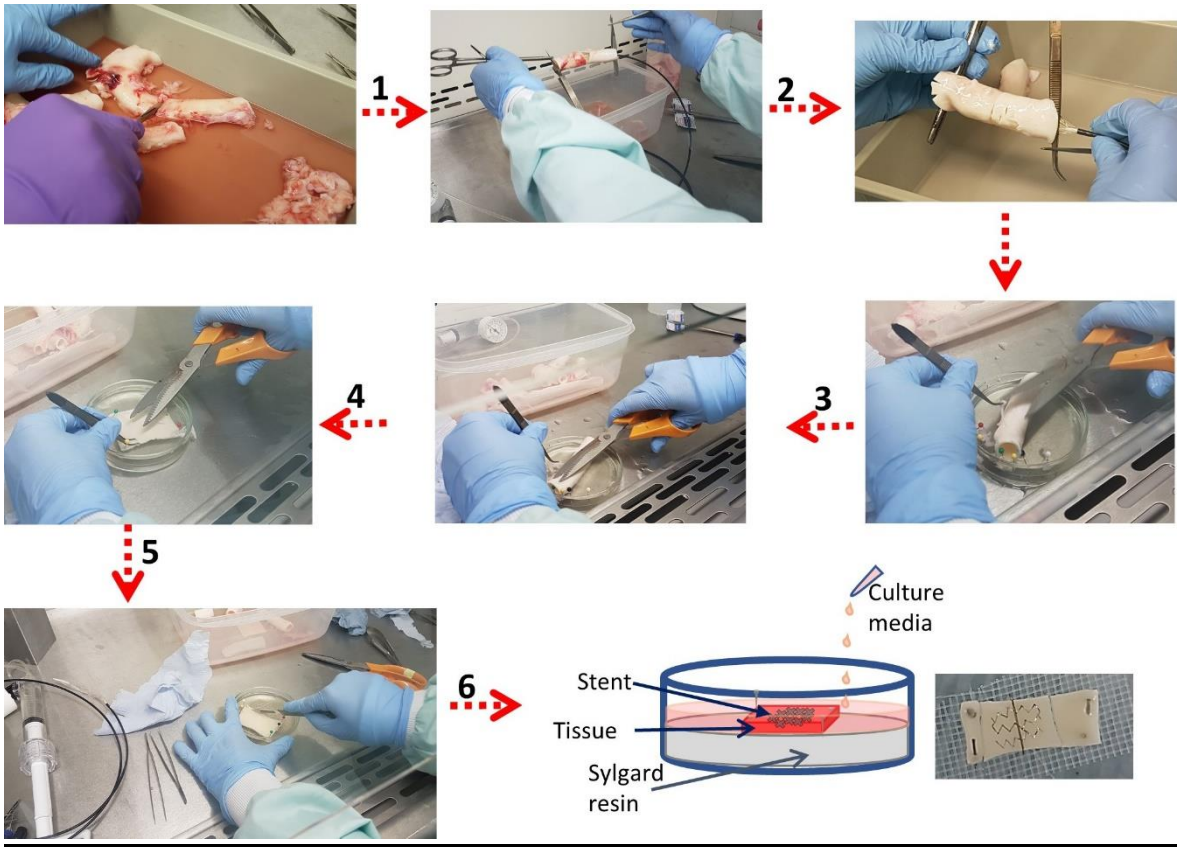

1) Thoracic aorta isolated
2) Aortic balloon inflated to cause lumen wall injury
3) Adventitia removed
4) Aorta cut opened and pinned open onto dish
5) Aorta cut into small segments for culture
6) Aorta/stent pinned into dish and culture media added into dish to incubate for 14 days at 37 ℃ and 5% CO_2.

Figure 2.8: Step by step outline of porcine aorta isolation and stent deposition for organ culture.

Table 2.2: The experimental set-up for porcine aortic organ culture.

Experimental group	Description
Ao- Day 0 Before injury	Aorta segment fixed after isolation and before inducing injury
Ao- Day 0 After injury	Aorta segment fixed after isolation and after inducing balloon injury
Ao- GAZELLE	Balloon injured Aorta segment fixed after 14 days of tissue co-culture with dH_2O spray coated GAZELLE stent segments
Ao-CHROMA	Balloon injured Aorta segment fixed after 14 days of tissue co-culture with dH_2O spray coated CHROMA stent segments
Ao-Graphene	Balloon injured Aorta segment fixed after 14 days of tissue co-culture with Graphene spray coated GAZELLE stent segments
Ao- Graphene Oxide	Balloon injured Aorta segment fixed after 14 days of tissue co-culture with Graphene Oxide spray coated GAZELLE stent segments
Ao- EES	Balloon injured Aorta segment fixed after 14 days of tissue co-culture with EES stent segments
Ao- Day 14	Balloon injured Aorta segment fixed after 14 days of tissue culture (Without any stent)

2.4.1.6 Coronary artery and aorta Tissue culture with/without stent segments

Each pre-prepared 50 mm glass petri dish (section 2.4.1.1) contained 10mL of RPMI 1640, Hepes Media (Gibco® Life Technologies, 42401-018) supplemented with 30% Foetal Bovine Serum (SIGMA, F9665), Penicillin- Streptomycin at 50Units/mL, 50µg/mL, respectively (SIGMA Aldrich, P4333), Glutamine at 2mM (SIGMA, G7513) and Amphotericin at 5µg/mL (Gibco® Life Technologies, 15290-026) (207). The dishes were incubated at 37 ˚C, 5% CO_2 for 14 days. The media was changed every day to every other day. The control tissues, day 0, were fixed after isolation and underwent exactly the same fixing, processing and staining procedures as those fixed after 14 days of organ culture. Two sets of each experiment were prepared; one for paraffin embedding for histological/ immunohistochemistry staining and the other for scanning electron microscopy visualisation which both require different fixing techniques.

2.4.2 Ex-vivo porcine tissue processing post- organ culture for histological and immunohistochemistry analysis

2.4.2.1 Fixation of porcine tissue for paraffin embedding

To determine the amount of neointimal formation, both coronary artery and aorta tissues intended for paraffin embedding were fixed by 10% Neutral buffered formalin. Tissue

segments in each dish were washed 2-3 times with PBS prior to adding 10% Neutral buffered formalin (SIGMA Aldrich) and incubated at 4˚C for 24 hours. The next day, fixing agent was removed and tissue washed 3x with PBS subsequent to adding 70% ethanol and incubating at 4˚C until ready for processing for paraffin embedding.

2.4.2.2 Tissue processing of porcine coronary artery and aorta in preparation for paraffin embedding

Fixed tissues (see section 2.6.1) were placed in pre-labelled histology cassettes and processed in the Leica ASP300 S Tissue Processor (Leica Microsystems, Nussloch, Germany) on an overnight programme starting through graded alcohols (70%, 20 minutes; 70%, 30 mins; 90%, 60 mins, 90% 60 mins; 100%, 30 mins; 100%, 45 mins; 100%, 60 mins) then moving to xylene (3 buckets; 20 mins, 30 mins, 40 mins), next ending in molten paraffin wax (3 buckets; 70 mins, 70 mins, 70 mins).

2.4.2.3 Paraffin wax embedding

Porcine coronary arteries and aortae were embedded into paraffin and positioned to enable vessel transverse sections on slicing. The embedding into the paraffin was performed using the Shandon Histocentre 2 (Fisher Scientific). Molten paraffin wax was poured into moulds, the vessel positioned and the top of the cassette was then embedded into the molten wax mould to provide grip for the microtome. Subsequently, the blocks were placed on a 4 ˚C cold plate and allowed to harden overnight.

2.4.2.4 Sectioning of embedded porcine coronary artery and aorta

To optimise the quality of the cut sections, paraffin blocks encompassing the embedded tissue were placed on ice prior to sectioning. 5 µm sections were obtained using a Leica RM2145 microtome, sections were floated onto a 45˚C distilled water bath (Leica HI1210) to remove wrinkles in the tissue, followed by collection of the tissue onto a Thermo Scientific Superfrost ® Plus glass slide (Braunschweig, Germany) after 2-5 minutes. Slides were then incubated vertically at 45°C, overnight to ensure complete adherence of the porcine coronary artery/aorta sections onto the glass slide.

2.4.2.5 Histology – Miller's elastin staining

Glass adherent 5µm thick paraffin coronary artery and aortic sections were de-paraffinised in xylene (Fisher Chemical) for 5 minutes (2 changes) in the fume cupboard. Next, the sections were re-hydrated by graded ethanol immersion into 100%, 75%, 50%

and then distilled water for 5 minutes each before staining. Subsequently, sections were oxidised in 0.5% potassium permanganate (Sigma Aldrich) (5 minutes), washed in distilled water, bleached in 2% oxalic acid (Sigma Aldrich) for approximately 9 seconds until sections decoloured, followed by rinsing in 95% ethanol and immersion in blue Miller's stain (3 hours). Afterwards, slides were rinsed in 95% ethanol followed by distilled water, and then counterstained with Van Gieson's stain for 5-10 seconds (1:1 dilution with water). Sections were then dehydrated gradually in 50%; 75%; 90%; 100%; 100% ethanol solution with a final double immersion in xylene (at least 5 minutes each). Sections were mounted using DPX mounting medium (Fisher Chemical) before placing the cover slip. This was allowed to dry overnight before visualisation and imaging via a 3D Histec Pannoramic 250 slide scanner (3DHISTECH Ltd., Hungary) and visualised for analysis using the Case Viewer with Histoquant licence.

2.4.2.5.1 Neointima measurements and analysis

Coronary artery and aortic tissue was separated into 4 and 8 equal segments, respectively (Fig. 2.9). Neointima was measured from the internal elastic lamina using the Case Viewer programme and all measurements collected into PRISM GraphPad software for analysis.

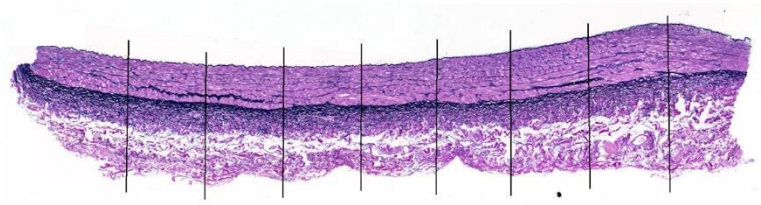

Figure 2.9: Representative tissue section of porcine aorta, Miller's elastin stained and divided into equal sections.

Average data were presented as mean ± standard error of the mean (SEM). Four different pigs were used for coronary artery tissue organ culture and ten different pigs for aortic organ culture. Statistical analysis was performed using PRISM GraphPad software, one-way ANOVA with Tukey's post-hoc test. Statistical significance was illustrated as $p<0.05$ (*) and $p<0.001$ (**).

2.4.2.6 Immunohistochemistry of sectioned porcine coronary artery and aorta – Endothelial cell staining

Sections were deparaffinised with xylene (Fisher Chemical) and then rehydrated by serial immersion in 100%, 95%, 75%, 50% ethanol and distilled H_2O (5 minutes each). Antigen retrieval was done by slide incubation in 0.01M citrate buffer (SIGMA) heated to 95 ˚C

and allowed to cool at room temperature (30-60 minutes). Next, slides were rinsed in 10mM PBS and blocked in 3% (v/v) H_2O_2 (SIGMA) for 7 minutes. Sections were rinsed twice in 10mM PBS, 5 minutes each time, before encircling using a hydrophobic pen and blocking in 2.5% normal horse serum (Vector) for 1 hour in humidified chamber (to avoid evaporation) at room temperature. Endothelial cells were specific stained by adding 1:50 primary antibody against CD31, (Rabbit pAb to CD31, ab28364, Abcam), prepared in TPBS (0.025% TritonX in PBS) and 1% Bovine serum albumen (Vector) and incubated in a dark humidified chamber at 4˚C, overnight. The next day, primary antibody was removed and slides were washed three times in PBS, each 5 minutes, before applying the ImmPRESS HRP reagent anti-Rabbit IgG (Vector) and incubating for 30 minutes at room temperature, again in humidified chamber. Washing of sections twice in PBS (5 minutes each) followed, with subsequent addition of ImmPACT DAB (SK-4105, Vector) for 4-5 minutes to allow staining to take place. DAB activity was stopped by washing in distilled water (5 minutes) and prepared for counterstaining by immersion in 95% ethanol. Slides were submerged in Miller's stain for a duration of 30 minutes before washing in 95% ethanol (3 changes). Slides were further dehydrated in 100% ethanol changes and then the alcohol removed in twice incubation in xylene (5 minutes) before mounting with DPX mounting medium (Fisher Chemical), placing the cover slip and left untouched overnight. Imaging was done using the 3D Histec Pannoramic250 slide scanner (3DHISTECH Ltd., Hungary) and analysis using the Case Viewer with Histoquant licence. Tissues were viewed and annotated for absence of endothelial cell/CD31 staining (-); some areas of staining (+-) and most areas of CD31 staining (+).

2.4.3 Ex-vivo porcine tissue processing post- organ culture for scanning electron microscopy analysis

In order to investigate further the healing potential of the vessel, scanning electron microscopy was used to determine endothelial cell coverage on the graphene coated, graphene oxide coated and control stents. This may provide more information about possible preferential growth of endothelial cells on the graphene coated or graphene oxide coated stents.

2.4.3.1 Fixation of porcine tissue for scanning electron microscopy

The second set of the tissues were immersion-fixed in 4% paraformaldehyde, 2.5% glutaraldehyde (AGAR Scientific, R1012) in 0.1 M Hepes. Incubated at room temperature

for 1 hour followed by incubation at 4˚C until ready for osmium staining. Tissue with pinned stents were stained in 1% osmium tetroxide for 1 hour (R1024, AGAR Scientific), and dehydrated via ethanol serial immersion (dH_20, 35%, 50%, 75% 95%, 100% Ethanol) each at 20 minutes duration. Subsequently, the tissues were critical point dried (CPD). CPD was performed using the K850 Critical point drier (Quorum Technologies, UK). Three incubations of 40 minutes each in the CPD was performed to dehydrate the tissue for visualisation by scanning electron microscopy (SCEM).

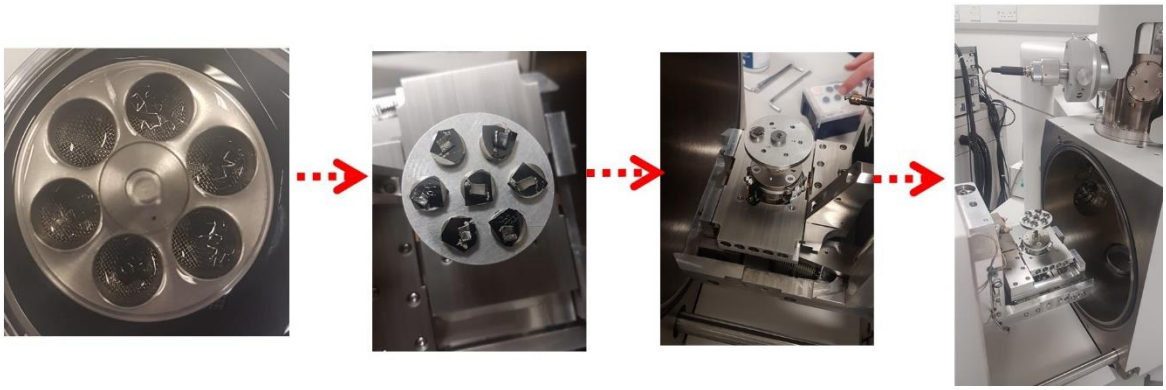

Figure 2.10: Step by step schematic of critical point drying and preparing for SCEM visualisation.

Subsequently, CPD samples were secured onto metal stubs using double sided tape (Fig. 2.10), and then gold splutter coated (Quorum Technologies, SC7620, Sputter Coater, UK). At least a few hours prior to visualisation with SCEM, on 1-2 corners of the tissue, drops of Acheson Silver DAG (G3648, AGAR Scientific) were added in order to form a thin highly conductive silver layer as means to visualise the samples. SCEM tissue and stent surface imaging was performed using an FEI Quanta 250 ESEM operating in high vacuum at 10.0 kV.

CHAPTER 3

Preparation and characterization of graphene based dispersions

3.1 Introduction

Graphene and graphene oxide manufacture by liquid phase exfoliation results in a dispersion. The material produced with the preparation methods is described in chapter 2.1.1. The concentration, thinness and lateral dimension of the Gr/GO flakes exfoliated require characterisation and this is typically determined by UV-Vis spectroscopy, Raman spectroscopy and atomic force microscopy, respectively. Each of these techniques will be described in this chapter. This chapter will also present the concentration, structural and quality characteristics for the graphene and graphene oxide dispersions produced in this study.

3.1.1 UV-Vis spectroscopy determining Graphene concentration

Ultraviolet-visible spectroscopy (UV-Vis) is typically utilised to determine the concentration of graphene. A beam of monochromatic light is passed through a diluted sample and absorbed light is measured by electronic detectors (208). To calculate concentration of the sample from absorbance values, the Lambert-Beer law (203) is utilised, as following:

$$A = \alpha c l$$

Where A is the optical absorbance of light, α is the molar absorption coefficient, equal to 2460 $Lg^{-1}m^{-1}$ (170) measured at 660 nm, c is the sample concentration and L represents the distance which the light travels through, i.e. the size of the cuvette (in this study, 0.01m).

A typical UV-Vis spectrum of graphene is illustrated in figure 3.1. The π-π interaction (transition of the electron within each carbon atom to a higher energy orbital) within the carbon atoms of the hexagonal graphene structure cause a UV-Vis peak at 268 nm (209). The absorbance of graphene is extrapolated at 660nm wavelength.

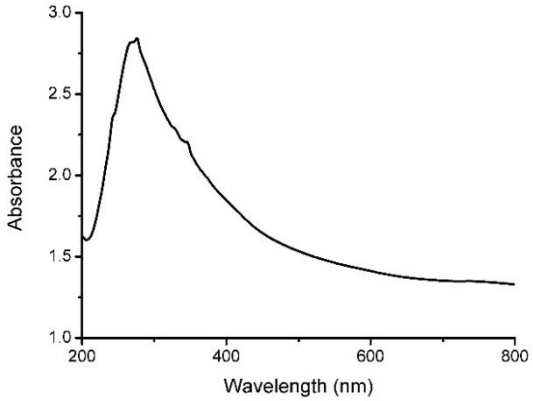

Figure 3.1: Typical UV-Vis spectrum of graphene dispersion in water.

3.1.2 Raman spectroscopy

The Raman effect was discovered by an Indian physicist, Chandrasekhara .V. Raman in 1928 (210). Raman spectroscopy is the method of choice as a diagnostic tool to analyse and identify material-specific structural fingerprint. This method involves applying monochromatic light (typically using a laser) onto the sample, causing atomic vibrations, which cause a change in the energy of the scattered light (Fig. 3.2). Looking at the difference between incident and scattered light energy, one can see specific peaks attributed to particular atomic vibrations (Fig. 3.3, 3.4). Thus, analysis of the Raman spectrum yields information on the structure of the molecule or material.

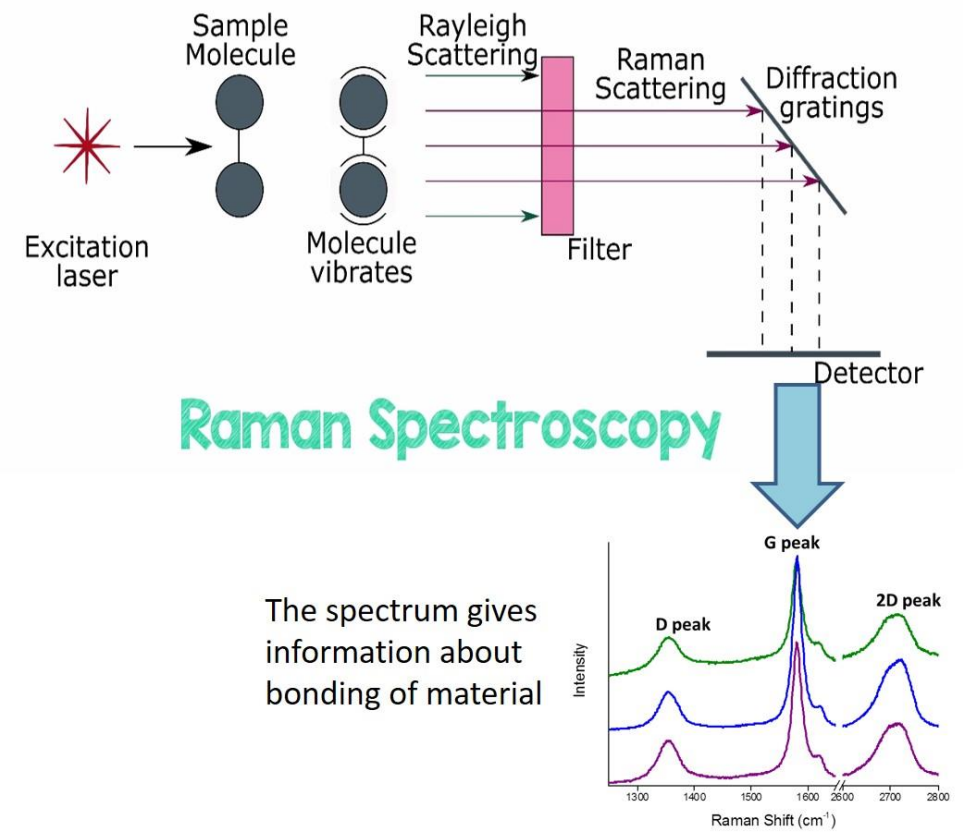

Figure 3.2: Principal of Raman spectroscopy, altered and annotated from (211).

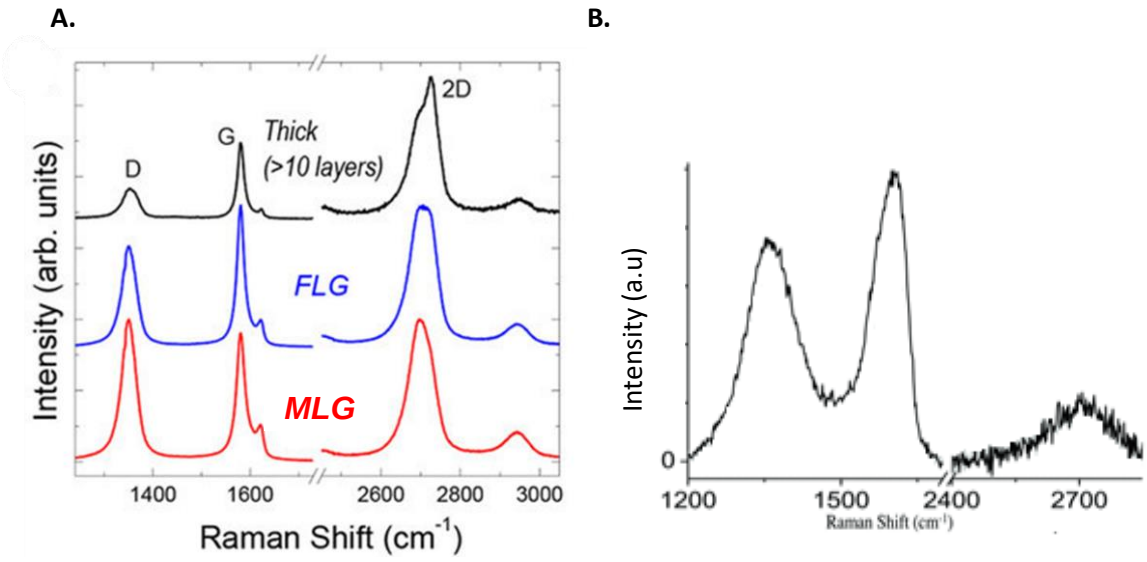

Figure 3.3: A: Typical Raman spectra of graphene produced by LPE and B: graphene oxide. Graphene from liquid phase exfoliation and image obtained from (212). **A:** Monolayer graphene (MLG), Few layer graphene (FLG), Graphite (Thick). **B:** Graphene oxide Raman spectrum (168).

The typical Raman spectrum of graphene shows two peaks, centred at 1580 cm^{-1} and at 2680cm^{-1}, known as the G and 2D peak, respectively (Fig. 3.3A) (213), which are associated with the atomic vibrations shown in figure 3.2. In the case of graphene produced by LPE, the Raman spectrum also shows a characteristic D peak (at ~1350 cm^{-1}) (170) which is a defect-activated peak (Fig. 3.3A), i.e. it appears only if there are defects in the material, while the 2D peak (which is associated to the same atomic vibration) is always present in the Raman spectrum. Although the Raman spectrum of graphene produced by LPE shows a prominent D peak, the material does not have any structural defects. In this case, the D peak is activated by the edges of the material (214): the flakes are very small, therefore the edges strongly contribute to the Raman signal. An edge, from a Raman point of view, is a defect because it breaks the symmetry of the crystal, hence why the D peak appears in the Raman spectrum.

The typical Raman spectrum of GO shows broad and intense G and D peaks, while the 2D peak is very weak (Fig. 3.3B). These changes are attributed to the defective nature of GO: the functionalisation breaks the symmetry of the graphene crystal, making this material equivalent to a very defective graphene.

One of the major problems of working with graphene produced by LPE is the quantification of the single layers and few layers in the dispersion. As mentioned in section 1.10.1, dispersion produced by LPE typically contains flakes with a distribution in thickness. In this project, the following parameters will be analysed in order to qualitatively estimate the thickness distribution:

i) The intensity ratio between the D and G peak, I (D)/I (G). This depends on the size of the flakes. During sonication the layers of graphite get exfoliated, but sonication also makes the layers smaller in size. Thus, smaller flakes are more likely to be single layers.

ii) The shape of the 2D peak, which allows for distinguishing between single/few layers and graphitic (i.e. >10 graphene layers) flakes (Fig. 3.3). The method (215) involves fitting a Lorentzian curve to the 2D peak and calculating the coefficient of determination (R^2), which indicates how well the fit reproduces the experimental line: A finely symmetrical and sharp peak with R^2 value above 0.987 presents mono layered graphene (MLG), whilst few layered graphene (FLG) is identified by

asymmetrical and rather broad 2D peak with $0.985<R^2 \leq 0.987$. Restacked graphene (FLG restacked), which describes graphene sheets bereft of AB Bernal stacking can be distinguished by the R^2 again; values between 0.985-0.987 indicate restacked graphene layers while <0.985 indicated few layered. Graphite is determined by the broad and double peaked 2D spectrum.

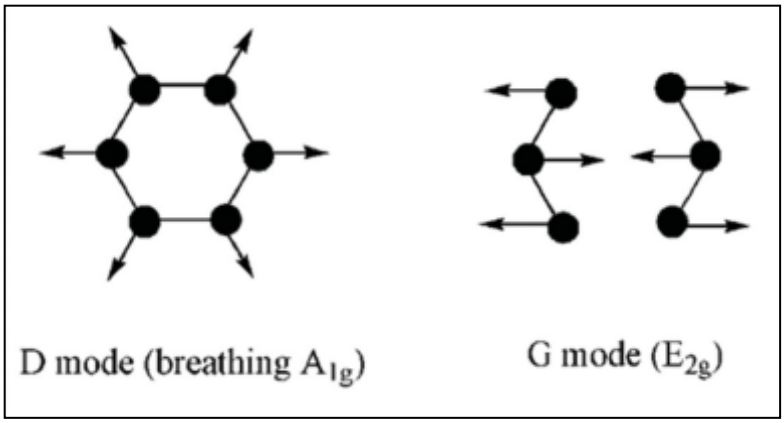

Figure 3.4: Atomic vibrations associated to the D (2D) and G peaks. Figure obtained from (216).

*3.1.*3 Atomic Force Microscopy

Atomic force microscopy (AFM) allows high-resolution surface imaging by scanning a very sharp probe along the surface. The probe is attached to a cantilever (mimicking a record player needle) that moves along with the probe and acts as a laser reflective surface. When the probe gets close to the surface, it moves over and along the material changing the cantilever angle, and therefore alters the angle of the reflected laser into the photodetector (Fig. 3.5). The tip often measures only nm across and movement of the cantilever is detected by laser. This then is output as an image. Graphene flakes appear as images on the AFM to identify shape and size of the flake. One could also extract the thickness, by looking at the height of the flake, measured at the substrate-flake edge. However, this method is known to be only qualitative, as contamination and water absorption on the flake may increase the apparent thickness of the flake. (217).

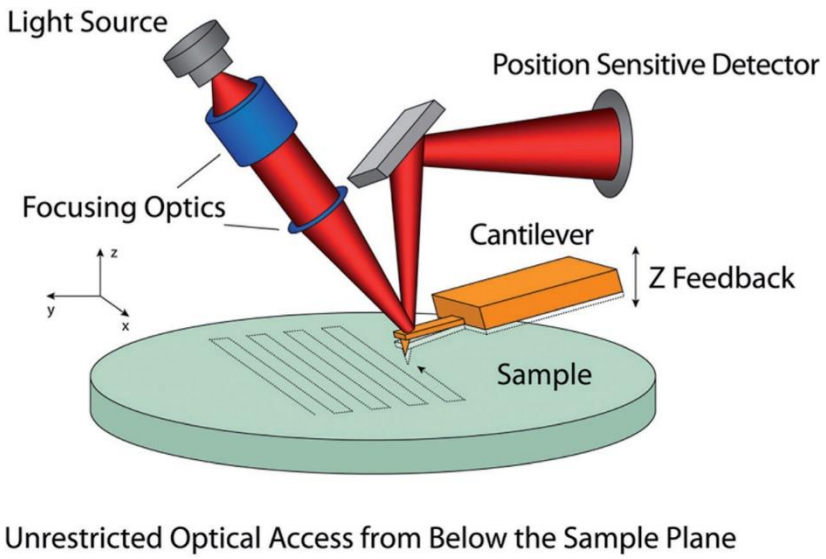

Figure 3.5: Schematic illustrating the atomic force microscopy set-up (218).

3.2 Methods

The graphene dispersion that was used for the main experiments performed in this thesis was prepared by Dr Daryl McManus in Prof Casiraghi's group, School of Chemistry, University of Manchester, using the method described in Chapter 2. Graphene oxide was prepared by the modified Hummer's methods in Prof Kostarelos's laboratory, School of Life Sciences, University of Manchester, as described by Ali-Boucetta and colleagues and illustrated in Fig. 2.2 (168).

In brief, to determine the concentration of the dispersions, a very diluted sample of the dispersion was used to measure concentration by UV-Vis (chapter 2 provides more detail). The number of layers within each flake was elucidated by Raman spectroscopy and the flake lateral size was determined by AFM.

3.3 Results

3.3.1 Graphene characterisation

The resulting concentration of the graphene dispersion as determined by UV-Vis was calculated as 1.07 $mgmL^{-1}$. The dispersed flake thickness and length were determined using Raman spectroscopy and atomic force microscopy, respectively (Fig. 3.6, 3.7) using the methods described in Chapter 2.

Figure 3.6A illustrates representative spectra of the produced material, with the D and G peaks (at 1350 $cm^{-1}$and 1580 cm^{-1}, respectively), while Fig. 3.6B shows the 2D (2700 cm^{-1})

peak. The R^2 value of 0.989 is indicated on the 2D peak suggesting single layered graphene (219).

Figure 3.7A shows a representative AFM picture of the graphene flakes deposited on the silicon substrate as a lighter sheet like structure. The majority of the flakes appeared to range between 100-300 nm in lateral size (Fig. 3.7B). The thickness as measured by AFM, was in the range of 3-35 nm, with the majority exhibiting analysis thickness of 5-10 nm.

As is displayed in Table 3.1, over 80% of the dispersion consists of few layered flakes (2-7 layers), whereas approx. 7.5% included mono layered graphene. Graphite, i.e. flakes with more than 7 layers, was also identified within the dispersion.

Table 3.1: Liquid phase exfoliated graphene flake layer distribution. Raman analysis at 514 nm wavelength was used to determine flake thickness identified from the 2D peak sharpness (determined by its r^2 value, see section 5.2.1) and shape. Monolayer graphene (MLG), Few layer graphene (FLG).

MLG	FLG – restacked	FLG	Graphite	Total
3	3	29	5	40
7.5%	7.5%	72.5%	12.5%	100%

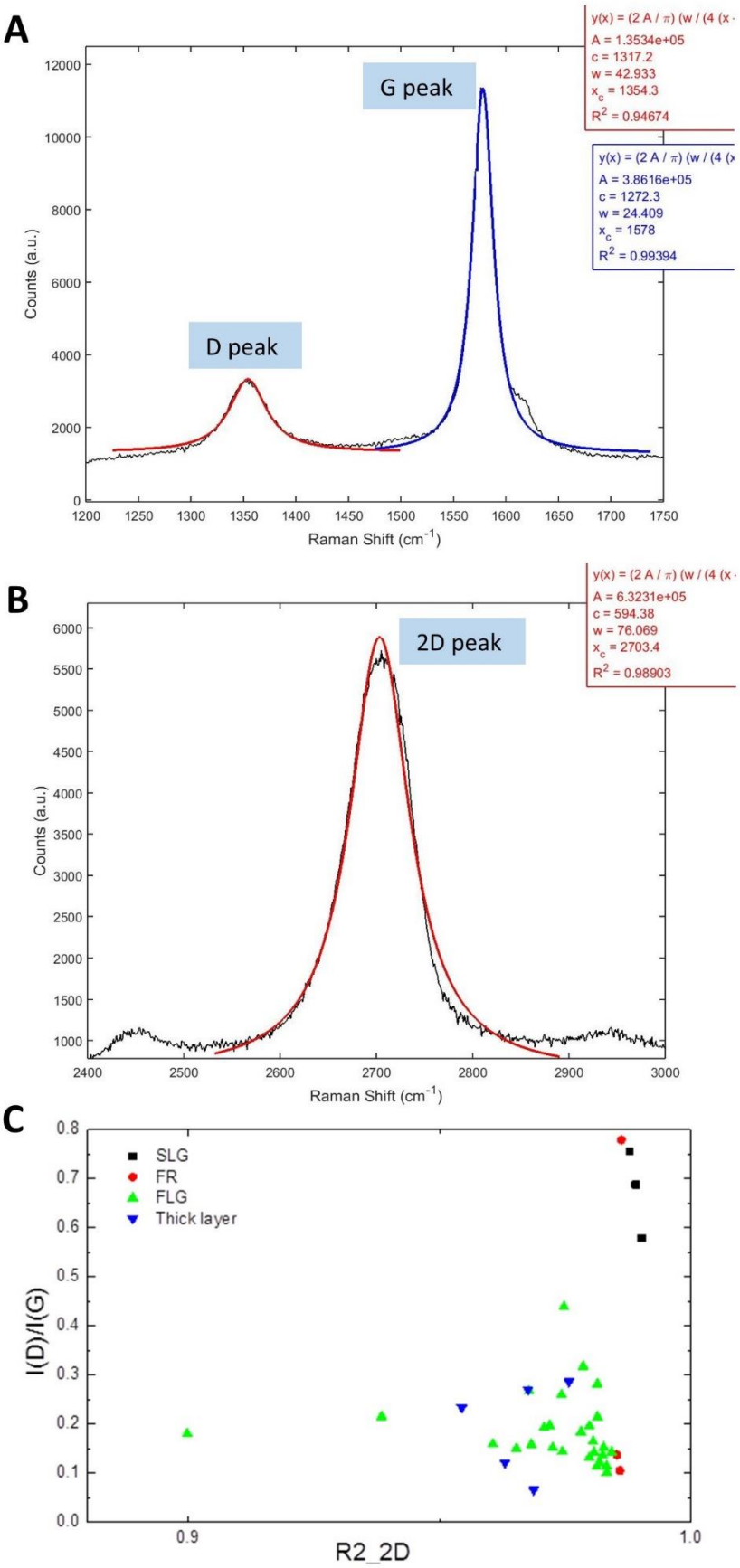

Figure 3.6: Characterisation of graphene using Raman spectroscopy. A-B: Representative Raman spectra attained at 514nm excitation line indicating a monolayer graphene flake, when analysing a drop casted 0.05 mgmL^{-1} LPE graphene dispersion on a SiO_2 wafer with the solvent evaporated. R^2 value of >0.987 indicates a monolayer. **C:** I(D)/(G) versus R^2 value of regression of the 2D peak value, so that I(D)/(G) ratio is compared to the flake thickness.

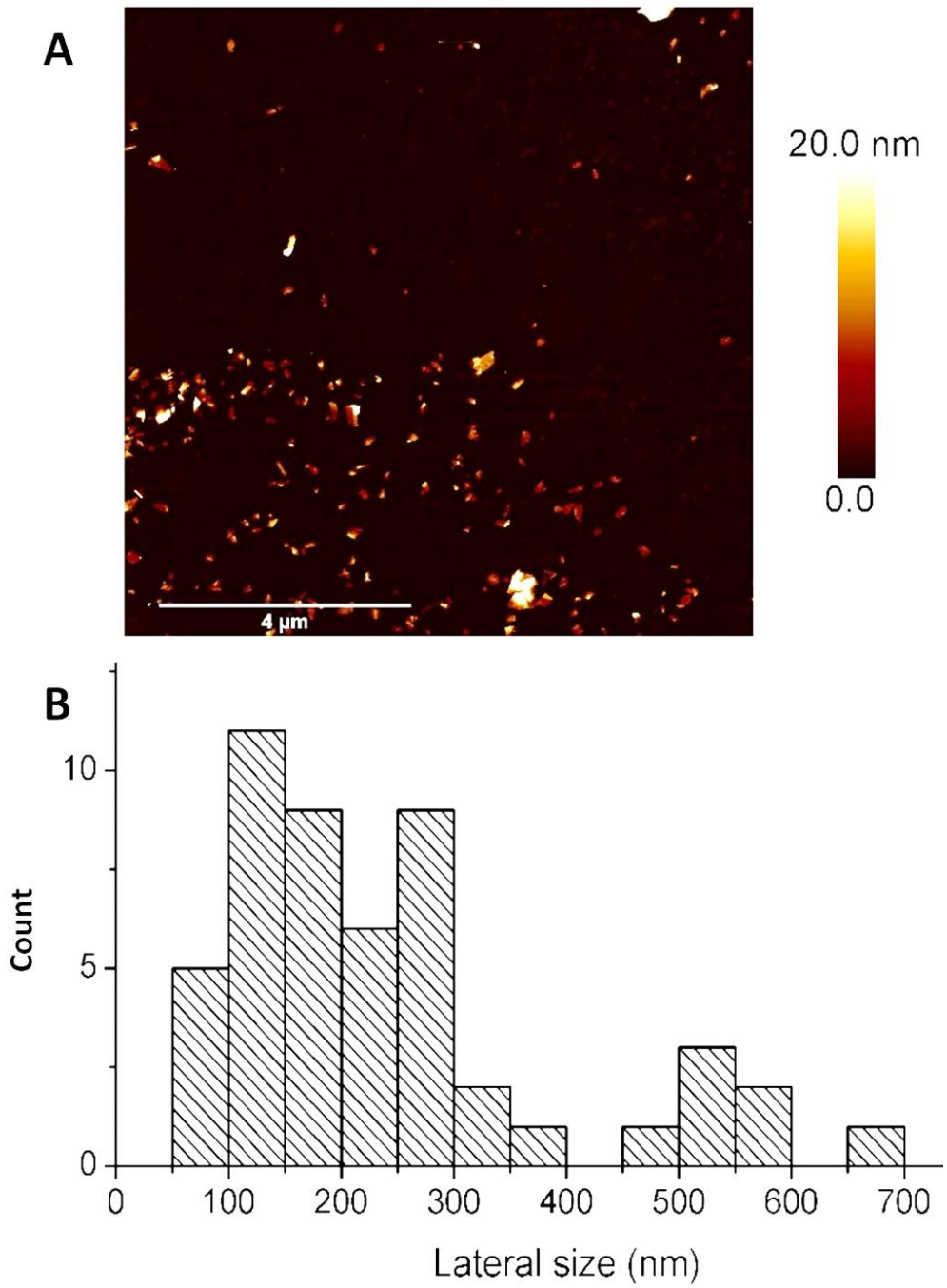

Figure 3.7: Characterisation of graphene using AFM. A: Atomic force microscopy (AFM) image of the same drop casted graphene sample, using the Tapping mode software option. **B:** Flake length distribution.

3.3.2 Graphene Oxide characterisation

The GO dispersion produced and used for this project, had a concentration of 1.0 $mgmL^{-1}$ and its corresponding characteristics, GO flake thickness and lateral size, was determined by Prof Kostarelos's team (Table 3.2) using methods previously described *(168, 220).*

Table 3.2. Graphene Oxide characterised by Raman spectroscopy and AFM.

I(D)/I(G) ratio	1.3±0.09
Thickness (AFM)	1 nm
Lateral size (AFM)	20 µm

3.4 Discussion

The thinness of the graphene flakes is critical for the unique properties attributed to graphene. It is the single layer thinness of the graphene material that gives it the properties that make it so unique. The lateral size and number of layers each flake is made up may have consequences in the experimental conduct of the project as well as potential influence on results. It is for this reason that both the graphene and the graphene oxide dispersions used in this project required structural (lateral size) and quality (layers of each flake) characterisation. In this chapter, the techniques to assess the quality and structural characteristic of the flakes were introduced and the resulting data from these techniques analysed for both Gr and GO dispersion examination.

3.4.1 Graphene dispersion dominated by few layered flakes

Our results revealed that the graphene dispersion contained ~80% of few layers graphene (2-7 layers). These data cannot be compared to the literature because the yield is dependent on the specific protocol, particularly the sonication time. By fitting the 2D peak (Chapter 2) the R^2 values were determined and it was observed that the thickness distribution was dominated by few layers graphene (Table 3.1). The intensity ratio between the D and G peak, I(D)/I(G), was also analysed and plotted as a function of R^2 (Fig. 3.6C). As expected, LPE graphene defect or I(D)/I(G) ratio was larger with fewer graphene layers and particularly with single layered graphene, because thinner flakes are likely to have small flake size (i.e. smaller than the laser spot) with the flake edges contributing to the I(D)/I(G) ratio. Thus, I(D)/I(G) is not representative of real defects in LPE graphene dispersions (214, 221).

Raman spectra denoted the characteristic G band at 1580 cm^{-1} caused by bond stretching of the sp2 carbon atoms and the 'defect' D band was at 1350 cm^{-1} (Fig. 3.6 A). In liquid phase exfoliated graphene, the D peak is often active due to edges of the graphene flake. The flakes in LPE Gr are small, <500nm, this leads to the edges being within the area of the laser, as the laser point itself is approximately 500nm in diameter. This is the main reason for the rise of the D peak in graphene flakes in this study. The D to G peak intensity ratio (ID/IG), corresponding to the metric of disorder in the single layered graphene was largest, dropping with increasing flake thickness (Fig. 3.6C); caused due to single layered graphene flakes being smaller than the LASER size thus flake edges contributing to the D peak, and thus in this instant, not representative of real defect (214, 221). The 2D band at 2680cm^{-1} was present with the sharp, single and symmetric peak suggesting pristine single layered graphene, with broader peaks representing increase in graphene sheets, few layered graphene (Fig. 3.6B) (221).

The subsequent structural characterisation by AFM, revealed a graphene thickness range of 3-35 nm, with the majority exhibiting Raman analysis thickness of FLG (2-7 layers) ~3 nm (222). Previous literature has reported an AFM measured flake size of 5 nm to be actually 1 nm or less after laser treatment to desorb molecule residues on the flake surface (183), therefore suggesting that AFM data should be considered as a qualitative measurement rather than quantitative. Therefore, it is not surprising that the flake thickness obtained by AFM and Raman do not correspond to each other. It is important to note the length of the flakes, as this will affect coating (may clog nozzle of spray gun) as well as potentially influence the biological components (223).

3.4.2 Graphene oxide lateral size larger than graphene flakes

The GO dispersion was characterised by Prof Kostarelos's group, University of Manchester. The results demonstrate a rather high ID/IG ratio (Table 3.2) as typically reported for GO (224). GO is expected to have a higher D peak, compared to graphene produced by LPE, due to the presence of oxygen-containing groups, which break the symmetry of the crystals and, hence, are considered defects. In addition, the GO flakes tend to have larger lateral size (1-20 μm) than graphene flakes produced by LPE, whose lateral size is mostly around 100-300 nm. This may later influence spray coating as larger flakes may aggregate and clog the spray pistol.

3.5 Key Findings of this chapter:

- Graphene and graphene oxide dispersion of 1 $mgmL^{-1}$ concentrations were achieved by LPE method.
- Graphene dispersion consisted mainly of ~ 80% few layered graphene (2-7 layers).
- Lateral size of 100-300 nm for graphene and 20 µm for graphene oxide were achieved.

CHAPTER 4

Selection of optimal graphene coating deposition technique

4.1 Introduction

The overall aim of this project is to improve restenosis risk associated with bare metal stents by coating BMS with a biocompatible material. Even though there is not enough data supporting the biocompatibility of graphene based materials, there is the potential that its unique properties of high strength, smoothness, anti-corrosion, high surface to volume ratio render it an ideal material for coating of medical implants. However, it is not clear which coating method would be more suitable. There are several coating methods available, however those achieving the most uniform, thin and precise coating arise from expensive, low yield and difficult upscaling methods such as chemical vapour deposition or rapid thermal processing, which 'grow' graphene onto the metal substrate (165).

In this chapter, several coating techniques were investigated in order to select the coating method that produced the most even, thin Gr/GO coating with optimum coverage of the substrate. Once the coating technique was selected, investigations were conducted in order to optimise the coating further on stainless steel coronary artery stents (GAZELLE stents donated by Biosensors Int.), producing uniform coating with higher substrate coverage.

4.2 Methods

Various coating methods were tested for selection followed by optimisation as outlined below. For this project, simple dip coating, dip coating with applied bias and spray coating was explored to select the coating method that would subsequently be optimised.

Medical grade, 316L stainless steel (SS) discs were used for preliminary investigation of coating techniques, as a substitute to coronary artery stainless steel bare metal stents. To identify the method that produces the most even and thin coating with maximal graphene coverage of 316L stainless steel discs, several coating methods were attempted and examined:

- Dip-coating; dipping the 316L SS discs wholly or partially into the graphene dispersion to show uncoated/coating boundary.
- Dip-coating with applied bias; applying voltage bias between the graphene based dispersion and the discs to force flakes onto the 316L SS substrate (Fig. 2.3).

- Spray coating; spraying graphene based dispersion onto the substrate whilst simultaneously allowing for annealing via solvent evaporation (Fig. 2.4).

To reiterate, for technique selection only graphene dispersions were utilised, and following selection, both graphene and graphene oxide dispersions were used for optimising the coating, on coronary artery stainless steel GAZELLE stents, for the highest substrate coverage with thin and even outcome. Since this involves a serial trial and consequent re-strategising approach, methods and results will be presented together in this chapter.

4.3 Methods and Results

4.3.1 Dip coating 316L (medical grade) stainless steel discs

Firstly, the discs were dipped into graphene or graphene oxide dispersions for a duration of approximately 3 seconds. Subsequent air-drying allowed solvent evaporation, leaving graphene flake deposition on the stainless steel disc substrate. The initial dip-coating illustrates a darker region in the middle of the disc while the rest of the disc appeared lighter in colour (Fig. 4.1A), indicating poor and uneven coating coverage. Following from this, and in order to visualise the boundary of coated versus uncoated 316L stainless steel discs, partial immersion in both Gr and GO dispersions for 24 hours were also performed. This partial immersion illustrated varying areas of darker regions on the disc (Fig. 4.1 and 4.2 A, B), but also demonstrated larger areas of coverage compared to the shorter immersion duration (Fig 4.1 B versus A).

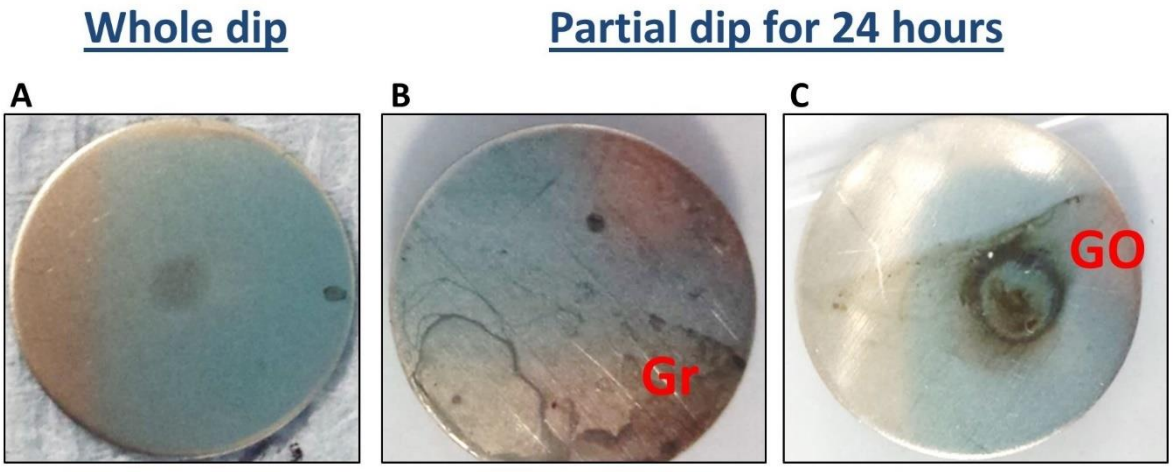

Figure 4.1: Uneven and poor coating coverage with dip-coating. A: 3 second dip-coating in 0.33 $mgmL^{-1}$ of graphene dispersion. **B:** Partial dip-coating for a duration of 24 hours into 0.33 $mgmL^{-1}$ of graphene and **C:** Partial dip-coating for a duration of 24 hours into 0.5 $mgmL^{-1}$ of graphene oxide dispersion. Images acquired using SAMSUNG cameraphone. Graphene (Gr) and graphene oxide coating (GO) region indicated on the images as is evident by dark and uneven areas/patches. Coating is visually very patchy.

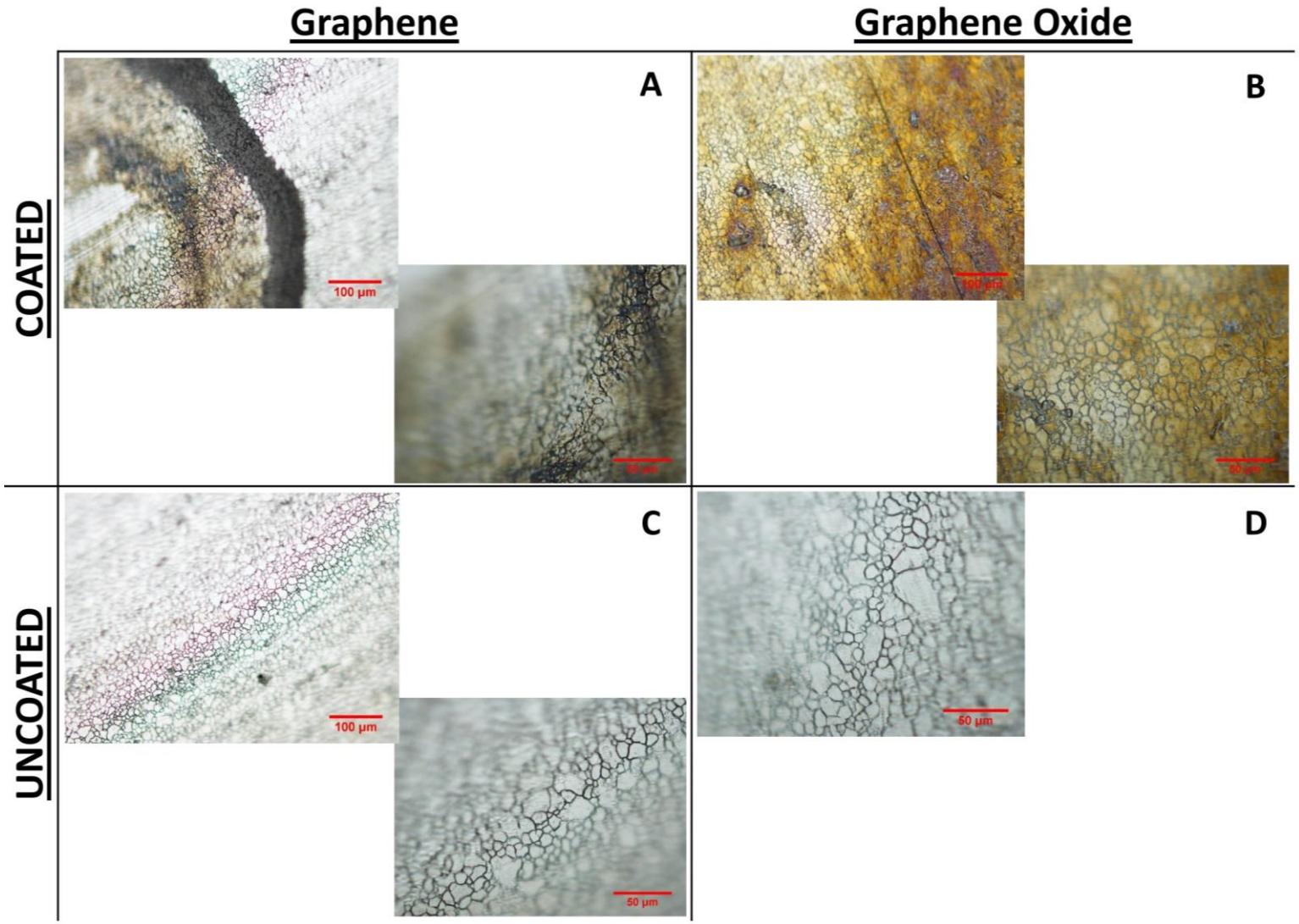

Figure 4.2: Partially dip-coated 316L stainless steel discs immersed in graphene and graphene oxide dispersions for a duration of 24 hours.
A: Graphene (0.33 $mgmL^{-1}$) coated area**. B:** GO (0.5 $mgmL^{-1}$) coated area. **A/B** illustrate the coated regions of the stainless steel discs, demonstrating visually uneven coating (light or thin to very dark or thick coating regions). **C/D:** Uncoated area of stainless steel disc, as was not immersed into dispersion. Nikon Eclipse LV100 microscope was used to view the disc and the TV lens 0.55x Ds camera. Scale bar 50 µm and 100 µm.

4.3.2 Dip-coating with simultaneous applied voltage bias

Coating on the dip-coated discs (above) was focused onto spots. In order to improve graphene coverage onto the stainless steel discs, an attractive force between the dispersion and substrate was applied in an attempt to improve coating uniformity. However, this was tested using the graphene dispersion only, as an initial investigation. Application of voltage bias to enhance coating has previously been described in the literature as electrophoretic deposition of graphene (225). The attractive force, in the form of bias voltage was utilised, since the graphene dispersion stabiliser, PS1, is negatively charged. Therefore, the discs were positively charged to attract the graphene flakes onto the stainless steel substrate, as illustrated in Figure 2.3. As the application of voltage bias produced a more uniform and visible graphene coating on the stainless steel disc when compared to simple dip-coating technique, the next step was to determine the optimal settings. The 1 $mgmL^{-1}$ graphene dispersion was diluted to 0.3 $mgmL^{-1}$ and the following parameters applied:

(i) Varying voltage 50V, 100V and 200 V for 20 secs once desired voltage was reached

Figure 4.3i and figure 4.4 demonstrate that relatively uniform coating was achieved at 200V bias when discs were dipped for 20 seconds. Increasing the voltage applied to the stainless steel increased the evenness of the graphene coating. Some thin coated patches were observed with 50V, but application of 100V visibly reduced the number of these patches, hence improving coating (Fig. 4.3i). There was a small area of thinner coating observed towards the centre of the disc with 100V (Fig. 4.3i). The most uniform coating was achieved by applying higher voltage, as observed with the application of 200V.

(ii) Varying disc immersion duration, 30 secs, 40 secs and 60 secs once 50V was reached

Coating was assessed by visualisation because the graphene coating was thick and therefore visible. Some uncoated or very thin coated patches were observed in all three immersion duration time points (Fig. 4.3ii). Increasing the immersion time period in the graphene dispersion did not improve the evenness of graphene coating, as patchy coating continued to be visible and visually to the same extent. AFM use to quantify thickness was not possible in this instance because the discs (sample) were not completely flat, which is a requirement for using AFM.

(iii) Varying dip frequency 1 x 20 secs and 4 x 5 secs dip once 50V was reached

Performing the dip-coating four consecutive times with each 50V applied voltage for 5 seconds revealed less effective graphene coating coverage with some parts of the disc appearing to be uncoated (Fig. 4.3iii). As illustrated (Fig. 4.3iii), graphene coating evenness was compromised with frequent dipping.

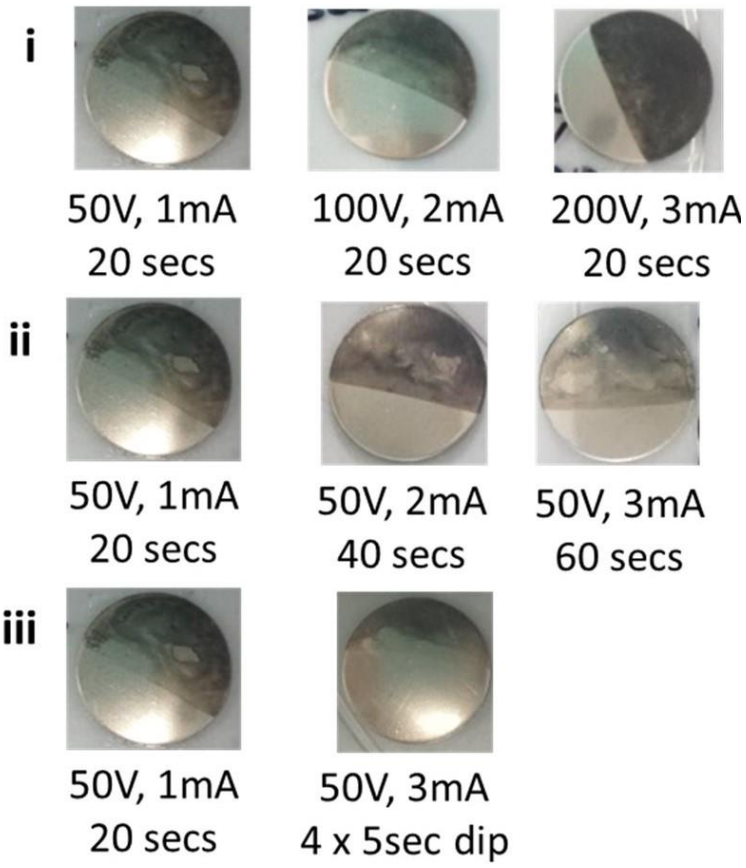

Figure 4.3: Optimising graphene coating onto stainless steel using applied voltage bias simultaneously with dip-coating. Graphene coating achieved when 14mm diameter 316L stainless steel discs were partially dip-coated in 0.3mgmL^{-1} graphene dispersion under the following conditions. (i) voltage was varied at 50V, 100V and 200 V for 20 secs once desired voltage was reached; (ii) varying disc immersion duration, 20 secs, 40secs and 60 secs once 50V was reached; and finally (iii) varying dip frequency 1 x 20 secs and 4 x 5 secs dip once 50V was reached. Images acquired using phone camera of Samsung Galaxy S4. Most optimum coating established at 200V, 3mA bias for an immersion duration of 20 seconds from the time 200V was reached. The black/dark deposit on the stainless steel denotes graphene coating.

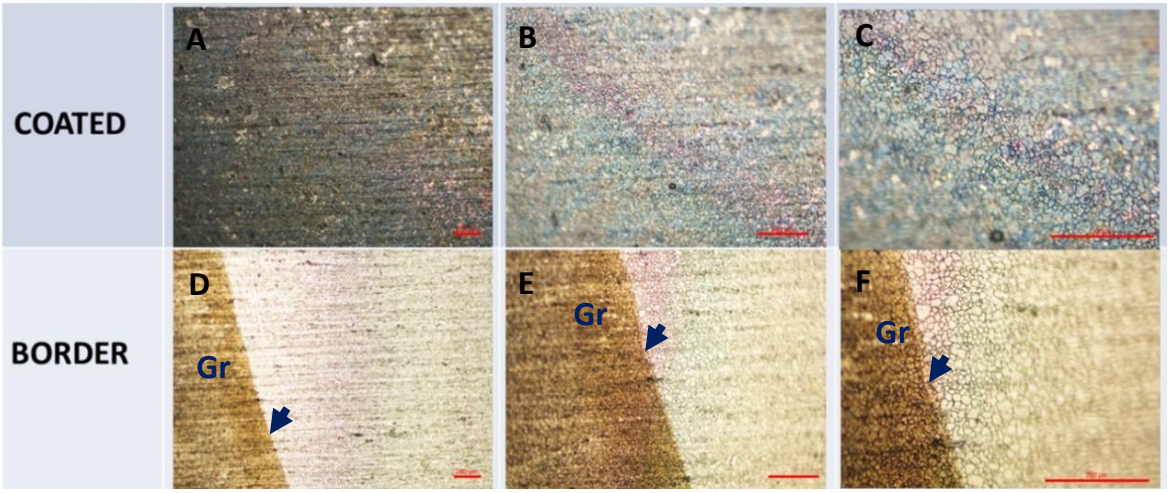

Figure 4.4: **Magnified image of partially graphene coated stainless steel disc.** Nikon Eclipse LV100 microscope was used to view the disc and the TV lens 0.55x Ds camera used to capture the images of the disc. 316L stainless steel disc was graphene (Gr) coated by partial dipping into 0.3 $mgmL^{-1}$ graphene dispersion, simultaneously applying 200V, 3mA for a duration of 20 seconds at different magnifications. **A-C:** Coated regions and **D-F:** coated/uncoated border region (arrows). Scale bars on bottom-right hand corner of each image equates to 200 µm.

Visibly, a more uniform and thick coating of graphene coating was established with application of a high voltage of 200V as opposed to longer duration of a lower voltage or more frequent dipping cycles (Fig. 4.3). Even though a more uniform coverage of coating was achieved using this method (visible to the eye but also confirmed via Raman spectroscopy), the thickness of the coating was not controllable and tended to be thick (Fig. 4.3 and Fig. 4.4). For the coating of medical implants, a thin (not visible by eye, or nm thick) coating of the graphene based material is preferable, thus a coating method achieving much thinner coating was required. Consequently, spray coating was investigated as a method for producing thin, uniform graphene based coating on medical grade stainless steel.

4.3.3 Spray coating

Spray coating has previously been described to provide homogenous coating and to allow control of the coating thickness as well as uniformity (226, 227). Figure 4.5 illustrates a stainless steel disc after spray coating of Gr, the coating is not visible by naked eye, but the presence of a carbon thin film was confirmed by Raman spectroscopy. Nine spots were selected on the disc for Raman spectroscopy. One of the nine randomly selected points on the coated disc was taken on an area without graphene coating (top panel on Fig. 4.5, area marked/indicated with red x on the disc), as shown by the absence of the G

and 2D peaks (Fig. 4.5A). The Raman spectra measured on the other eight points on the disc showed graphene specific G and 2D peaks, indicating presence of graphene (Fig. 4.5 B). This indicates the potential for thin graphene coating with relatively good coverage using the spray coating approach, however optimisation of this technique was essential to yield maximal and even coverage, particularly, to coat the coronary artery GAZELLE stents. Consequently, the next step was to investigate parameters that further improve coating by maximising coverage.

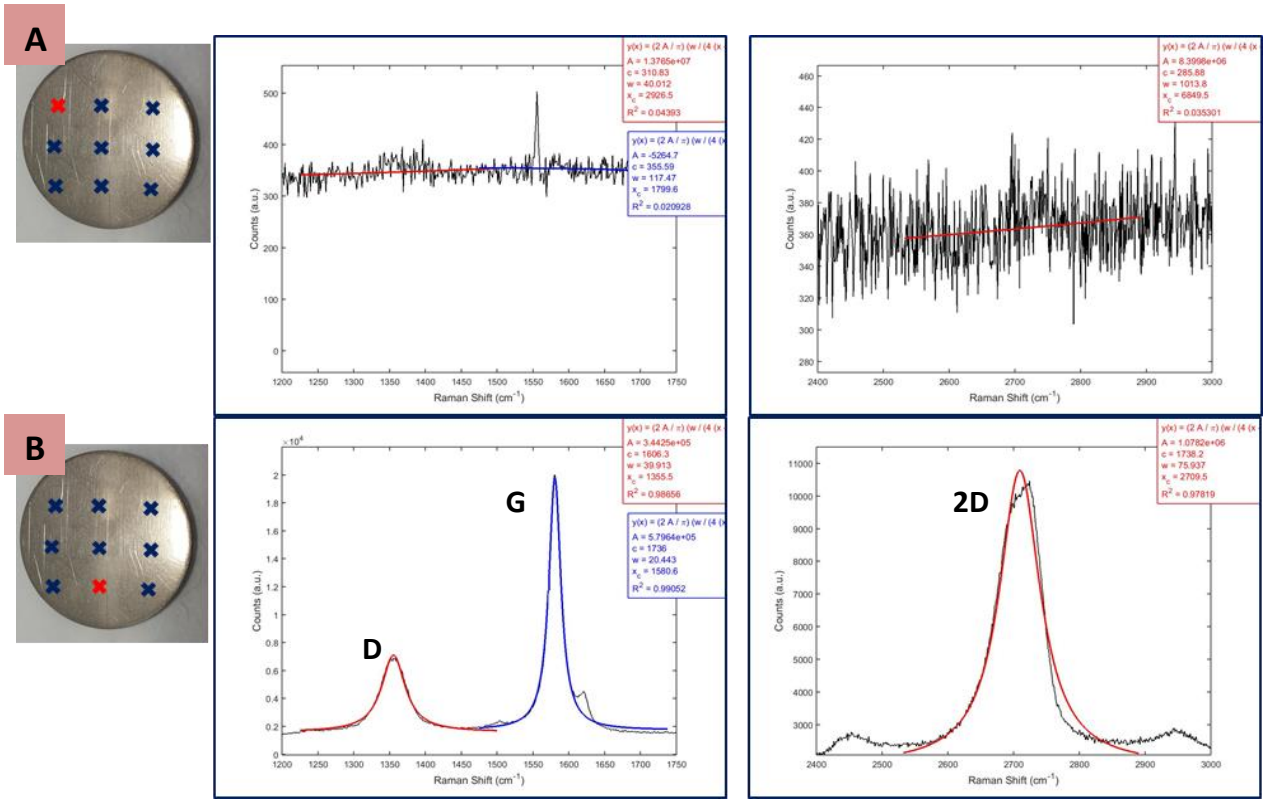

Figure 4.5: Raman spectra of graphene spray coated disc. Three layers of 0.3mgmL^{-1} LPE graphene dispersion spray coated onto a pre-cleaned 14mm diameter 316L stainless steel disc. Raman spectroscopy measurements were undertaken at 514nm excitation line. **A:** Top panel illustrates spectra from the point highlighted with a red cross on the coated disc, there was no graphene coating at this spot because there was no G or 2D peak in the spectra. **B:** The bottom panel is representative of spectra attained from eight of the nine spots Raman analysed, suggesting relatively good coverage and thin graphene coating (not visible coating). The Raman spectra of the respective position shown with a red cross on the disc is represented on the right.

4.3.4 Optimisation of spray coating of graphene onto coronary artery stents

In order to maximise graphene and graphene oxide coverage with relative uniformity on the GAZELLE stents, spray coat conditions such as pre-plasma cleaning, spray distance and various other parameter were investigated.

4.3.4.1 Plasma cleaning of stent surface

The spray coating method was repeated on GAZELLE stents (Biosensors Int.) producing coating that appeared as graphene aggregates on the coated stents (Fig. 4.6A, 4.7A). In an attempt to improve coverage and dispersibility of coating material on stainless steel GAZELLE stents, the effect of Argon plasma cleaning on the coating coverage was investigated (details in section 2.2.2.1). Plasma cleaning achieves surface cleaning by removing thin layers of natural contaminants such as hydrocarbons from the surface of the sample by bombarding high-speed argon particles onto the surface of the sample stent, consequently knocking away any contaminant particles (206). Argon was used due to its inert quality, avoiding change in surface chemistry of the stainless steel bare metal stent.

The company providing the stents (Biosensors Int.) suggested that plasma cleaning of the GAZELLE stents prior to graphene coating should decrease aggregation of coating material on the substrate surface, by promoting a more uniform coating (Fig. 4.6/4.7 A vs. Fig. 4.6/4.7 B). Raman mapping was performed, showing the presence of the Gr and GO characteristic Raman peaks (Chapter 2), confirming the coating to be made of graphene and graphene oxide. More area without graphene coating is visible on the coating without plasma cleaning (Fig. 4.6A iii/iv and 4.7A ii/iii) when compared to the pre-plasma cleaned surface coating (Fig. 4.6 B iii/iv and 4.7 B ii/iii), as is shown by the Raman maps illustrated in Figures 4.6iii and 4.7ii, and respective Raman spectra of the purple, green and blue points (circular points indicated on the Raman mapping (purple, green and blue) depicted in figure 4.6iv and 4.7iii. Figures 4.6iii and 4.7ii illustrate a larger area of higher intensity mapping after plasma cleaning (Fig. 4.6 B iii and Fig. 4.7 B ii) when compared to spray coating without pre-plasma cleaning (Fig. 4.6A iii and Fig. 4.7A ii), suggesting more coverage and less aggregate formation of coating with plasma cleaning prior to spray coating. This is confirmed when comparing percentage coverage of Gr (49.2%), GO (80%) without pre-plasma cleaning and percentage coverage of Gr (88.1%), GO (100%) after plasma cleaning. This may have been due to increased wettability/ hydrophilicity of the

surface attributed to plasma cleaning; decreasing water contact angle and thus dispersibility of the graphene based flakes once solvent had evaporated (228, 229). Decrease of contact angle means less water droplet like depositions on the stent, resulting in further distance between flakes within the spray drop, thence, leading to drop in van der Waals forces between flakes and consequently reduced agglomeration of the Gr/GO flakes that would have resulted in aggregate-like coatings (Fig. 4.6 and Fig. 4.7) (230, 231).

These results show that plasma cleaning prior to spray coating must be included in the protocol for spray coating GAZELLE stents in order to achieve dispersion of the graphene material, giving rise to a uniform coating. Surface plasma treatment prior to coating can also aid adhesion of the coating material onto the substrate, as well as improving thickness distribution, again attributed to the influence from increased dispersibility (232), but also plasma cleaning induced surface activation, leading to stronger bonding potential (233).

Even though plasma cleaning had a positive influence on maximising both uniformity and coverage of Gr and GO coating on the GAZELLE stents, it did not produce complete coverage. Thus, as a further attempt to improve coating, the spray distance between the substrate (stent) and the spray gun nozzle was studied. Spray coating up to this point had been performed from a distance of 20 cm. Subsequently, the coating was examined when Gr/GO dispersion was spray coated from a height of 10 cm.

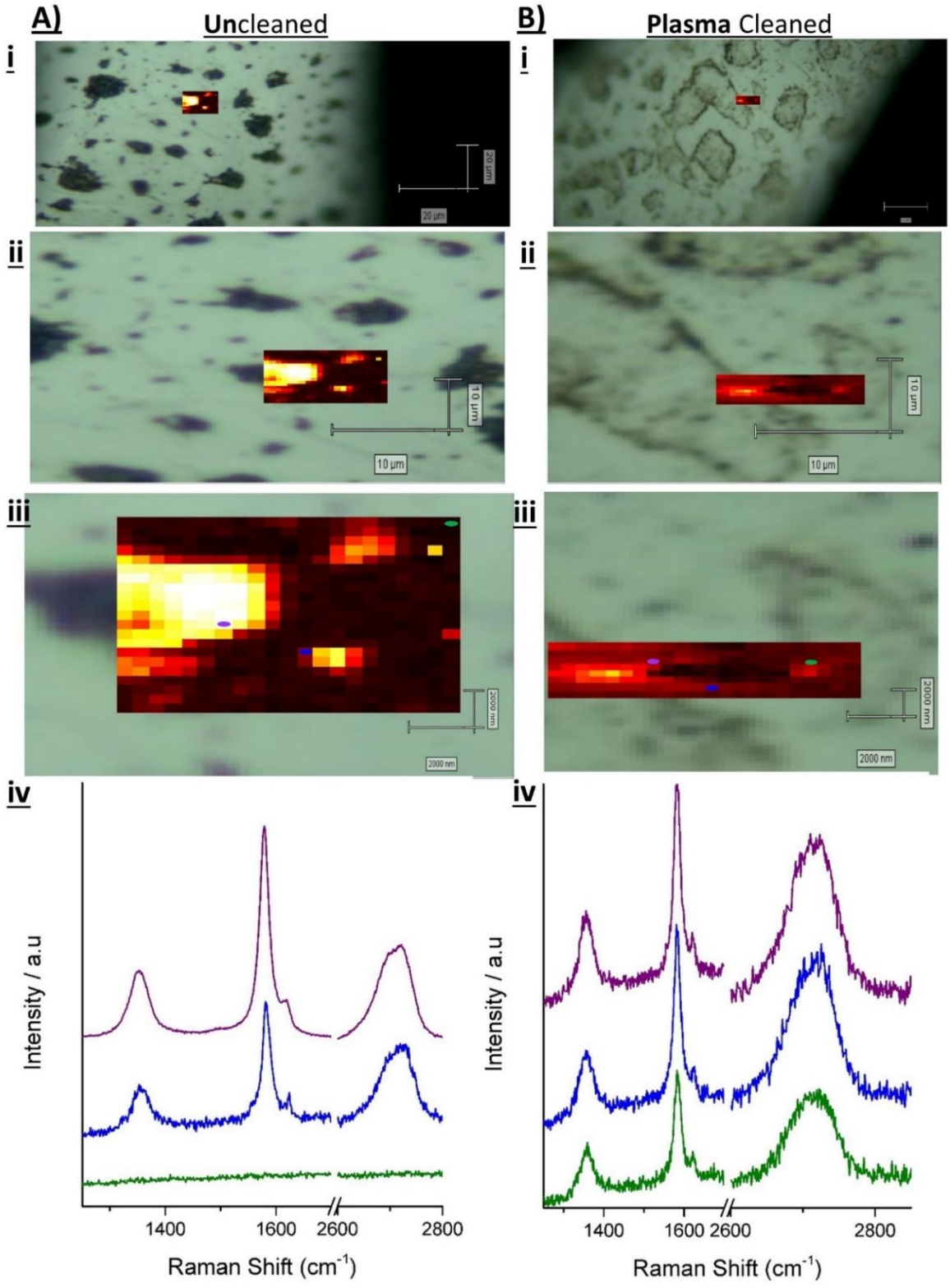

Figure 4.6: Plasma cleaning prior to graphene coating improves coating dispersibility.
A) Spray coating without pre- plasma cleaning and **B)** WITH pre-plasma cleaning. Plasma cleaning using Argon gas for 2 minutes. GAZELLE stainless steel stents were spray coated with 1 mL graphene dispersions at 0.4 $mgmL^{-1}$ concentration. The height from which dispersion was sprayed onto the stent was 20cm height, hotplate temperature at 75 °C. Optical image (i-iii); Raman spectroscopy mapping illustrating distribution of coating (white/yellow/red denotes coating, black area indicates no graphene coating) (i-iii). **iv:** Illustration of representative Raman spectra, colour coded corresponding to spots on iii.

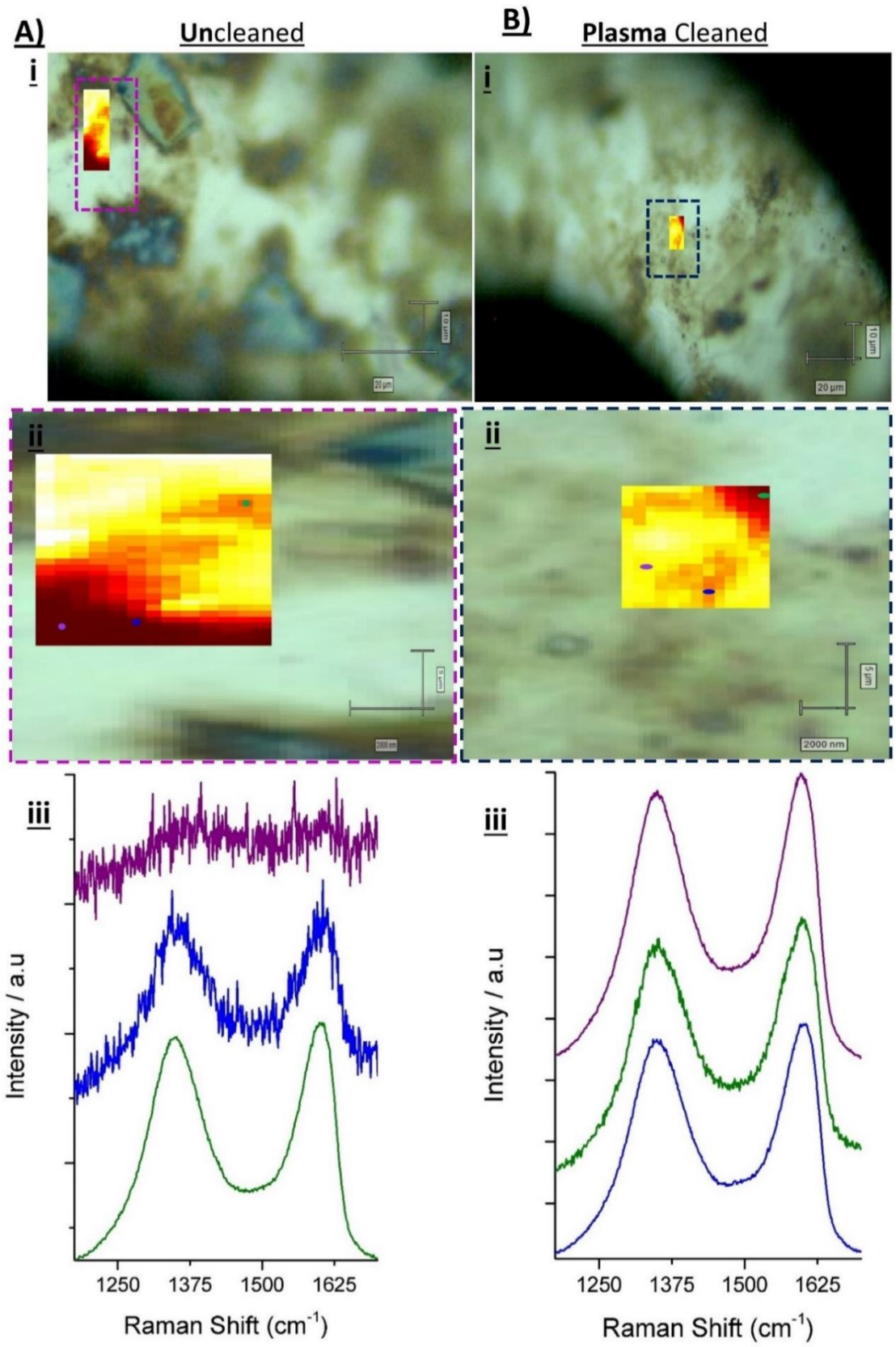

Figure 4.7: Plasma cleaning prior to GO coating improves coating dispersibility.

A) Spray coating without pre- plasma cleaning and **B)** WITH pre-plasma cleaning. Plasma cleaning using Argon gas for 2 minutes. GAZELLE stainless steel stents were spray coated with 1 mL GO dispersions at 0.4 $mgmL^{-1}$ concentration. The height from which dispersion was sprayed onto the stent was 20cm height, hotplate temperature at 75 °C. Optical image (i-ii); Raman spectroscopy mapping illustrating distribution of coating (white/yellow/red denotes coating, black area indicates no GO coating) (i-ii). **iii:** Illustration of representative Raman spectra, colour coded corresponding to spots on ii.

4.3.4.2 Determination of spray distance for graphene coating onto stents

The height from which the graphene dispersion is sprayed onto the stent has been described as the main factor affecting uniformity of the coating (234, 235). The distance from which to spray the graphene dispersion onto the substrate was therefore investigated. In the Casiraghi group, spray coating distance of 20cm were being studied, for coating of various materials, including graphene, for non-biomedical purposes. As an initial starting point, a spray distance of 20 cm was investigated followed by half the distance to promote higher coating coverage by means of reducing spread. Spray distance of 20 cm and 10 cm were investigated by preparing a chamber of height 20 cm and 10 cm (Fig. 2.4). An improved graphene coverage was observed with the shorter spray distance, 88.1%/100% (Gr/GO) at 20 cm versus 99.1%/99.8% (Gr/GO) at 10cm, (Fig. 4.8B and 4.9B), as well as a reduced spray volume requirement; 1.0 mL of Gr and GO at 20 cm versus 400 µL of Gr and GO dispersions at 10 cm, both at 0.4 $mgmL^{-1}$. The coverage of the spray coated stents was examined by Raman spectroscopy mapping, measured at 0.5 µm intervals, denoting improved coverage (Fig. 4.8A iii/iv versus Fig. 4.8B iii/iv and 4.9A ii/iii versus 4.9B ii/iii). At 10 cm spraying distance (Fig.4.8B and 4.9B), a lower volume of both graphene and graphene oxide was required to produce optimal covered and relatively uniform coating (demonstrated as reduced variation of Raman mapping colours (2D peak intensity) when compared to spraying at 20cm distance (Fig. 4.8A and 4.9A). Complete coverage was demonstrated with 10 cm spray distance (99.1% (Gr)/99.8% (GO)) and less Gr/GO dispersion.

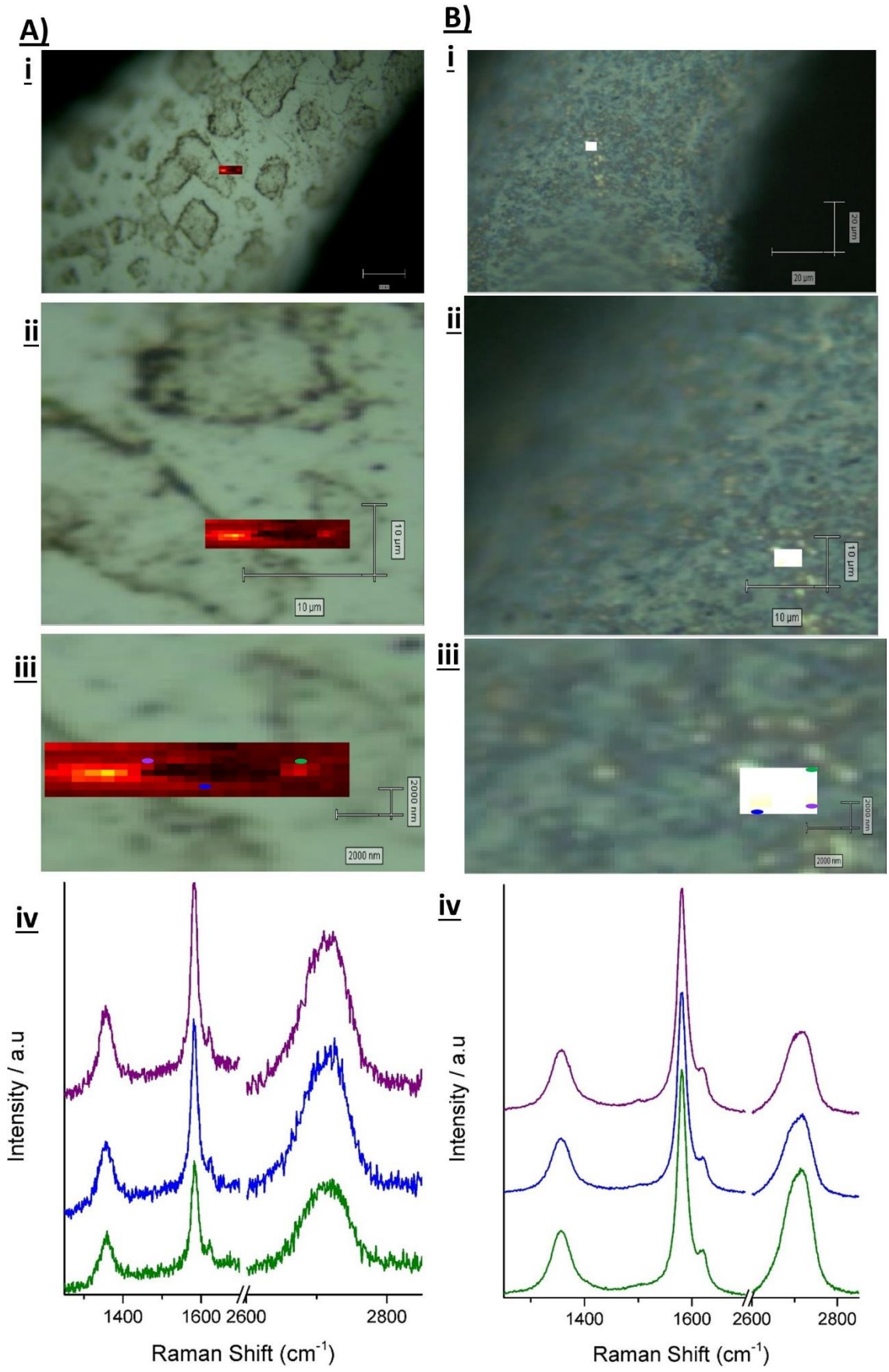

Figure 4.8: Spray coating from a shorter distance achieved complete graphene coverage. **A)** Spray coating from a height of 20 cm using 1.0 mL graphene at 0.4 mgmL^{-1} **B)** Spray coating from a height of 10 cm using 0.4 mL graphene at 0.4 mgmL^{-1}. Hotplate temperature at 75 °C. Optical image (i-iii); Raman spectroscopy mapping illustrating distribution of coating (white/yellow/red denotes coating, black area indicates no graphene coating) (i-iii). **iv:** Illustration of Raman spectra, colour coded corresponding to spots on iii.

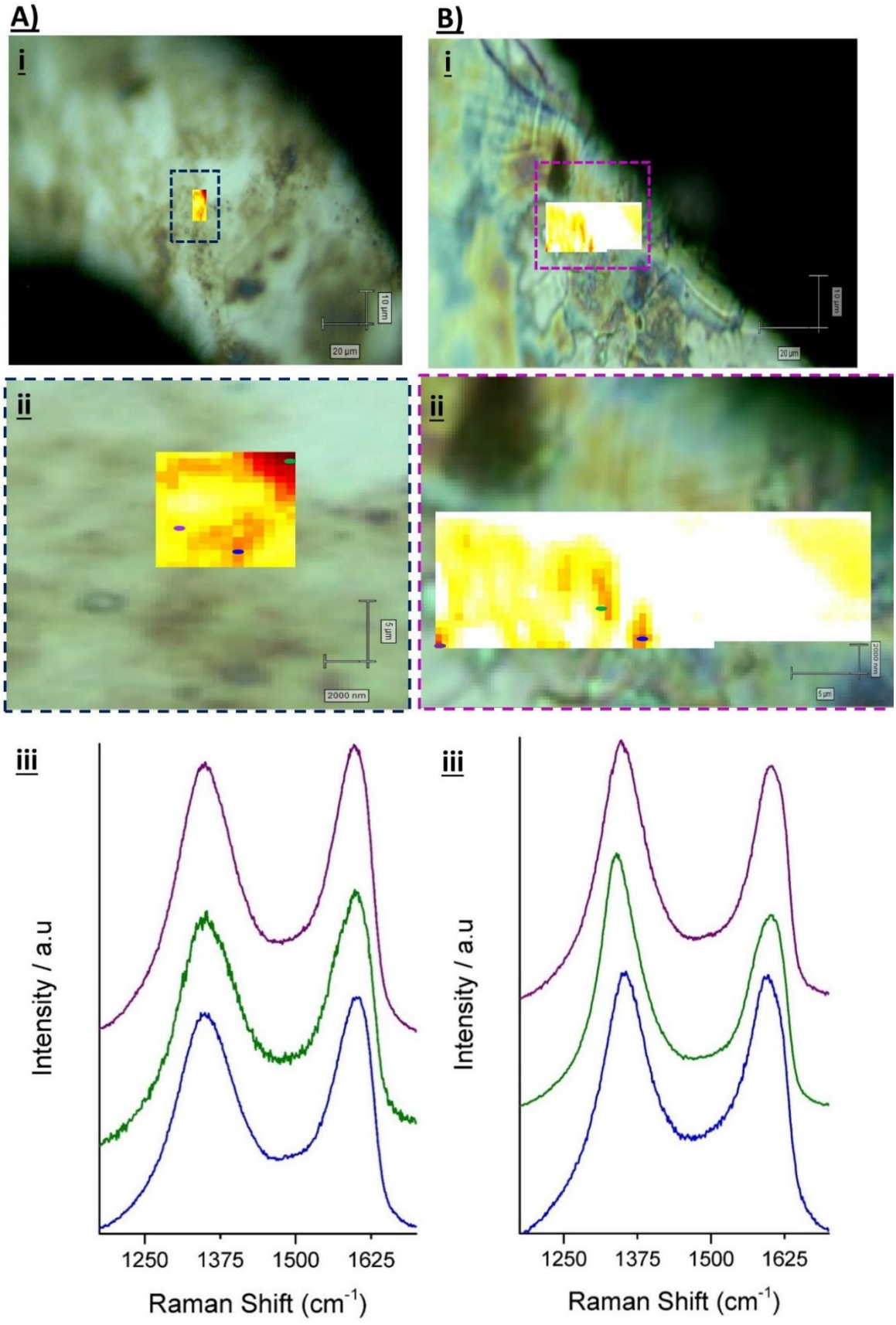

Figure 4.9: Spray coating from a shorter distance achieved complete GO coverage. **A)** Spray coating from a height of 20 cm using 1.0 mL GO at 0.4 mgmL^{-1} **B)** Spray coating from a height of 10 cm using 0.4 mL GO at 0.4 mgmL^{-1}. Hotplate temperature at 75 °C. Optical image (i-ii); Raman spectroscopy mapping illustrating distribution of coating (white/yellow/red denotes coating, black area indicates no GO coating) (i-ii). **iv:** Illustration of Raman spectra, colour coded corresponding to spots on ii.

4.3.4.3 Scanning electron microscopy of spray coated GAZELLE stents

Stents coated with graphene and graphene oxide, were viewed under the SCEM as an additional approach to examine the graphene and graphene oxide coating compared to the uncoated (water coated) stents. Gr and GO coating was visible on the stent by the round-like material deposited on the stent surface, this perhaps illustrating small Gr (Fig. 4.10 D-F) and GO (Fig. 4.10 G-I) aggregates, this was absent in the uncoated stents (Fig. 4.10 A-C).

The 'uncoated' stents were treated with the identical coating conditions as the coated stents but were sprayed with distilled milliQ water rather than Gr or GO, in order to minimise the introduction of variation and bias; dH_2O ('uncoated') vs Gr vs GO.

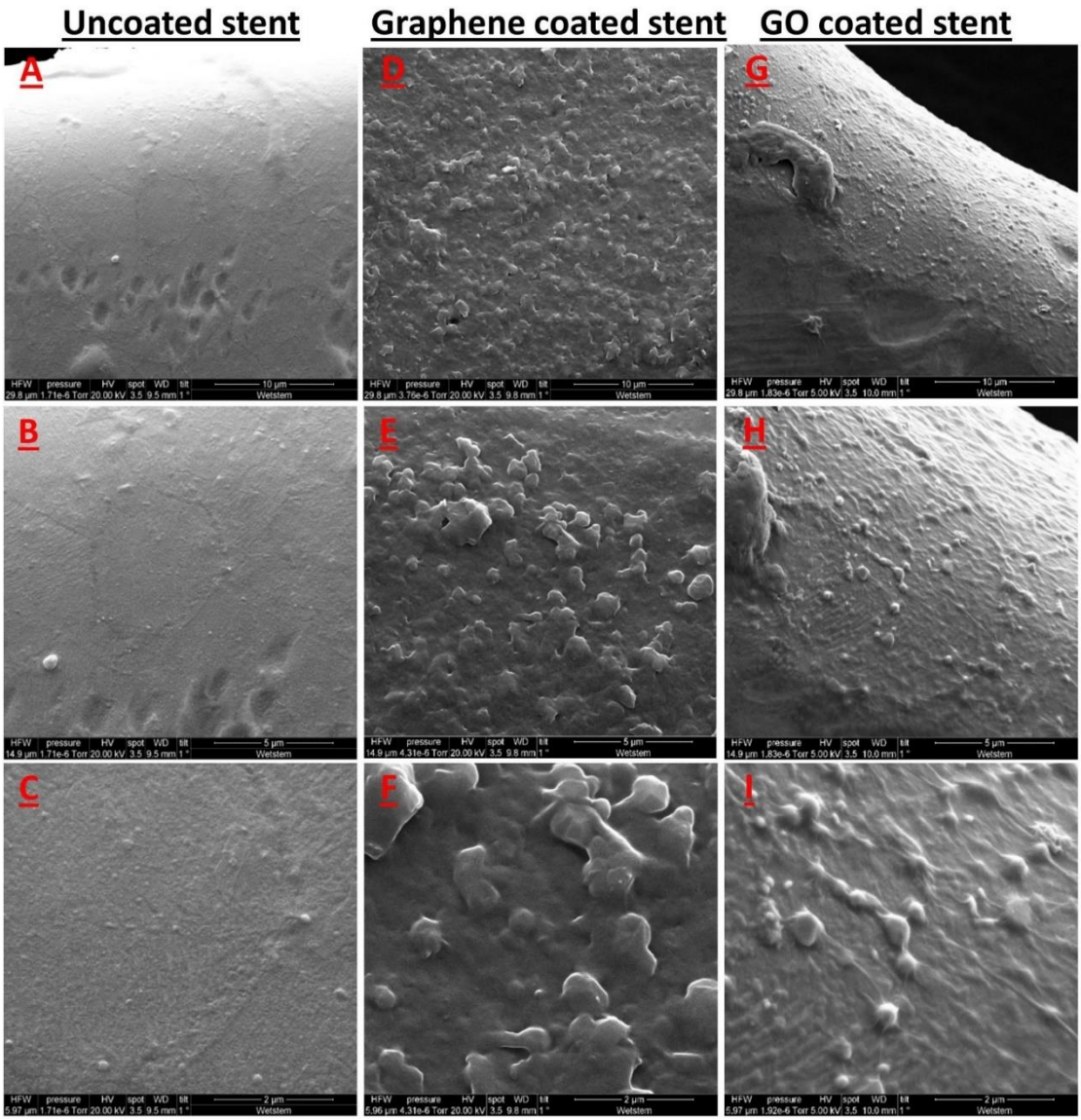

Figure 4.10: Scanning electron microscopy illustrating surface topography of uncoated vs coated stents. A-C: 'Uncoated stent' – spray coated with distilled H_2O. **D-F:** Surface of Gr spray coated stent (0.4 mL at 0.4 $mgmL^{-1}$, 10cm). **G-I:** Surface of GO spray coated stent (0.4 mL at 0.4 $mgmL^{-1}$ 10 cm). Scale bar denoted at bottom right hand side, from top to bottom: 10µm, 5 µm, 2 µm.

In summary, figure 4.11 clearly illustrates the improvement in percentage coverage of Gr/GO coating with pre-plasma cleaning of the GAZELLE coronary artery stents. While optimum coverage was achieved with this step for GO, further optimisation steps were necessary for graphene coating. Reducing the spray distance not only saved valuable Gr and GO dispersions but also achieved the optimum, complete Gr/GO coverage of the stent (Fig. 4.11).

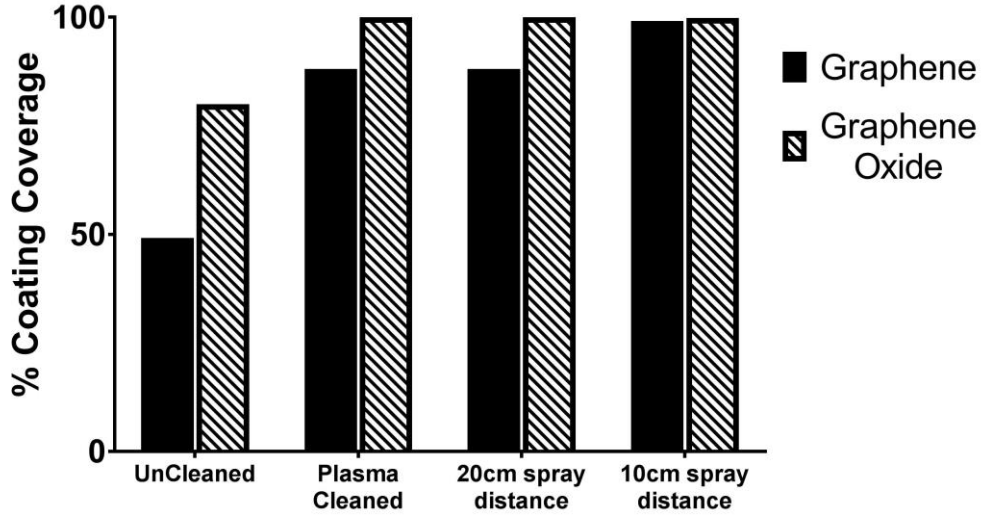

Figure 4.11: Improving percentage coverage of Graphene and Graphene Oxide on the GAZELLE coronary artery stents by incorporation of optimisation steps. Summary of the optimisation steps demonstrated as % coating coverage: Without plasma cleaning (Uncleaned) and with pre-plasma cleaned stent surfaces in addition to investigations of spray distance.

4.3.5 Evaluating the graphene and graphene oxide coating on the GAZELLE stent

4.3.5.1 Determination of longevity of Gr and GO coating onto stent surface

A thin layer of graphene or graphene oxide on medical implants should be adequate to provide an impermeable membrane between the metal and the biological conditions (236, 237). The thicker a coating the more susceptible it may be to wear as the outer coating layer has no direct interaction with the substrate itself but rather interacting with the underlying graphene coats. To determine if the Gr/GO coating is stable on the stent and whether it remains intact on the stent, coated stents were immersed into cell culture media and aggitated on a shaker for 7 days. Both the stents and the effluent media were examined for graphene and graphene oxide presence using Raman spectroscopy (Fig. 4.12). Raman spectroscopy of the drop-cast effluent media did not detect any graphene signature peaks at 2700cm^{-1} and 1600 cm^{-1} and Raman mapping of the coronary stent surface demonstrated 100% of graphene coverage in three of the randomly selected areas on the stent. This illustrated intact graphene coating onto the stent.

In addition, adhesion of coating onto stent was futher examined by Raman mapping of coated stents after culture for 14 days pinned onto porcine aortic tissue at 37 ˚C and 5% CO_2 (Fig. 4.13). Intact graphene and GO coating on the stent surface was detected after both 7 days washing under high agitation and post 14 days in culture, suggesting strong adhesion of the coating material onto the GAZELLE bare metal stent. However, small areas of thinner GO coating were observed in figure 4.13B, indicating possible partial denudation of the GO coating after 14 days of culture, even though percentage coverage of both Gr and GO on the stent remained at 100%.

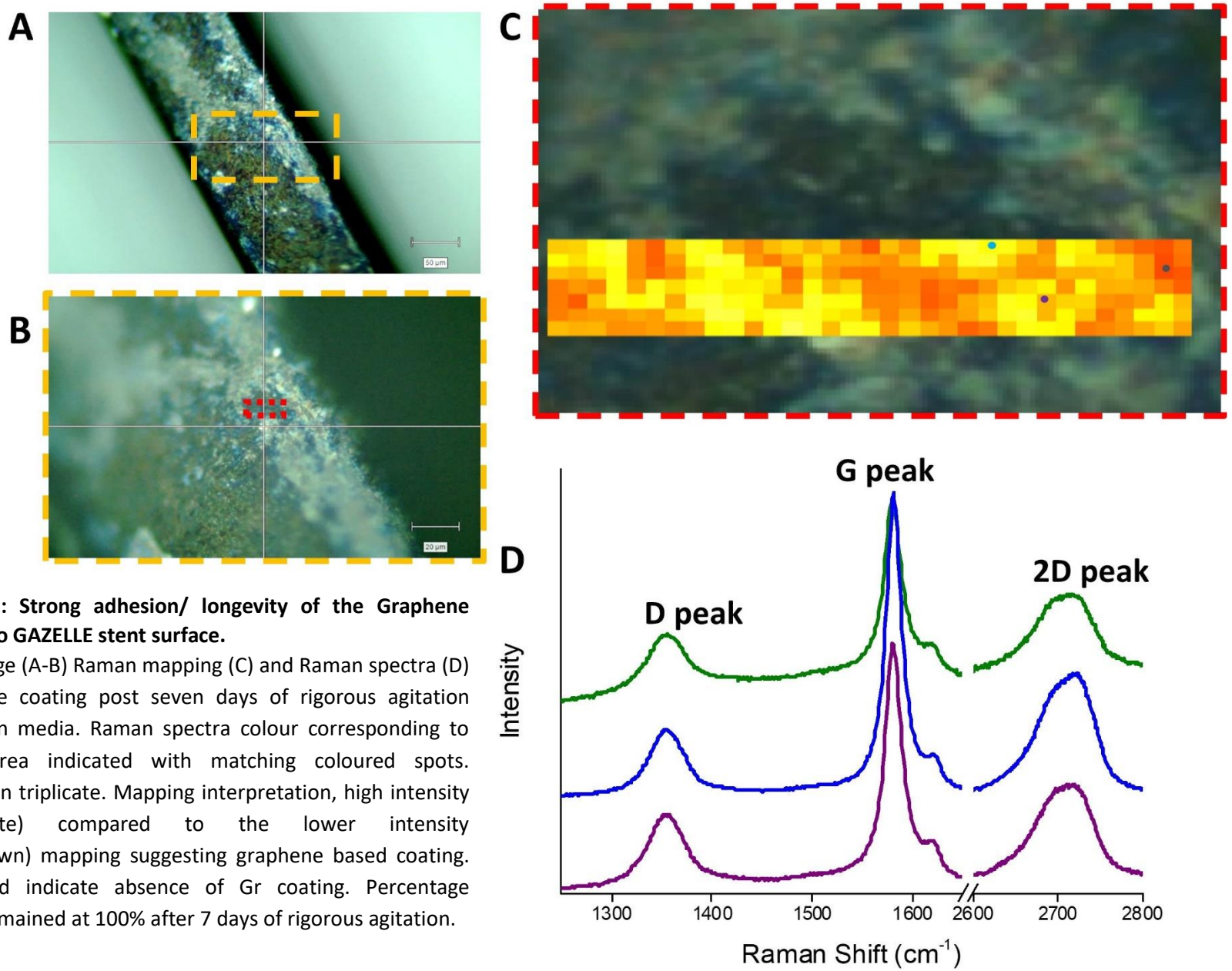

Figure 4.12: Strong adhesion/ longevity of the Graphene coating onto GAZELLE stent surface.

Optical image (A-B) Raman mapping (C) and Raman spectra (D) of graphene coating post seven days of rigorous agitation immersed in media. Raman spectra colour corresponding to mapping area indicated with matching coloured spots. Performed in triplicate. Mapping interpretation, high intensity (yellow/white) compared to the lower intensity (darker/brown) mapping suggesting graphene based coating. Black would indicate absence of Gr coating. Percentage coverage remained at 100% after 7 days of rigorous agitation.

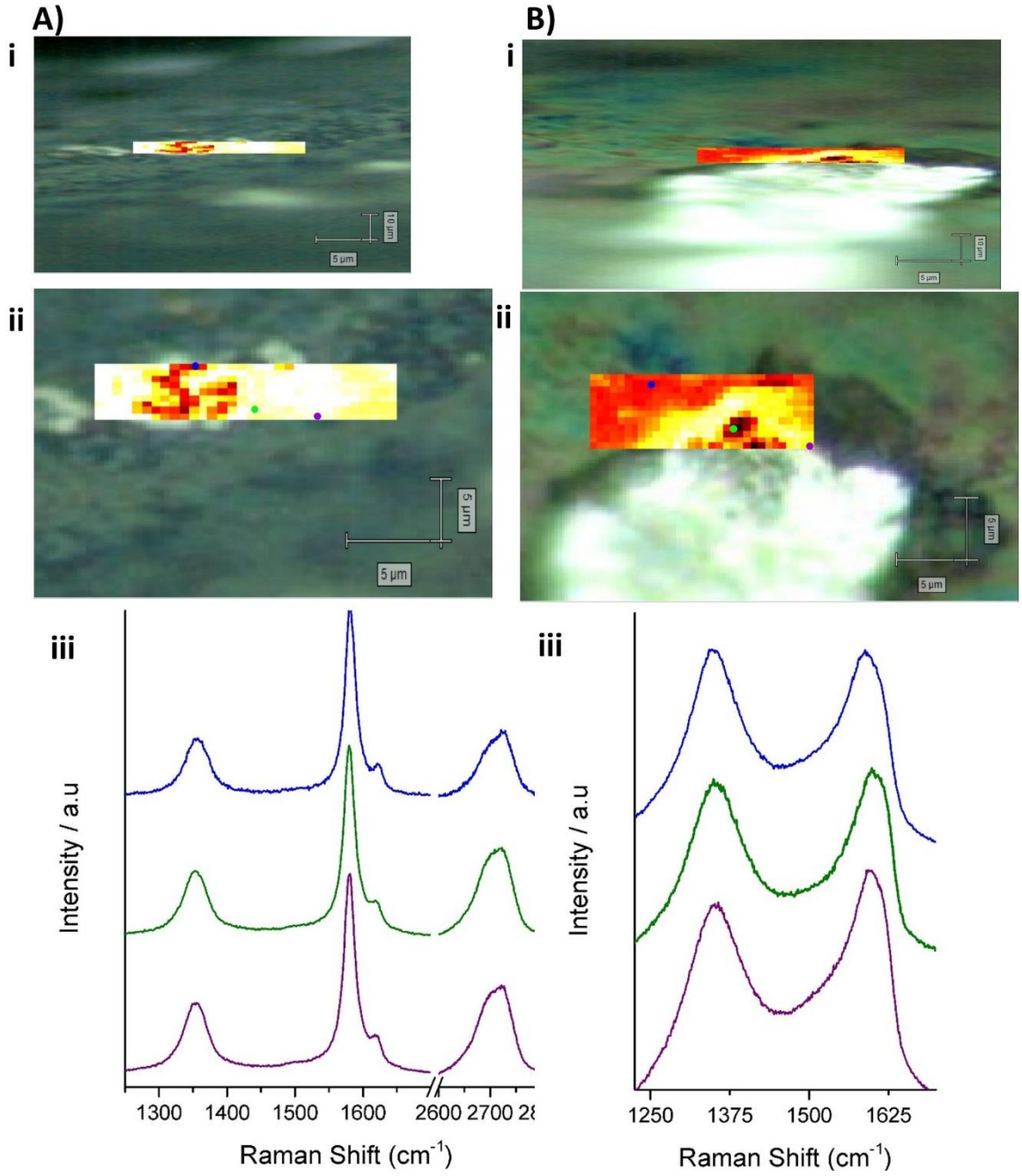

Figure 4.13: Determination of longevity of Gr and GO on stent surface.

A) Porcine aortic tissue facing surface of Gr and **B)** surface of GO. Gr/GO coated stents analysed by Raman spectroscopy. **i-ii:** Optical images with Raman mapping. White/ yellow/ red denotes coating, black area indicates no Gr/GO coating. **iii:** Raman spectra colour corresponding to mapping area indicated with matching coloured spots on ii. Analysing each point in the mapping region revealed 100% coverage with Gr/GO.

4.3.5.2 Sterilisation by Ultraviolet radiation does not influence graphene and graphene oxide coating as determined by Raman spectroscopy

The potential effect of ultraviolet irradiation on graphene and graphene oxide coating has not been widely investigated. For the purpose of *in vitro* and *ex vivo* use of the stents, sterilisation is essential. Assessment of the possible influence of UV irradiation with the purpose of sterilisation for biomedical use requires assessment prior to undertaking *in vitro* and *ex vivo* investigations. Raman spectra for Gr and GO coated stents before and after UV irradiation (4 minutes at 40W) was studied to determine if there was an effect on the Gr/GO surface chemistry.

No peak shifting and no peak changes were observed, i.e. ratio of the I(D)/I(G) peak observed when comparing D and G peaks before and after 4 minutes of UV irradiation (Fig. 4.14). If there were any changes induced by UV irradiation, such as reduction (removal of oxygen groups from the graphene flakes), the D peak would have decreased significantly to the G peak. It has been reported that GO would be more susceptible to structural changes when compared to graphene due to the ability of the UV irradiation to break the C-O bond whereas it is incapable of breaking the C-C bonds in graphene (238). UV sterilisation did not appear to affect the Raman spectra of either graphene or graphene oxide, suggesting stability of the Gr and GO coating post UV sterilisation.

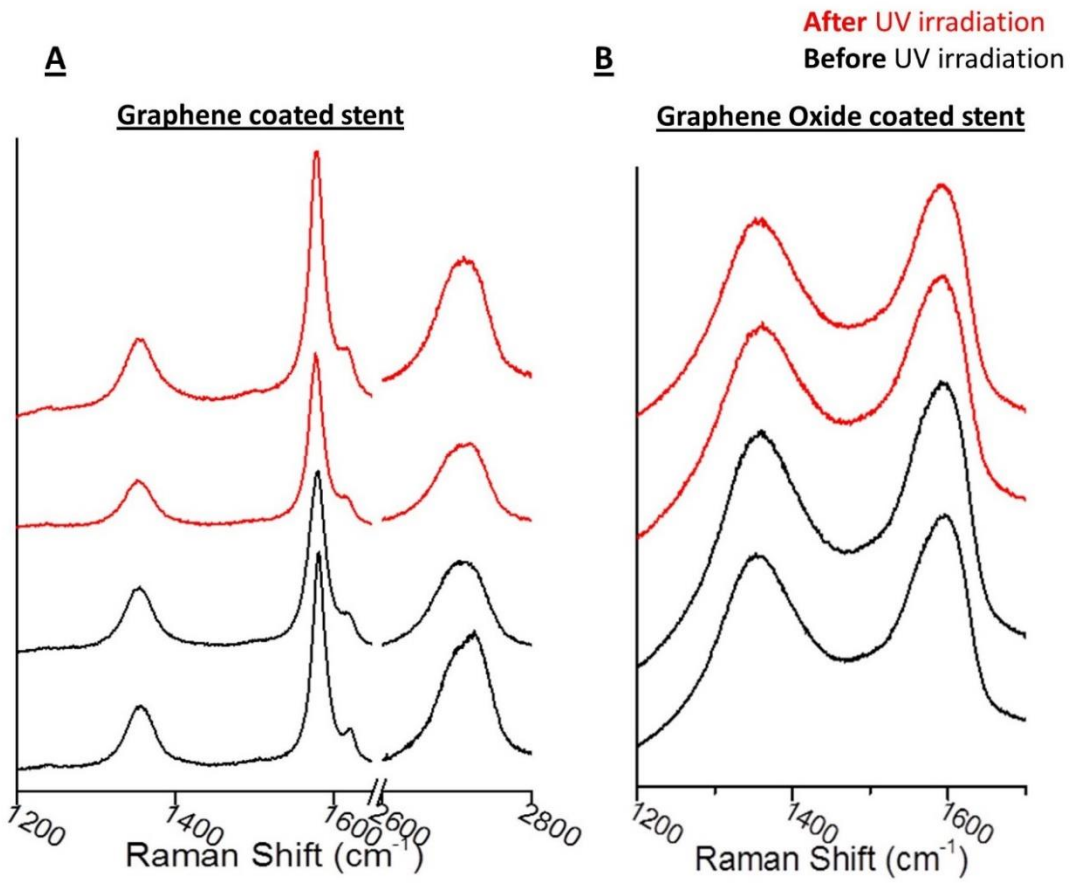

Figure 4.14: UV irradiation did not cause any structural changes to the Gr and GO coatings on the stent. UV irradiation at 40W for a duration of 4 minutes proved to have no effect on **A:** Graphene and **B:** GO, as studied under Raman spectroscopy.

4.4 Conclusions

The second objective for this project was to prepare an optimal graphene based coating of stainless steel bare metal stents. This required selecting an optimal coating method, which mandated a few techniques to be trialled. In this chapter, several techniques were investigated with the final aim of obtaining a thin and uniform film of Gr and GO, offering maximal coverage of the coronary stent.

Spray coating was optimised and standardised for each spray coating of GAZELLE stents. The following parameters produced the highest coverage, dispersibility and uniformity: 10 cm spray distance, 400 µL at 0.4 mgmL^{-1} graphene or graphene oxide dispersion (with 90˚ x-axis rotation of the substrate at each 100µL spraying), substrate temperature of 75 ˚C, spray duration of 60-80 minutes and added 15 minutes annealing time at the end. The annealing temperature allows for solvent evaporation and improved adhesion of the graphene based coating onto the stent as had been previously reported although at significantly higher temperatures (239).

As reported previously, graphene has remarkable properties including metal leaching, wear and friction protection, which are ideal properties for application in blood flow environment where shear/force and pH variations exist (200, 240). To our knowledge, this is the first study to report on the stability of both graphene and GO coating under ultraviolet radiation. The results also demonstrate the longevity, durability and low wear of the Gr and GO coatings on the stainless steel stent in stressed fluid flow environment as is consistent with the anti-wear property of graphene (165).

4.5 Limitations

Contrary to our study, some changes have been reported by others, however the limitation of this project is that a complete examination of the effect of UV were not performed. This could be performed by X-ray photoelectron spectroscopy (XPS) analysis, which determines the exact composition of the material. This was out of the scope of this PhD project due to 1) time restriction and 2) outside the theme/focus of this project.

4.6 Key findings

- Spray coating was selected as the optimal technique to produce the thinnest, uniform and largest stainless steel substrate coverage with LPE Gr/GO.
- Spray coating of GAZELLE stainless steel was optimised at spraying 0.4 $mgmL^{-1}$ of 400 µL Gr or GO dispersion at 10 cm (spray distance), 75 ˚C, spray duration of 60-80 minutes onto pre-plasma cleaned GAZELLE bare metal stents.
- Coating longevity was shown to be satisfactory in the laboratory settings, with coating remaining on the stent.
- UV sterilisation does not affect graphene or graphene oxide surface chemistry.

CHAPTER 5

Human coronary artery endothelial cell adhesion and proliferation on graphene and graphene oxide coated coronary stents

5.1 Introduction

The arterial endothelium exhibits selective permeability between blood and the underlying tissue. It is capable of secreting molecules that regulate inflammation, thrombosis, vascular remodelling and tone (241). As described in chapter 1.4, expansion of coronary artery stents as a therapeutic strategy to tackle CAD, leads to denudation of endothelial cells. After deploying DES, re-endothelialisation is delayed, exposing the intimal layer to blood components, including platelets, that adhere and lead to thrombosis (77, 78). It has been described that the erosion of the endothelial layer leads to a surge in smooth muscle cell migration and proliferation that dwindles once the endothelium is re-established (10). The endothelium consequently is paramount to the healthy function of the vasculature. Re-establishing the endothelium after injury is a critical step in healing the vessel wall following stent deployment. Thus, there is a requirement of studying endothelial cell adhesion and proliferation on novel coronary artery stent designs.

The chemical composition, size and shape of nanomaterials are some of the factors associated to cytotoxicity, as has also been documented of the interaction of cells, tissues and organisms with carbonaceous materials (242). To this end, biocompatibility of graphene based coatings on the coronary artery stent necessitate confirmation. Others in the literature have, however, documented healthy cell adhesion, growth and function on graphene based coatings of medical implants (194, 196, 197, 243).

In this chapter coronary artery endothelial cell adhesion and growth will be investigated *in vitro* on uncoated control, Gr and GO coated bare metal stent segments, in order to determine any influence from the graphene and graphene oxide coating on the endothelial cell adhesion or proliferation.

5.1.1 Chapter objectives

The objective of this chapter is to investigate the effect on human coronary artery endothelial cell (HCAEC) adhesion and proliferation from Gr or GO coated stent segments in comparison to uncoated control stent segments.

1) To determine whether Gr and GO coated GAZELLE stent segments influence HCAEC adhesion after 1 day of *in vitro* culture.

2) To determine whether Gr and GO coated GAZELLE stent segments affect HCAEC proliferation after 8 days (compared to 1 day culture) of *in vitro* culture.

5.2 Methods

Human coronary artery endothelial cells (HCAEC) are anchorage-dependant cells that require surface adhesion for survival and proliferation (244). As is described in chapter 2, 5000 HCAECs were seeded into a tissue culture well of approximately 100 mm^2 base area at Day 0, equating to a cell density of 50 HCAECs/mm^2. It should of course be considered that this area encompasses a resin base and coronary stent segment. The resin base was used to prevent stent segments from floating into the culture medium. UV sterilised uncoated control (dH_2O sprayed GAZELLE stent segment) and Gr or GO coated (GAZELLE) stent segments were each positioned into separate wells. Three replicates in each experiment were included: Uncoated (dH_2O spray coated), graphene coated and graphene oxide coated stent segments.

HCAECs were cultured for one day and eight days. HCAECs were cultured for eight days in order to allow ample time for metal leaching or any other potential impact from either the stents or the coatings to affect proliferating HCAECs. HCAECs were fixed one day after seeding in order to assess HCAEC adhesion and obtain 'baseline cell numbers' for later proliferation calculation. Fixation was also performed at eight days post-seeding, followed by phalloidin (f-actin, green) and Hoechst 33342 (DNA, blue) staining (details in chapter 2). Subsequently, numerous fields of view were imaged, covering the whole of the stent. Since it was not possible to completely flatten the stent segments, areas of the fluorescent images did appear out of focus requiring several images of the same field of view to be captured after adjusting focus.

Due to the uneven stent surface, overall stent area and cell count was not determined. Cell density (HCAEC count per stent mm^2 area) was therefore determined. Each experiment was performed using endothelial cells of similar passage, performed in triplicate and repeated three times, (n=3). Cell density results are presented as mean± SEM.

5.3 Results

5.3.1 Human coronary artery endothelial cell viability/adhesion onto Gr/GO coated and uncoated stent segments

Human coronary artery endothelial cell adhesion and viability was assessed by determining HCAEC number per mm^2 area of uncoated/coated stents, 1 day after cell seeding versus seeding cell density at day 0. Human coronary artery endothelial cells were seeded at a density of 50 HCAECs/mm^2 and one day later calculated to have a HCAEC density of 18.7±5.4, 13.8±5.6 and 23.6±3.5 (HCAECs/mm^2) on uncoated, Gr coated and GO coated stent segments, respectively. HCAEC density (HCAECs/mm^2) at day 1 compared to the seeding density appears to be substantially lower. Comparing HCAECs per mm^2 of each stent area at day 1, there were no significant difference identified between the groups (Control vs. Graphene, Control vs. Graphene Oxide and Graphene vs. Graphene Oxide), even though impaired as compared to seeding density (Fig. 5.1).

5.3.2 Proliferation of human coronary artery endothelial cells

In order to assess proliferation of HCAECs, an increase of cell density from day 1 to 7 days later was studied. Overall, an increase in cell density was evident in all groups from day 1 to 7 days later, with a 30 fold increase in HCAECs/mm^2 on the uncoated and GO coated stent segments (Fig. 5.1B). Of note, substantially higher number of HCAECs on the graphene coated stent segments was observed, with 70 times more HCAECs per mm^2 of graphene coated stent segment at day 8 than day 1. A substantial increase of HCAEC count per mm^2 is attributed to the proliferation of cells during the 8 days in culture (Fig. 5.1).

The capacity of HCAECs to proliferate on each stent group was assessed and compared to each other at day 8, revealing a significantly higher HCAEC density on the graphene coated stent segments (1099±158 (HCAECs/mm^2)) compared to both uncoated and GO coated stent segments (Fig. 5.1). Statistically, the influence of Gr/GO coating and culture conditions on HCAEC proliferation was analysed using the one-way ANOVA test, and HCAEC count/mm^2 at day 8 demonstrated significance, $p=0.005$. Subsequent post-hoc Turkey test revealed a significantly higher HCAEC count/ mm^2 on the graphene coated stent segments at day 8 compared to both control uncoated stent segments (1099±158 vs. 505±127 HCAEC count/mm^2, respectively; $p=0.01$) and GO coated stent segments (1099±158 vs. 703±136 HCAEC count/mm^2, $p=0.03$)), n=3 (Fig. 5.1). This is an approximate

doubling of HCAEC count per mm^2 stent area on the graphene coated versus on the uncoated stent segments (Fig.5.1B).

5.3.3 Human coronary artery endothelial cell morphology

Cell morphology was studied by observation of the cell via the cell actin-f staining. There appeared to be no difference in the shape of the cells cultured on Gr and GO coated and uncoated stents, although it was difficult to examine this appropriately as substrate was not completely flat resulting in difficulty acquiring completely focused and clear fluorescent images on each field of view.

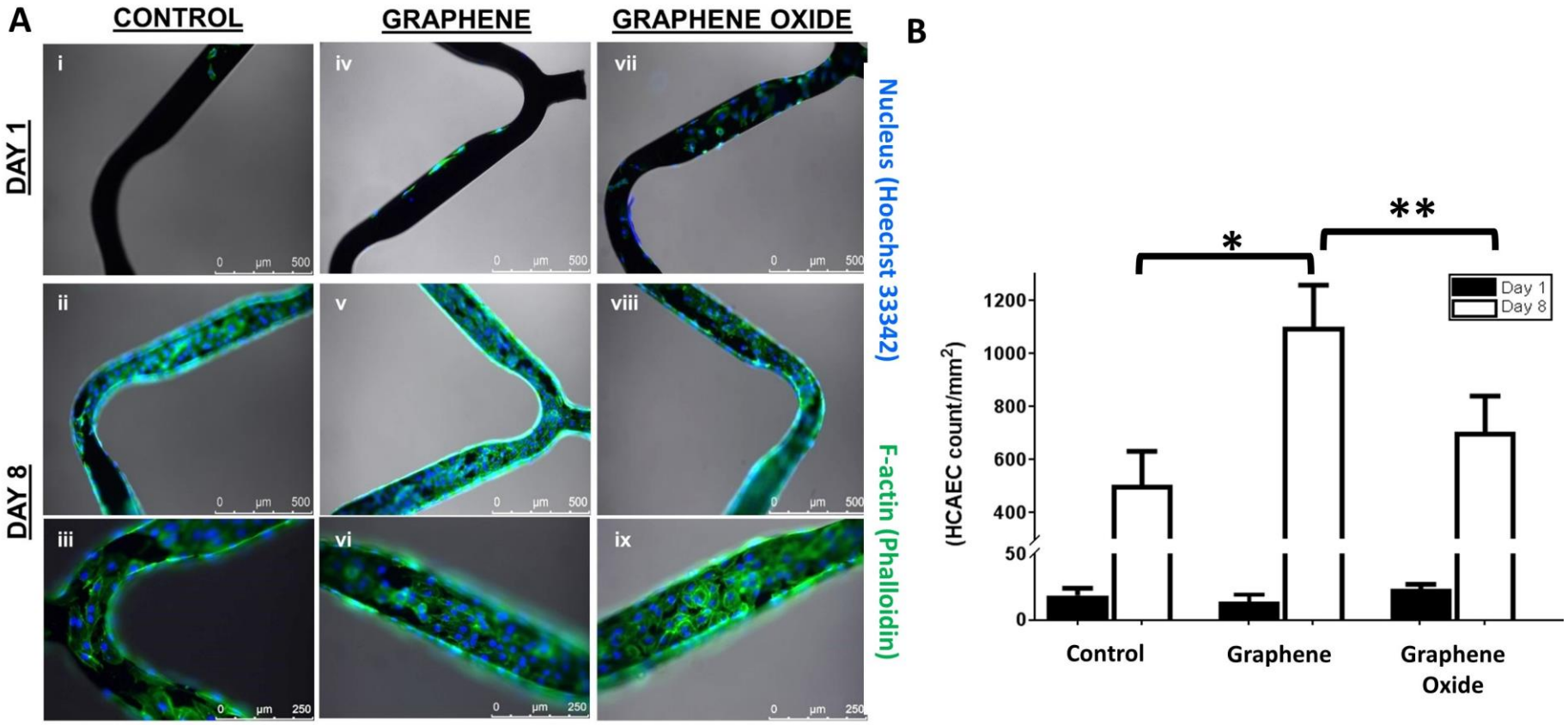

Figure 5.1: Proliferation of human coronary artery endothelial cells (HCAEC) on uncoated control, graphene (Gr) and graphene oxide (GO) coated stents. **A:** Fluorescent images illustrating coverage and cell morphology of HCAECs on uncoated control (i-iii), Graphene coated (iv-vi) and Graphene Oxide coated (vii-ix) GAZELLE stent segments. DNA stained using Hoechst 33342 (blue fluorescence) and Actin-F stained using phalloidin (green fluorescence). Fluorescence images acquired using the LEICA DFC 30000 G camera. Scale bar = 500µm (top two panels); 250 µm on the bottom panel (n=3). **B:** More endothelial cells were detected per mm^2 area on graphene coated stents than both uncoated control stent segments and graphene oxide coated stents. Cell count and stent area of each stent was measured, and results illustrated as HCAEC count/mm^2. HCAEC count/mm^2 at day 1 in comparison to day 8 was significantly higher in all groups, indicating proliferation of HCAECs on all uncoated and Gr/GO coated stent segments. Significantly higher HCAEC count/mm^2 of graphene coated stent segment was observed when compared to uncoated control (*) and GO coated stents (**), $P<0.05$, n=3. Error bars denote variability of the three repeats, standard error of mean (SEM).

5.4 Discussion

In order to assess the adhesion and proliferation of cells on graphene and GO coatings, it was essential to study biologically relevant cells to coronary artery and restenosis. The first objective of this chapter was to study human coronary artery endothelial cell adhesion (or survival) on the Gr/GO coated stent segments compared to the uncoated stent segments, i.e. whether the coatings have any toxic influence on the cells, which would impact number of cells adherent on the stent segments. Secondly, to determine if HCAEC proliferation (HCAEC count/mm^2 at day 1 vs. HCAEC count/mm^2 at day 8) is affected when cultured on graphene and graphene oxide coated stents compared to 'uncoated' stents.

The endothelium is fundamental to the healthy function of the vasculature. Re-establishing the endothelium after it has been eroded following stent implantation is a healing process that is delayed by currently available stents, particularly DES. If coronary artery stents displayed an improved endothelial cell proliferation, this could implicate an enhanced vessel healing with potential of avoiding the stent associated complications (section 1.3.3). Endothelial cells are anchorage dependent cells, where their adhesion/affinity to the substrate is fundamental in the cell's migration, survival and proliferation (244).

In this chapter, HCAEC adhesion to the graphene and graphene oxide coated coronary stent was assessed and compared to control uncoated stents in order to determine if there was an enhanced endothelial cell affinity to the graphene based surface coatings. In addition, the proliferation of HCAECs on these stents was examined to determine whether the graphene based coatings create a more favourable condition for endothelial cell mitosis.

5.4.1 Graphene and graphene oxide coatings did not influence HCAEC adhesion

A lower density of HCAEC in relation to HCAEC seeding density was observed one day after seeding. This indicates a low initial HCAEC attachment, but this is not uncommon, as at seeding not all HCAECs are viable and able to attach to the substrate. Some of the factors that may affect initial cell attachment in our experiment are that the stent substrate did not cover the entire base of the cell culture plate/well, due to its stent shape and size (space between stent struts). This along with the static culture design, could have caused some HCAECs to fall away from the stent struts, losing contact with the

stent strut. Comparing to other reports of general cell attachment to stent surfaces, our experiments demonstrate an at least 28% adherence efficiency compared to a maximum of 30% reported by others working on stents, suggesting acceptable cell attachment and confirming any effect on cell attachment in the *in vitro* experiment is from stent strut design and not influenced by surface coating (spaces between stent struts) (245). In order to delineate the effect from surface coatings, HCAEC attachment between the uncoated, Gr and GO coated stent segments were compared at day 1 and found to be not significantly different in each group, suggesting HCAEC adhesion to be unaffected by the Graphene or Graphene oxide coating.

Even though a higher HCAEC density was observed in the GO coated stent, the standard error of the mean was too large to conclude a real effect from the actual GO coating. Comparing each group to the uncoated control group at day 1, it is evident that there is no significant difference between the HCAEC count per mm^2 of stent area, indicating no influence from the graphene or the GO coatings on the affinity or the adhesion capability of the endothelial cell. This is contrary to recent report from Wawrzyńska and colleagues, who demonstrated enhanced endothelial cell adhesion on the graphene coated stainless steel discs (197). Moreover, and again contrary to adhesion results in this chapter, Aryaei and others documented improved adherence of cells towards the graphene coatings (194, 246). Our data, denote no favourable surface for initial endothelial cell attachment; and this is also contrary to reports of enhanced initial adhesion of mammalian cells (embryonic, osteoblast, kidney, L-929 cells) onto GO coatings (247). In this study, the Gr or the GO coating is not significantly affecting HCAEC survival/adherence at day 1 in comparison to the uncoated stent segment.

5.4.2 Enhanced HCAEC proliferation observed on graphene coated stainless steel stent compared to uncoated and GO coated stents

The data in this chapter denote an almost doubling of HCAEC count per mm^2 of graphene coated stent segment in comparison to HCAEC count per mm^2 of uncoated control stent segment, during a 7 day static cell culture, indicating graphene as favourable surface coating for enhanced proliferation of HCAEC (Fig.5.1). This result is compatible with those available in literature, illustrating an improved proliferation of murine osteoblast, rat aortic and human coronary artery endothelial cells on graphene coated stents (194, 196, 197). This has implications for improved re-endothelialisation in coronary artery settings and thus an enhanced coronary artery stent design.

Endothelial cells are anchorage dependant cells, enhanced HCAEC number on the graphene coated stent after 7 days of culture could be due to a stronger long-term adhesion between the cell and graphene coated surface, in other words influence of graphene coating on HCAEC detachment and thus survival and consequently growth (194). Speculatively, this could be attributed to either improved adhesion of the cell adhesion proteins, vinculin and fibronectin to the graphene surface or the high in-plane stiffness of graphene that enables strong anchor points of the cytoskeleton (194, 197).

Numerous studies have reported on the biocompatibility of GO at low doses i.e. (<20µg/mL free GO (248, 249)). Results from this chapter also suggest biocompatibility of both GO and Gr coating, because even though there was no significant increase in HCAEC count per mm^2 on GO coated than control uncoated stent segments, there was also no decrease in cell number/density that would have suggested cytotoxicity. Biocompatibility of Gr and GO coatings is confirmed as has been documented by others in literature (197, 247).

5.4.3 Absence of morphological influence on HCAEC from the graphene or graphene oxide coating

In terms of cell spreading which is important in determining degree of adhesion, the actin-f filaments stained with phalloidin were further examined for differential spreading of the cells and were generally (visually) found to be no different from each other (Gr vs GO vs uncoated). As this is a qualitative observation and not quantitative, bias (subjective) can be introduced (Fig. 5.1A).

Overall, graphene and GO coating both support the adhesion and proliferation of human coronary artery endothelial cells, while graphene coating appears to display a greater support for HCAECs to proliferate upon. This has the potential implication of reducing in-stent restenosis. The robust mechanical properties exhibited by the stainless steel scaffold in addition to the graphene surface coating demonstrates a suitable candidacy for coronary artery implant, confirming biocompatibility as with supportive data from Podila *et al*. and Wawrzyńska *et al.* Long term effects of the coated stents under shear stress cannot be excluded/ignored.

5.5 Limitation

The incomplete flatness of the stents caused difficulty imaging to precisely visualise the actin-f of the HCAECs. The static (no flow) *in vitro* conditions and the absence of any influence from normal physiological conditions means this data, although promising, are to be used as an indication for further investigations only.

5.6 Key findings

- No difference in HCAEC adhesion capacity between the Gr, GO coated stent segments and the uncoated stent segment.
- At least a 30 fold increase in HCAEC/mm^2 on surface of uncoated and Gr/GO coated stent segments from day 1 to 7 days later, indicating proliferation of cells.
- Significantly greater proliferation of HCAEC onto graphene coating of stainless steel GAZELLE stent segments compared with GO coated and uncoated stent segments.

CHAPTER 6

Ex vivo porcine organ culture of coronary artery and aortic tissue to examine neointimal hyperplasia following incubation with Gr/GO coated coronary artery stents

6.1 Introduction

The results in chapter 5 demonstrated significantly improved growth of HCAECs on graphene coated stents, potentially indicating graphene as a favourable surface for HCAEC adhesion and proliferation. Studies from various investigations have documented biocompatibility of graphene with enhanced cell adhesion and proliferation of a variety of cells, however there are currently no *ex vivo* or *in vivo* studies in relation to coronary artery stenting and graphene based coating materials. In chapter 4, a novel method of coating bare metal stents using a LPE Gr and GO dispersion was developed. Therefore, it is vital that investigations are conducted to assess the performance of these stents in physiologically relevant settings. The most physiologically relevant and thus reliable technique to study this would be in the *in vivo* setting, however in order to reduce the number of animal experiments, it is important that first preliminary trials are conducted *ex vivo* on animal tissues prior to conducting *in vivo* studies. Moreover, to address the three Rs of the principles of Humane Experiment techniques: Replacement, Reduction and Refinement, it was decided to first investigate neointimal formation under *ex vivo* conditions, i.e. collecting porcine aorta and heart from the abattoir. Therefore, reducing the number of animals used to study neointimal formation and thus restenosis.

Why study neointimal formation?

Identifying neointimal formation is an important prognostic indicator of restenosis. Neointimal formation marks the early stages of restenosis following vascular stenting and therefore is an important measurement to determine success/efficacy of a stent coating. Following stent insertion, injury to the vessel wall often occurs causing damage or denudation of the endothelial cell layer that is vital as a protective film on the luminal surface of the vessel wall.

The endothelium lining acts as a barrier between blood components and the subendothelial layers of collagen and elastin fibres, regulating molecular/fluid traffic between blood and subendothelial tissue, vascular tone via secretion of nitric oxide as well as secreting smooth muscle cell (SMC) and inflammatory cell regulatory factors (250).

Endothelial cells are capable of influencing the migration and proliferation rate of the underlying SMCs as well as modulating haemostasis and thrombolysis (251-254). The anti-proliferative influence of endothelial cells on vascular SMCs (3), means that the inhibiting effect is lost with erosion of the endothelium, which triggers the proliferation of the SMCs, leading to extracellular matrix protein secretion that eventually results in neointimal formation (254). Moreover, the endothelium also regulates coagulation via expression of binding sites specific to pro- and anti- coagulant factors (2, 3), hence protecting against thrombosis.

With promoted re-endothelialisation, the arterial wall will recover to its healthy state and modulate SMC proliferation and thus neointimal formation, as has been shown by Kipshidze and colleagues, patches where endothelium regeneration occurred resulted in minimal neointima formation (10, 254).

To investigate the efficacy of Gr coated and GO coated stents in comparison to controls (unstented and uncoated stents), the extent of neointimal formation was explored. This is predominantly and ideally performed *in vivo* to minimise variation by yielding data from models that undergo physiological conditions similar to humans i.e. undergo stress by blood pressure, along with similar inflammatory responses.

Restenosis of a stented coronary artery occurs as a complication and as a consequence of vessel wall injury caused during stent deployment; either by the stent itself or inflation of the balloon that can result in medial distention. Stents that have these qualities may have significant potential in preventing restenosis. The effect of graphene and graphene oxide coated bare metal stents on neointimal formation, in these settings is unknown. To study this, uncoated, Gr and GO coated stents as well as control unstented porcine coronary artery and aortic tissue were cultured for 14 days as outlined in Table 2.1 and 2.2 respectively.

Why porcine aorta and coronary artery tissues?

Coronary artery (255, 256) and aorta (251, 257, 258) *ex vivo* organ culture has previously been shown to be a useful model to investigate neointimal hyperplasia after vessel wall injury and stent implantation; studying pathogenesis of balloon and stent induced injury and possible recovery effected by stent coating. These are also the most relevant tissues for studying coronary artery stent efficacy. These porcine *ex vivo* models have often been used as an *in vivo* replacement model and an effective model of studying neointimal

hyperplasia, due to their structural, functional, size and inflammatory response similarity to human coronary artery and aorta (259). Thus, providing data relevant to humans, making the pig the most commonly and relevant used model of studying restenosis and general cardiovascular research (260), and hence why it is being used in this project.

6.1.1 Chapter objectives

The objective of this chapter is to investigate the effect of Gr or GO coated stent segments in comparison to unstented control, and contemporary stents (uncoated GAZELLE, uncoated CHROMA stents and everolimus eluting stent (EES)) on neointimal formation as an indicator of restenosis/in-stent restenosis on porcine coronary arteries and aorta. Experimental groups described/outlined in Table 2.1 and Table 2.2 for coronary artery and aortic organ culture, respectively.

1) To determine whether Gr and GO coated GAZELLE stent segments influence neointimal formation in comparison to no stent, uncoated GAZELLE/CHROMA stent segments in porcine coronary artery organ culture.

2) To determine whether Gr and GO coated GAZELLE stent segments affect neointimal formation compared to no stent, uncoated GAZELLE/CHROMA and EES segment in porcine aortic organ culture.

3) To determine whether Gr and GO coated GAZELLE stent segments influence endothelial cell re-growth in comparison to no stent, uncoated GAZELLE/CHROMA stent segments in porcine coronary artery organ culture.

4) To determine, whether Gr and GO coated GAZELLE stent segments in relation to no stent, uncoated GAZELLE/CHROMA and EES segments have an influence on endothelial cell re-growth on porcine aortic organ culture, after denudation following balloon inflation and stent insertion.

6.2 Methods

Porcine hearts and aorta were harvested from pigs undergoing euthanasia in an abattoir (section 2.4.1.2). The tissues were transported in cold PBS supplemented with penicillin (200 units mL^{-1}), streptomycin (200 µg mL^{-1}), glutamine (4mmol L^{-1}) and amphotericin (5 µg mL^{-1}). Previous literature suggested 14 days vessel culture to be adequate time to produce neointimal formation (261, 262). The graphene and graphene oxide coated GAZELLE stents were coated as described in Chapter 2 and Chapter 4. The dH_2O coated

GAZELLE and CHROMA stents, referred in this project as 'uncoated' stents, were prepared as described in Chapter 2. The EES was unpacked, expanded to open and cut into segments for use *ex vivo* on aortic tissue organ culture. Briefly, porcine coronary artery and aortic tissue as well as the expanded stents were cut open along the longitudinal axis and cut into small segments (approximately 5 x 10 mm). To a section of the thoracic aorta, an aortic balloon was inflated for seven minutes to induce injury, denuding the endothelial layer. The purpose of inducing deliberate injury to aortic wall, was to mimic endothelial cell (EC) denudation that occurs in the clinical setting during stent deployment. It is the act of injury and EC denudation that triggers SMC proliferation and finally restenosis (263, 264).

At day 0 for control, and upon completion of the culture period of 14 days, the tissues were fixed using 10% neutral buffered formalin and 2.5% glutaraldehyde based fixative for paraffin embedding and scanning electron microscopy visualisation, respectively. To characterise the vessel layers in both the aorta and the coronary arteries, histological staining with Miller's elastin stain incorporating Van Gieson stain was performed on 5µm thick transverse paraffin sections. The stained sections would easily identify the elastin fibres, collagen and importantly the internal elastic laminae (IEL), essential as a start point from which to measure the neointimal thickness.

In order to identify endothelial cells, antibodies against CD31, were used on both aortic and coronary artery paraffin embedded sections. The Miller's stain alone without potassium permanganate, oxalic acid and Van Gieson's was used as a counterstain to highlight the elastin fibres. The presence/absence of endothelial cells is an important indicator of whether there was healing, and re-establishment of endothelial cell layer that would lead to vessel wall repair and possibly prevention of restenosis or any other deleterious response.

A further method to examine the luminal surface topography of the aorta and coronary artery before and after culture was undertaken by scanning electron microscopy (SCEM). The endothelial cell integrity both on the surface of the vessel wall and also on the surface of co-cultured and pinned stents was investigated. See section 2.4.3 for detailed methods.

6.3 Results

6.3.1 Neointimal thickening in porcine coronary artery and aortic organ culture

Culture of both coronary artery and aorta for a duration of two weeks resulted in development of neointimal formation in all categories: Day 14, GAZELLE, CHROMA, Graphene, and Graphene Oxide (Fig. 6.1 and 6.2). Neointimal thickness was measured in both coronary artery and aorta from the IEL denoted by a blue arrow head in Figure 6.1A and 6.2A, respectively. The navy coloured structures illustrate the elastic fibres, pink areas denoting collagenous material and the neointimal section formed above the IEL (Fig. 6.1A and 6.2A).

Neointimal formation in Coronary artery organ culture

Comparing the extent of neointimal formation, neointimal thickness measurements revealed a substantial but non-significant increase in thickness from Day 0 (2.08µm ± 1.08µm) to Day 14 (6.96µm ± 6.96µm) for the coronary artery organ culture specimens (Fig. 6.1). In the CoA-Day 14 specimens, two sections and for CoA-Day 0, one section were unmeasurable, due to ambiguity in vessel structures such as the IEL (technically difficult vessel appearance, unable to distinguish vessel structures), resulting in a reduced sample size. Moreover, the one-way ANOVA test revealed no significant difference in thickness of neointima within any of the coronary artery groups ($p=0.75$) (Fig. 6.1B). The mean neointima thickness for stented coronary arteries cultured for a duration of 14 days: CoA-GAZELLE (9.48µm ± 4.03µm), CoA-CHROMA (6.39µm ± 3.50µm), CoA-Graphene (4.46µm ± 0.89µm) and CoA-Graphene Oxide (6.23µm ± 3.48µm), all $n=4$ (Fig. 6.1A). Even though a clear increase in neointimal thickness is evident from CoA-Day 0 (unstented) to Day 14 (CoA-GAZELLE, CoA-CHROMA, CoA-Graphene, CoA-Graphene Oxide and CoA-Day14) coronary artery cultures, Tukey's multiple comparisons revealed no significance, indicating neointimal thickness on the coronary arteries to be unaffected by 14 days of culture or stenting (whether uncoated GAZELLE/CHROMA or Gr/GO coated GAZELLE stent segments).

CoA-Graphene demonstrated the lowest neointimal thickness (4.46µm ± 0.89µm), half the thickness of CoA-GAZELLE (9.48µm ± 4.03µm) (Fig. 6.1B). As this is not statistically significant, a robust and clear conclusion cannot be made, but perhaps with an increased n number, a reduction in neointima thickness may occur with graphene coated stents.

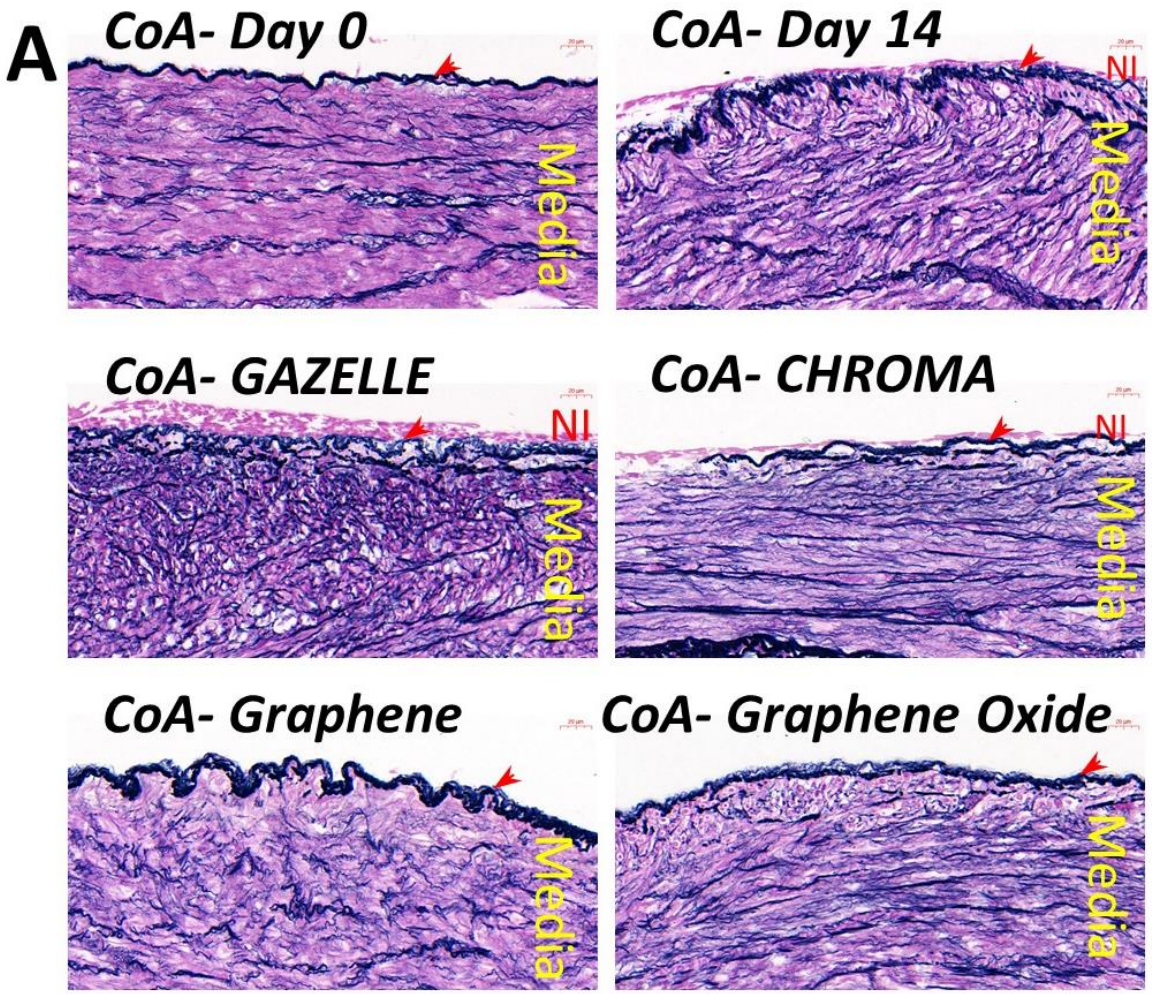
A
CoA- Day 0
Media
CoA- Day 14
NI
Media
CoA- GAZELLE
NI
Media
CoA- CHROMA
NI
Media
CoA- Graphene
Media
CoA- Graphene Oxide
Media

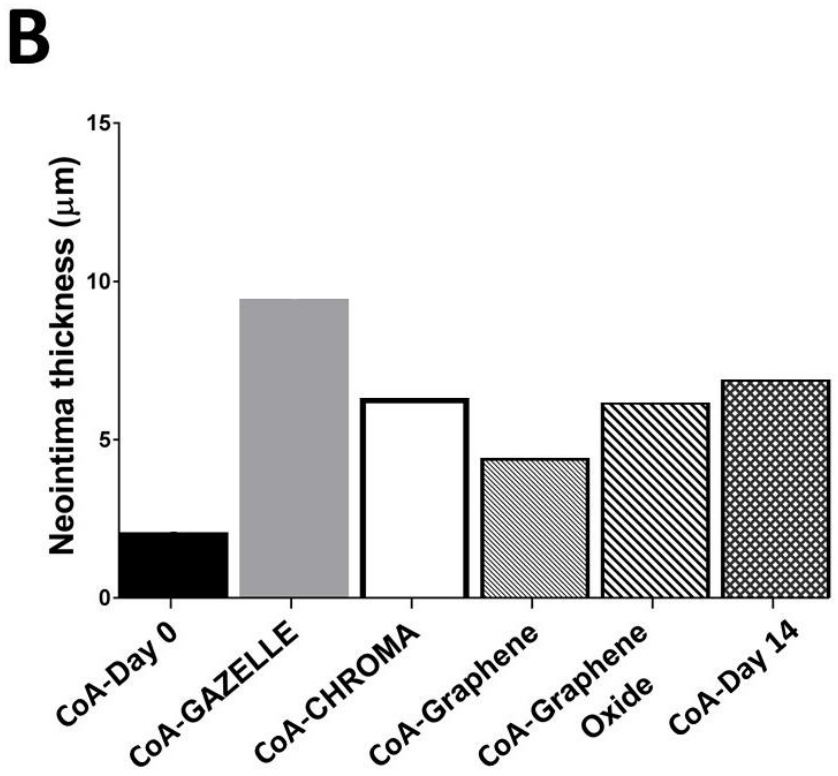
B
Neointima thickness (μm)
15
10
5
0
CoA-Day 0
CoA-GAZELLE
CoA-CHROMA
CoA-Graphene
CoA-Graphene Oxide
CoA-Day 14

Figure 6.1: Neointimal formation on porcine coronary arteries occurred in all groups after 14 days in culture, although the differences were not significant. Porcine coronary artery isolated from freshly sacrificed pigs in the abattoir were harvested, following which it was opened flat and pinned down for 14 day culture with/without stents. Details of experimental group can be found from Table 2.1. CoA-Day 0 (n=3) as well as CoA-Day 14 (n=2) were coronary artery tissue. All coated and uncoated stent segments (n=4); CoA-Graphene, CoA-Graphene Oxide and CoA-GAZELLE, were stainless steel bare metal stent (GAZELLE) substrate. CoA-CHROMA represented the newer bare metal stent (CHROMA). **A:** Miller's elastin staining of all tissue completed after paraffin embedding. Blue/black= elastin fibres; pink-= collagenous material. Arrows indicate the internal elastin laminae (IEL). Neointima labelled as NI and Tunica media of the vessel also labelled. **B**: Neointimal thickness was measured, µm and displayed. Statistical significance was determined by using one-way ANOVA with Tukey's post-hoc test, though none showed significance, $p>0.05$.

Neointimal formation in porcine aortic organ culture

Comparing Ao-Day 0, the neointimal layer was significantly thicker after 14 days of culture in all cultured groups with the exception Ao-EES. The Ao-EES remained without neointima (3.3µm ± 1.32µm), comparable to Ao-Day 0 after injury (2.29µm ± 1.23µm) and not significantly different to Ao-Day 0 before injury (0.70µm ± 0.36µm) (Fig. 6.2). As is depicted in figure 6.2B, almost all aortic tissue cultured for a period of 14 days (Ao-GAZELLE, Ao-CHROMA, Ao-Graphene, Ao-Graphene Oxide and Ao-Day 14) illustrated a thicker neointima than Ao-EES, indicating a suppression of neointimal formation by the EES.

The neointimal thickness of Ao-CHROMA (16.58µm ± 4.76µm) increased compared to the control Ao-Day 0 fixed tissues, (before injury (0.70µm ± 0.36µm; p=0.12)); after injury (2.29µm ± 1.23 µm; p=0.14)); although this was not significant.

Matched Tukey's multiple comparison of the experimental groups revealed a significantly thicker neointima in the Ao-Graphene (14.85µm ± 3.72µm) group, in comparison to Ao-Day 0 after injury (2.29µm ± 1.23µm; p=0.02), whereas no significant difference in relation to Ao-Day 0 before injury (0.70µm ± 0.36µm; p=0.06) was identified. Neointima thickness of unstented Ao-Day 14 aortic tissue (16.55µm ± 2.5µm) was not observed to be significantly different to any of the stented tissues cultured for 14 days (Ao-GAZELLE, Ao-CHROMA, Ao-Graphene, and Ao-Graphene Oxide), except Ao-EES (Fig. 6.2B). Figure 6.2A illustrates neointimal formation that thickened over the 14 days period, except in the Ao-EES group.

To determine any potential effect from either Gr or GO coating, neointima thickness comparisons between uncoated GAZELLE stent segments was performed. A neointima thickness of 14.0µm ± 3.17µm was measured on the Ao-GAZELLE, similar to thickness from Ao-Graphene, 14.85µm ± 3.72µm and Ao-Graphene Oxide, 11.97µm ± 1.33µm, n=10.

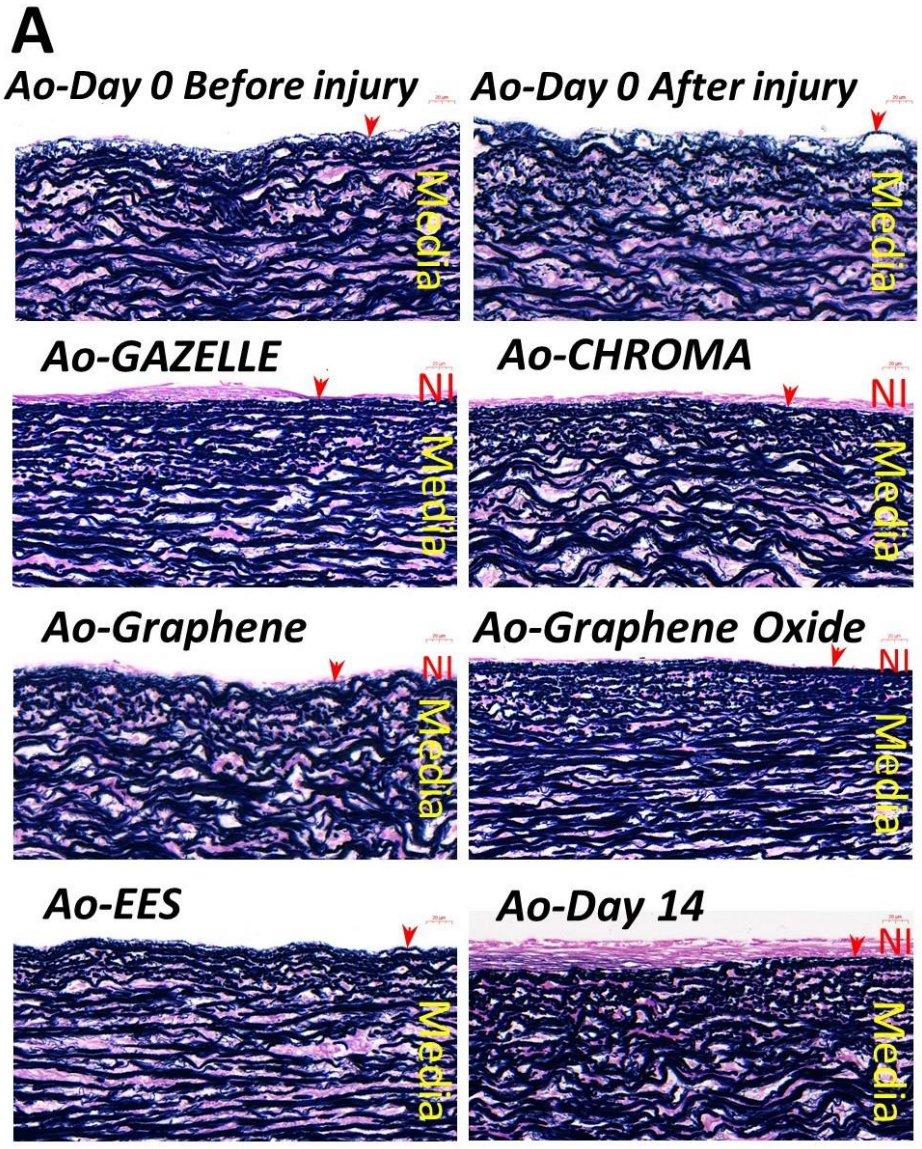
A
Ao-Day 0 Before injury
Ao-Day 0 After injury
Media
Ao-GAZELLE
Ao-CHROMA
NI
Ao-Graphene
Ao-Graphene Oxide
Ao-EES
Ao-Day 14

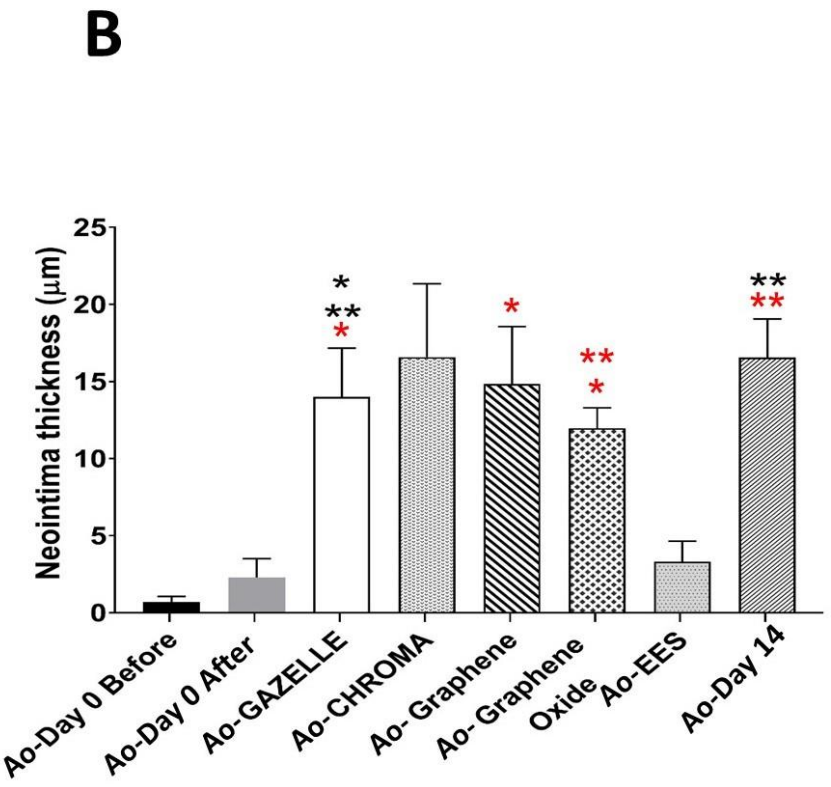
B
Neointima thickness (μm)
25
20
15
10
5
0
Ao-Day 0 Before
Ao-Day 0 After
Ao-GAZELLE
Ao-CHROMA
Ao- Graphene
Ao- Graphene Oxide
Ao-EES
Ao-Day 14

Figure 6.2: Significant increase in porcine aortic neointimal thickness occurred in all groups after 14 days of culture except in Ao-EES group.
Porcine aortic tissue isolated from freshly sacrificed pigs in the abattoir were harvested, balloon injured, following which it was opened flat and pinned down for 14 day culture with/without stents. Details of experimental groups in Table 2.2. Ao-Day 0 before and Ao-Day 0 after injury as well as Ao-Day 14 after injury (in 14 day organ culture) were all the unstented control groups of aortic porcine tissue. All coated and uncoated stent segments, Ao-Graphene, Ao-Graphene Oxide and Ao-GAZELLE, were stainless steel bare metal stent (GAZELLE) substrate. Ao-CHROMA represented the newer bare metal stent (CHROMA) and Ao-EES representing a contemporary drug eluting stent. **A:** Miller's elastin staining of all tissue completed after paraffin embedding. Blue/black= elastin fibres; pink-= collagenous material. Arrows indicate the internal elastin laminae (IEL). Neointima labelled as NI and Tunica media of the vessel also labelled. **B**: Neointimal thickness was measured, µm, mean and standard error of the mean calculated and displayed. Statistical significance was determined by using one-way ANOVA with Tukey's post-hoc test. (black *****: $p < 0.05$ versus Ao-Day 0 Before injury; red *****: $p < 0.05$ versus Ao-EES; black ******: $p < 0.01$ versus Ao-Day 0 After injury, red ******: $p < 0.01$ versus Ao-Day 0 Before injury, n=10.

6.3.2 Assessment of endothelial cell coverage before and after organ culture of porcine coronary artery and aortic tissue

Immunohistochemistry for CD31

As described in Chapter 5, significantly higher HCAEC count was observed per mm^2 area of graphene coated stents in comparison to HCAEC per mm^2 area of uncoated GAZELLE stent (Fig. 5.1). Leading on from this work, EC preservation and regeneration was assessed on both coronary artery and aortic tissue cultured for a period of two weeks as described in chapter 2.

An EC specific marker, CD31, was used to identify endothelial cells. CD31 is typically expressed on the cell junction membrane border of cells. Figures 6.3 and 6.4 illustrate immunostaining against CD31 with a Miller's elastin counterstain. The monolayer dark brown pigmentation above the internal elastic lamina (illustrated by a red arrowhead), indicates the presence of endothelial cells (Fig. 6.3 /6.4 on Day 0), as is also visible on the vasa vasorum in the peri-adventitial segment (6.4C). On the other hand, positive immune staining was observed above the IEL tissue cultured for 14 days, but lighter brown in colour as well as exhibiting a multilayer phenotype that is inconsistent with endothelial cells (Fig. 6.3/6.4 A Day 14). During 14 days of organ culture, very few aortic and coronary artery tissues exhibited the flattened, monolayer CD31 staining on the surface (Fig. 6.3/6.4 A).

Endothelial cell staining of sectioned, paraffin embedded porcine coronary artery organ culture specimens

CD31 positive cells were clearly visible on the luminal surface of two out of four coronary artery specimens fixed at Co-Day 0 and some patches of CD31 positive cells on two out of the three measurable specimens of CoA-Day 14 (Fig. 6.3 A, red arrowhead). On the other hand, in all other categories; CoA-GAZELLE, CoA-CHROMA, CoA-Graphene and CoA-Graphene Oxide, no CD31 positive cells were identified, indicating no EC preservation or regeneration. From a total of four specimens, CoA-Graphene and CoA-Graphene Oxide included three and two measurable specimens respectively, because the immeasurable specimens were ambiguous in vessel structure and technically difficult to assess CD31 positive staining, thus decreasing sample size.

A

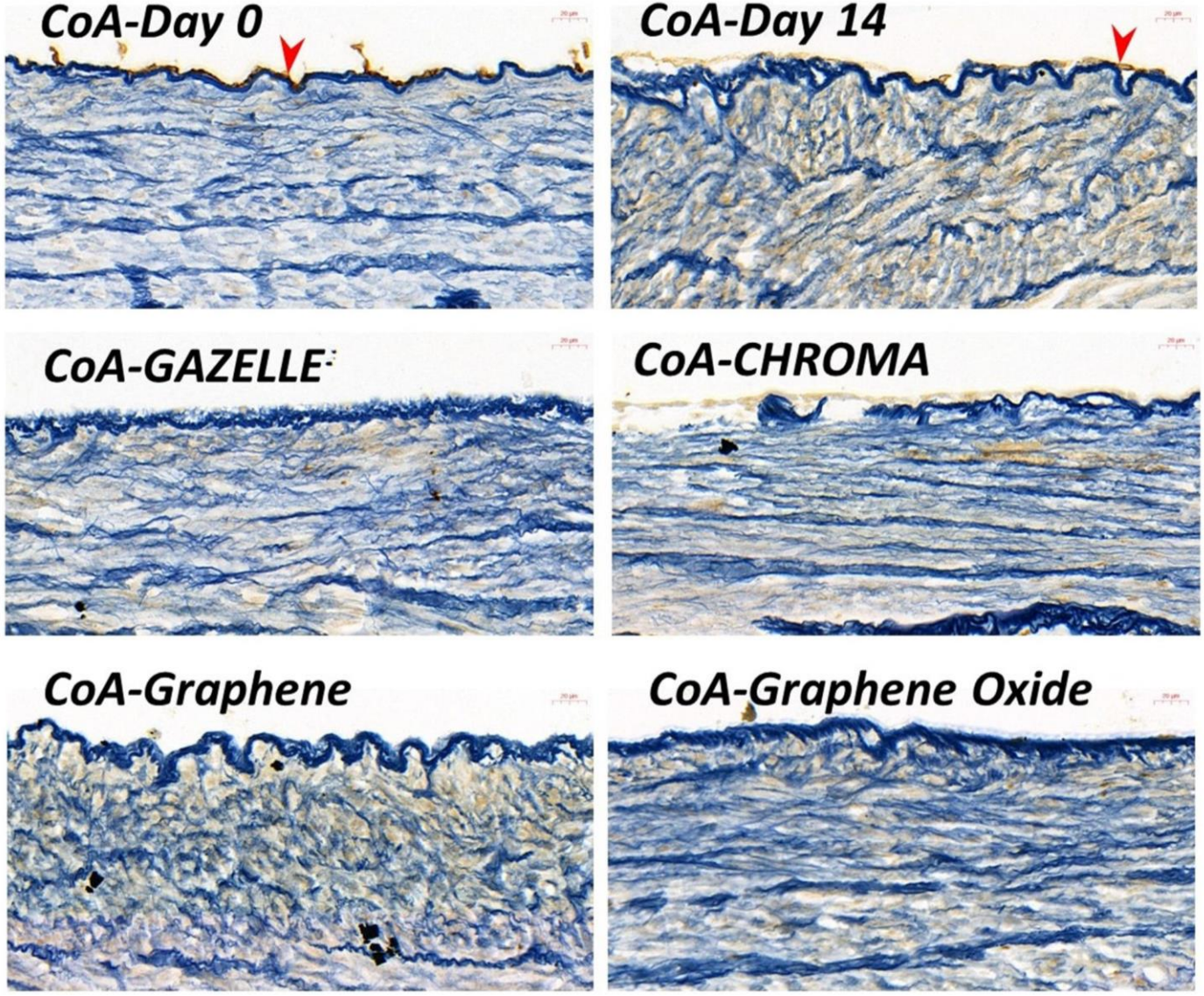

B

Coronary artery n=	1	2	3	4
CoA- Day 0	-	+	-	+
CoA-GAZELLE	-	-	-	-
CoA-CHROMA	-	-	n/a	-
CoA-Graphene	-	-	n/a	-
CoA-Graphene Oxide	-	n/a	n/a	-
CoA-Day 14	-	+-	n/a	+-

Figure 6.3: CD31 immunostaining of endothelial cells in porcine coronary arteries after 14 days of organ culture. Porcine coronary artery isolated from freshly sacrificed pigs in the abattoir were harvested, following which it was opened flat and pinned down for 14 day culture with/without stents. Details of experimental group can be found from Table 2.1. CoA-Day 0 (n=4) as well as CoA-Day 14 were coronary artery tissue. All coated and uncoated stent segments, CoA-Graphene, CoA-Graphene Oxide and CoA-GAZELLE, were stainless steel bare metal stent (GAZELLE) substrate. CoA-CHROMA represented the newer bare metal stent (CHROMA). **A:** Immunohistochemistry staining against CD31 to identify endothelial cells (dark brown colour, indicated with red arrowhead). Counterstain with Miller's elastin stain to locate elastic fibres. **B**: Table indicating the presence (+), absence (-), or partial presence (+-) of CD31 positive staining and hence endothelial cells. Scale bar=20 µm. n/a= data not available, n=4.

Endothelial cell staining of sectioned, paraffin embedded porcine aorta organ culture specimens

Coronary artery investigations presented above, clearly demonstrate the need for increased sample size to identify any significant differences. However, due to the technical challenges faced in isolating coronary arteries in a timely manner from the time of collection of the porcine tissue to culture from the abattoir, another technically easier porcine tissue, aorta, was selected to further study EC integrity on the luminal surface.

CD31 positive cells were predominantly identified on Ao-Day 0, both before and after balloon injury. Studying EC preservation by immunohistochemistry and SCEM visualisation of aortic tissue, four out of the ten (4/10, all from different pigs) Ao-Day 0 before injury specimens, and 6/10 of Ao-Day 0 after balloon injury, demonstrated moderate to strong CD31 positive staining with Ao-Day 0 after injury presenting more specimens with intact endothelium. There were aortic tissue demonstrating barren ECs at Day 0 prior to inducing injury, whereas the autologous (from same aorta/anima) aortic tissue specimens after injury showed presence of EC layer (Fig. 6.4B). This was also viewed in one of the autologous (from same aorta/animal) tissues examined by SCEM (n=3). Areas bereft of ECs were observed, though there remained areas showing intact ECs after injury (Fig. 6.4, 6.5).

In total, 2 out of the 10 (2/10) aortic specimens of Ao-GAZELLE, 2/10 of Ao-CHROMA stents and 1/10 of Ao-Graphene samples exhibited moderate patchy CD31 positive staining (Fig.6.4 B), whereas 2/10 of Ao-Graphene Oxide coated stents presented with strong CD31 staining and 1/10 of Ao-Graphene Oxide showed moderate patchy staining (Fig. 6.4B). Either, ECs survived balloon induced injury to Ao-Day 14 or regrowth of ECs took place. Unstented aortic tissue cultured for 14 days, Ao-Day 14 (Fig. 6.4A/B) illustrated light staining but perhaps not indicating CD31 positive cells due to the lighter colour and also the multi-layer phenotype of the staining. Endothelial cells typically are single layered. There was no CD31 staining on the Ao-EES coated stents. There doesn't appear to be a distinct affinity of the ECs to Gr or GO coating, with similar CD31 positive presentation in all experimental groups cultured for 14 days.

A

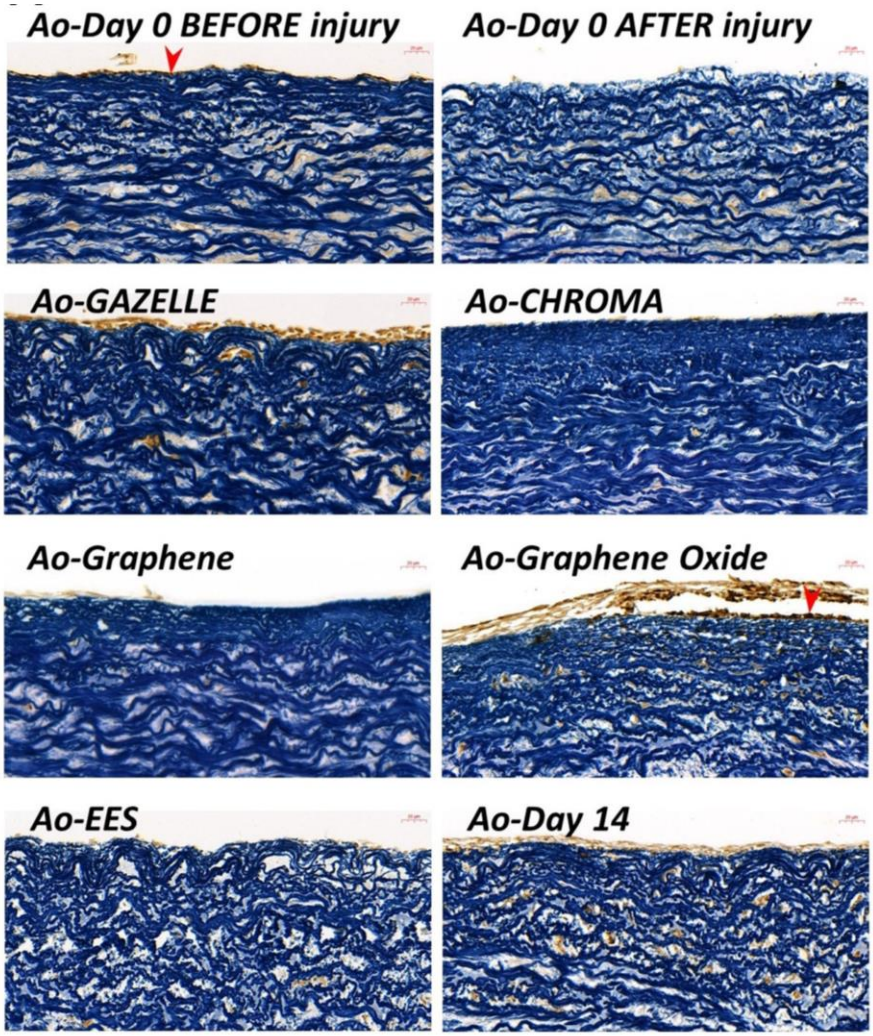

B

Aorta n=	1	2	3	4	5	6	7	8	9	10
Ao-Day 0 BEFORE	-	-	+-	-	+	+-	+-	-	-	-
Ao-Day 0 AFTER	+-	+	+	+-	+-	-	-	-	+-	-
Ao-GAZELLE	-	-	-	-	-	-	+-	+-	-	-
Ao-CHROMA	+-	-	-	-	-	-	-	+-	-	-
Ao-Graphene	-	-	-	+-	-	-	-	-	-	-
Ao-Graphene Oxide	+	-	-	+	-	+-	-	-	-	-
Ao-EES	-	-	-	-	-	-	-	-	-	-
Ao-Day 14	-	-	-	-	-	-	-	-	-	-

C

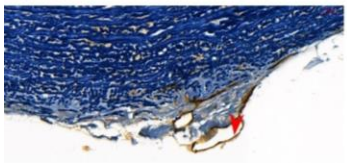

Figure 6.4: Immunostaining of endothelial cells in porcine aorta after 14 days of culture. Porcine aortic tissue isolated from freshly sacrificed pigs in the abattoir were harvested, balloon injured, following which it was opened flat and pinned down for 14 day culture with/without stents. Details of experimental groups in Table 2.2. Ao-Day 0 before and Ao-Day 0 after injury as well as Ao-Day 14 after injury (in 14 day organ culture) were all the unstented control groups of aortic

porcine tissue. All coated and uncoated stent segments, Ao-Graphene, Ao-Graphene Oxide and Ao-GAZELLE, were stainless steel bare metal stent (GAZELLE) substrate. Ao-CHROMA represented the newer bare metal stent (CHROMA) and Ao-EES representing a contemporary drug eluting stent. **A:** Immunohistochemistry staining against CD31 to identify endothelial cells (dark brown colour, indicated with red arrowhead). Counterstain with Miller's elastin stain to locate elastic fibres. **B**: Table indicting the presence (+), absence (-), or partial/patchy presence (+-) of CD31 positive staining and hence endothelial cells. Scale bar=20 μm. **C:** Endothelium in vasa vasorum in the adventitial layer of aorta pointed at by red arrowhead.

6.3.3 Surface topography of aortic tissue and stent

The purpose of visualisation by SCEM was to determine EC growth onto the stent surfaces. Cobblestone appearance is present on porcine aortic tissue luminal surface on the Ao-Day 0 both before and after balloon injury (Fig. 6.5 a-f). This is not present in the entirety of the tissue segment, but present in patches (Fig. 6.5 a, d). The cobblestone appearance is absent from tissue surface and stent surface in all other experimental groups consisting of all 14 day cultured tissues: Ao-GAZELLE, Ao-CHROMA, Ao-Graphene, Ao-Graphene Oxide, Ao-Day 14 and Ao-EES (Fig. 6.5 g-x). Stents and tissue, all 14 day cultures, are covered by unknown elongated cellular structures that mimic the elastin fibres/fibroblasts/SMCs (Fig. 6.5 g-x).

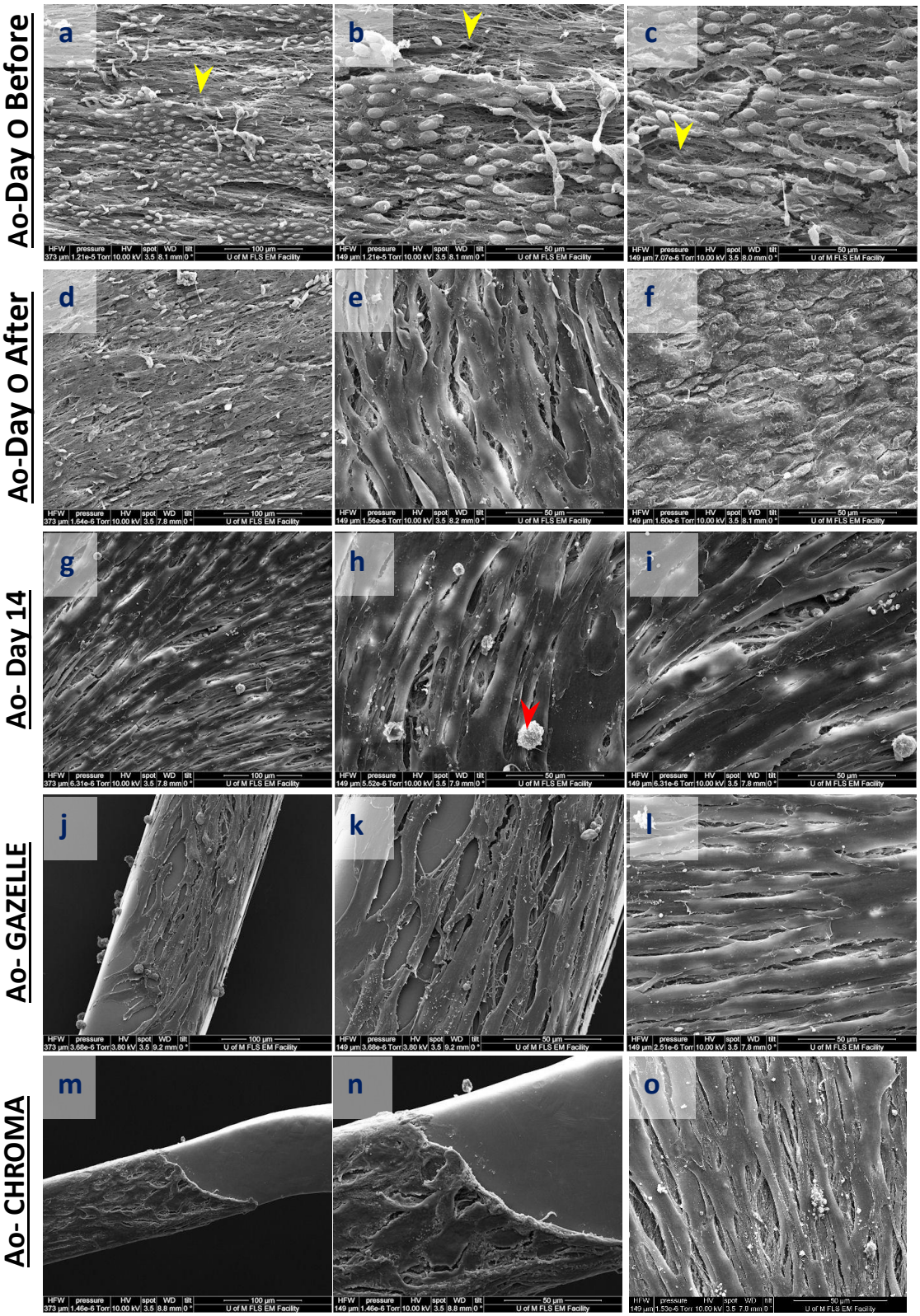
Ao-Day O Before
Ao-Day O After
Ao- Day 14
Ao- GAZELLE
Ao- CHROMA
a
b
c
d
e
f
g
h
i
j
k
l
m
n
o

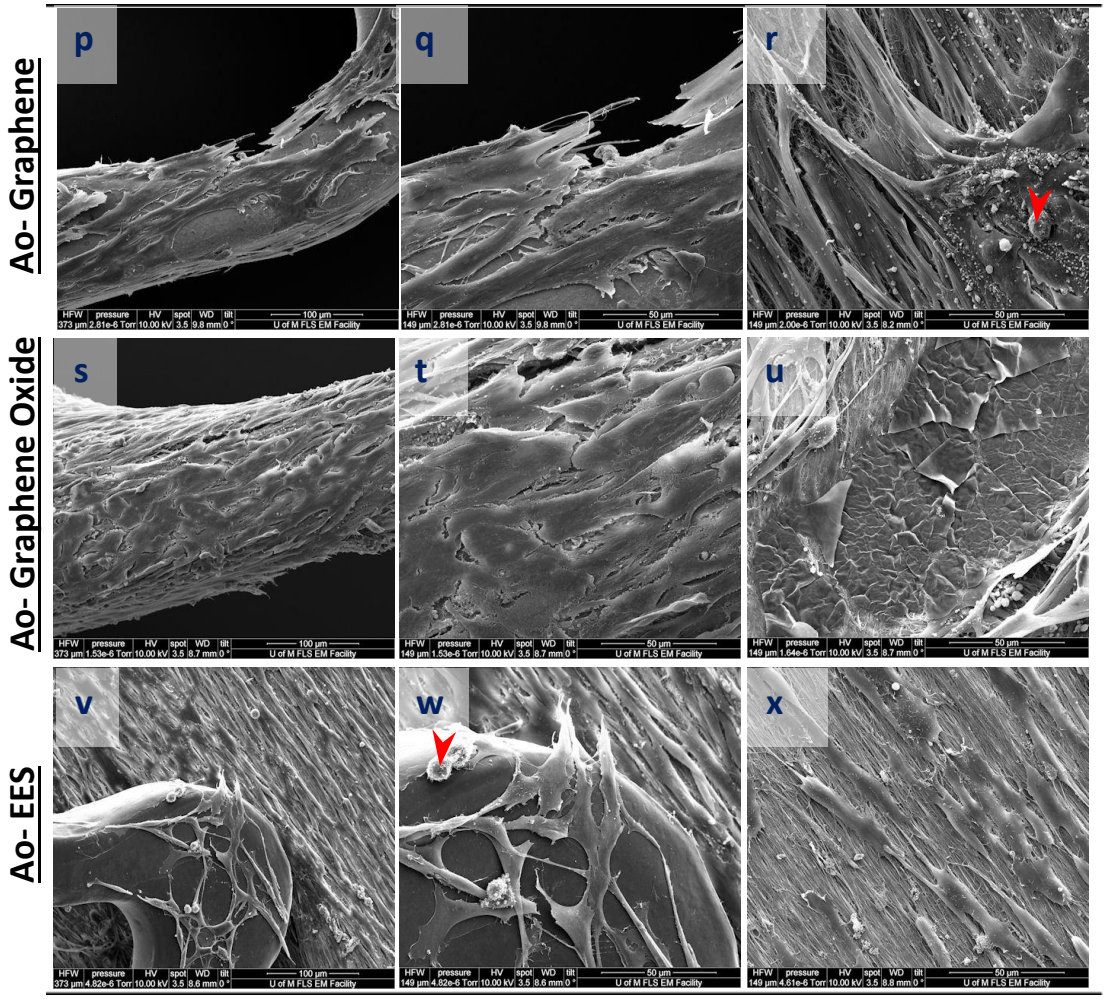

Figure 6.5: Scanning electron microscopy images of porcine aortic tissue surface and stent surface after 14 days of culture. Porcine aortic tissue isolated from freshly sacrificed pigs in the abattoir were harvested, balloon injured, following which it was opened flat and pinned down for 14 day culture with/without stents. Details of experimental groups in Table 2.2. Ao-Day 0 before (a-c) and Ao-Day 0 after injury (d-f) as well as Ao-Day 14 after injury (g-i) were all the unstented control groups of aortic porcine tissue. All coated and uncoated stent segments, Ao-Graphene (p-r), Ao-Graphene Oxide (s-u) and Ao-GAZELLE (j-l), were stainless steel bare metal stent (GAZELLE) substrate. Ao-CHROMA (m-o) represented the newer bare metal stent (CHROMA) and Ao-EES (v-x) representing a contemporary drug eluting stent. SCEM scanning parameters are displayed at the bottom of each image collected. At Day 0 (a-f), cobblestone shaped cells are the endothelial cells with yellow arrowheads denoting the gaps in the endothelium. Aortic luminal tissue surface (g-i,l,o,r,u,x) and stent surfaces (j,k,m,n,p,q,s,t,v,w) cultured for a period of 14 days, present a more elongated, parallel cell appearance, that has clearly also proliferated onto the stents. Red arrowheads points to adhered leukocytes. n=10; Scale bar = 100 µm (left panel of images); 50 µm (central and right side panel).

6.4 Discussion

This chapter presents a histological, immunohistochemical and scanning electron microscopy analysis of an *ex vivo* porcine model of neointimal thickening and re-endothelialisation in porcine coronary artery and aorta. Neointimal thickening is the early/initial phase restenosis development and is predominantly caused by de-endothelialisation and increased SMC proliferation within the vessel wall. The inflammatory and cell response may differ if stents were to have enhanced affinity towards endothelial cell growth and the contrary towards SMCs. Stents that have these qualities may have significant potential in preventing restenosis. The effect of graphene and graphene oxide coated bare metal stents on neointimal formation, in these settings is unknown. To study this, uncoated, Gr and GO coated stents as well as control unstented porcine coronary artery and aortic tissue were cultured for 14 days as outlined in Table 2.1 and 2.2, respectively.

Initially experiments were conducted using the coronary artery organ culture model due to its relevance to coronary artery stenting as an intervention for coronary artery disease, however due to its technical challenges, and limited time, the aortic organ culture model was later employed to increase sample size.

6.4.1 Graphene and graphene oxide coated stents formed similar neointima thickness to uncoated stents

Neointimal formation was evident in the 14 day coronary artery organ cultures; CoA-GAZELLE, CoA-CHROMA, CoA-Graphene, CoA-Graphene Oxide and CoA-Day 14, when comparing to neointimal thickness of baseline CoA-Day 0 (Fig. 6.1 B). A trend towards decreased coronary artery neointimal thickness was observed with the CoA-Graphene experimental group compared to CoA-GAZELLE, but this was not statistically significant (Fig.6.1B). The lower neointima thickness of CoA-Graphene versus CoA-GAZELLE allows speculation of possible neointima preventative/reducing influence from Graphene coating though replicates are vital to deduce the true impact of graphene coated coronary artery stents on neointimal thickness. One of the reasons for non-significance between any of the 14 day coronary artery organ cultures (CoA-GAZELLE, CoA-CHROMA, CoA-Graphene, CoA-Graphene Oxide and CoA-Day 14) versus CoA-Day 0 was probably attributed to the large SEM arising from the small sample size.

The sample size for all coronary artery organ culture experimental groups was n=4, however some difficulties to measure specimens were present leading to missing data. The reason for missing measurements, was the absence of discernible and distinct coronary artery structures such as the IEL, from which point the neointimal measurements initiated. The following had lower n numbers to the rest of the experimental groups: CoA-Day 14 (n=2) and CoA-Day 0 (n=3). The decrease in sample size does lower reliability and power for significance, however this did not affect all experimental groups and an n=4, for this study did not have adequate power to determine significance. As a result, a larger sample size was necessary.

The technical challenge of maintaining the heart cold and moist, during isolation of the coronary artery and particularly the potential influence this may have on the integrity of the coronary artery prompted a change of experimental protocol to a less technically challenging tissue to dissect, though still relevant to the study of neointimal hyperplasia. In an attempt to speed up time from tissue collection to culture and increase sample size, porcine aortic tissue was selected as a reliable model of studying neointimal formation.

A larger sample size (n=10) for aortic organ culture consisting of experimental groups outlined in Table 2.2 was undertaken. Data presented in figure 6.2B, demonstrated the development of neointima to similar extent for all experimental groups (Ao-GAZELLE, Ao-CHROMA, Ao-Graphene, Ao-Graphene Oxide and Ao-Day 14) cultured for a duration of 14 days, except Ao-EES, where neointimal thickness was comparable to CoA-Day 0 after injury (Fig. 6.2 B). This means that EES was the only stent capable of inhibiting neointima thickening, whereas Gr and GO coated stents did not appear to influence neointimal thickness. The benefits of the EES are clear, the stent elutes a potent anti-proliferating drug specifically targeting SMC cell cycle (69), inhibiting SMC proliferation and consequently intimal thickening (265). The restenosis inhibiting effect of EES is known and our data are congruent with most studies, confirming the efficacy of EES in lowering the incidence of restenosis (266, 267). The performance of EES on intimal thickening and in comparison to Ao-GAZELLE/CHROMA was as expected (266, 268), but the unknown was on its performance in relation to Ao-Graphene and Ao-Graphene Oxide and on the possible effects from Gr or the GO, which showed no neointima inhibiting effect. Hence, Gr and GO coating on the GAZELLE stents failed to have any influence on neointimal

thickness (Ao-Graphene and Ao-Graphene Oxide versus Ao-GAZELLE (Fig. 6.2B)). This is addressing the first and second aim of this chapter, demonstrating no effect of the Gr and GO on intimal thickening in the coronary artery organ culture and again significantly no difference identified between the 14 day aorta organ culture groups, except Ao-EES, as described above.

6.4.2 No influence of graphene or graphene oxide coating on endothelial cell regeneration

To address the third and fourth objective of this chapter, CD31 staining and SCEM surface visualisation was used as a means to examine endothelial cell denudation and regeneration within the luminal surface of coronary artery and aortic tissue as well as stent surfaces. Coronary artery segments did demonstrate patches of preserved EC integrity after 14 days of culture where EC layer was intact at Day 0 on the same coronary artery, though injury to these vessels was not intentionally induced on coronary arteries (Fig. 6.3). CoA-Day 14 data were only available for three out of the four coronary artery experiments performed but only two presented patches of ECs (Fig.6.3). It may be that injury was caused to vessels when dissecting tissue or it may be an indication of poor EC regeneration. These data are contrary to reports of preserved and regenerative capability of the endothelium within 14 days culture (255, 257, 263). Importantly, for the CoA-Graphene Oxide experimental group (Table 2.1), the sample size was halved due to indistinguishable structures, making it difficult to form a reliable conclusion. However, the CD31 staining of coronary artery specimens does not provide conclusive evidence of either preserved or regenerative luminal EC layer, necessitating an increase of sample size. To assess this further, 10 porcine aortic tissue segments, as described previously, were stained to identify CD31 positive cells (indicative of endothelial cells).

Studying EC preservation by immunohistochemistry and SCEM visualisation of Ao-Day 0 before versus Ao-Day 0 after balloon injury, implies poor induction of deliberate balloon injury to the aortic wall. Areas bereft of EC were observed on the luminal surface of Ao-Day 0 before injury, indicating injury to have already occurred, possibly through handling and dissection, however, there also remained areas intact of ECs after injuring, Ao-Day 0 after injury (Fig. 6.4/6.5). Interestingly, there was also aortic tissue that demonstrated barren ECs at Ao-Day 0 before injury, whereas the autologous (from same animal/aorta)

aorta after injury (Ao-Day 0 after injury) showed presence of EC layer (Fig. 6.4B). This was also the case in one of the autologous aortic tissues examined by SCEM. This suggests injury to the aortic wall may not have been achieved by balloon inflation, however it should be considered that perhaps injury may have been achieved without the removal/erosion of the endothelium. It may be that in some aorta collected, unintentional injury may have occurred in handling, during adventitial removal and cutting/segmenting of the tissue or between animal slaughter until tissue collection (in the abattoir). (255). Aortic tissue specimens before inducing injury, was collected anterior to the aortic region where injury by balloon inflation was induced. Although, considering these are from autologous tissue, efforts were made to carefully dissect aortic tissue segments after injury, close to tissue before injury (few mm apart). The reason for less endothelium integrity/adhesion on the aortic tissue luminal surface prior to inducing balloon injury remains unclear (few aortic segments denoted CD31 staining, Fig. 6.4). The extent of EC denudation varies depending on severity of injury induced, it is not complete denudation (269).

The remaining endothelial cells, or the ECs that have not eroded and are intact on the aortic tissue after injury (example for visualisation, Ao-Day 0 after injury (Fig. 6.5 d-f)), are the source of endothelial cell replication and regeneration, and this has been shown to be the case in the literature (61) . In the instance of complete EC loss after injury, the source of ECs would typically be from distal or proximal areas of the vessel in the *in vivo* settings. However, if complete EC denudation had indeed occurred in our *ex vivo* tissue segments, then there would be no source of EC for regeneration, a limitation of the *ex vivo* study.

As described previously, the everolimus drug incorporated on stents in the Ao-EES experimental group plays a role in inhibiting cell cycle progression rather than influencing cell viability or adhesion, specifically SMC proliferation (270). The lack of endothelium on the EES experimental group at day 14, implies that CD31 positive cell staining in the other experimental groups identifies proliferated cells rather than surviving of the original/mother cell. The reason for this conclusion is that if original endothelial cells survived until 14 days, some would also be identified/ stained for the EES experimental group, so any CD31 staining must be attributed to repopulated (daughter) cells. Consequently, it must be assumed that if CD31 positive staining was observed at any

experimental group that was cultured for 14 days, was an indication of ECs regenerated rather than preservation of the original/source/mother cells. This is mirrored by a study demonstrating the suppression of EC activation by the everolimus stents (271).

Even though EC regeneration is generally initiated during the first 24 hours after endothelium denudation (272), when comparing unstented and balloon injured aortic tissue at Day 0 and Day 14 (Ao-Day 0 after injury versus Ao-Day 14, Fig. 6.4), there was no evidence of EC regeneration after the 14 days of aortic culture. It is noteworthy that CD31+ cells were present on the sections, but these appeared to be stained lighter in colour and in multiple layers. These cells were therefore considered not to be endothelial cells, due to the expected monolayer phenotype of endothelial cells. Further investigation is required to determine the phenotype of the cell, co-staining against fibroblasts or α-SMA could be advantageous, as myofibroblast and SMCs have been documented to be involved in restenosis (273). These data disagree with the data presented in Chapter 5, where significantly more human coronary artery endothelial cells were present after 8 days of culture on the Graphene coated stent segment when compared to the uncoated or the GO coated stent segment. This was not shown to be the case in the *ex vivo* investigations.

6.4.3 Scanning electron microscopy revealed structural growth on tissue and stents

Scanning electron microscopy of fixed tissue at Day 0 showed a cobblestone appearance on the aortic luminal surface, indicating endothelial cells (Fig. 6.5 a-f). ECs were visualised on aortic tissue fixed at Day 0 prior to balloon injuring (Fig. 6.5 a-c) as well as some patches of endothelium observed on tissue fixed after balloon injury (Fig. 6.5 d-f), suggesting erosion of ECs with balloon distension. Even before inducing deliberate balloon injury, the endothelium exhibits gaps between ECs, exposing the subendothelium (Fig. 6.5 b, c yellow arrowheads). This suggests wall injury prior to induced injury by balloon distension, as was also demonstrated above with immunohistochemistry against CD31.

The absence of cobblestone structures on the stent surfaces (Ao-GAZELLE, Ao-CHROMA, Ao-Graphene, Ao-Graphene Oxide and Ao-EES) and aortic luminal surface cultured for 14 days, suggests the absence of endothelial cell preservation and regeneration (Fig. 6.5 g-x). In addition, in place of the cobblestone structures, there appears to be spindle-shaped,

elongated structures both on the aortic luminal surfaces and on the stent surfaces (Ao-Day 14, Ao-GAZELLE, Ao-CHROMA, Ao-Graphene, Ao-Graphene Oxide and Ao-EES) of the 14 days cultured tissues. The elongated growth, adherent to one another, and aligned parallel to one another are recognised to be smooth muscle cells (274, 275). On the other hand their striated appearance may be representative of connective tissue, elastic fibres or even fibroblasts (273, 276, 277), pointing to the exposure of subendothelial tissue; mostly consisting of connective tissue and IEL. On the surface of these, small, irregular-shaped and spherical deposits are also visible, and these have been deduced by Holt *et al.* to be very likely leukocytes (Fig. 6.5, red arrowheads) (263). SCEM imaging results of aortic tissue cultured for 14 days (Ao-Day 14, Ao-GAZELLE, Ao-CHROMA, Ao-Graphene, Ao-Graphene Oxide and Ao-EES) is in agreement with the results presented by staining against CD31. Figures, 6.4 and 6.5, clearly demonstrate an absence of endothelial cell layer on aortic luminal surface after 14 days of incubation, again indicating the denudation of the endothelial layer post injury without subsequent repair of the endothelial layer. Endothelial staining was observed in two out of the four coronary artery cultures on Day 14 (Fig. 6.3 B), suggesting either EC preservation or regeneration. This is different to the aortic tissue, one explanation for this could be ascribed to the different time courses for re-endothelialisation that has been described between animals but also between the specific artery/organ (254, 269). Deposition of leukocytes were also apparent on the injured surfaces, covered by what looks like to be SMCs (278, 279), though this would need to be validated, potential by immunohistochemistry against alpha-smooth muscle actin. These SMC like structures were also visible at Ao-Day 0 after injury, indicating perhaps aggressive balloon injury, that caused over distension of the wall exposing the medial layer of the aorta, that also further delaying of re-endothelialisation (254). Using currently available *ex vivo* tissue sections, staining against α-SMA and fibroblasts (vimentin or S100A) simultaneous with CD31 could provide further information, particularly determining the phenotype of the cells showing as multi-layered in the immunohistochemistry results presented above (Fig. 6.4). On the other hand, this may also resemble collagen rather than SMC, since it was stained pink in colour on the Miller's elastin stain and could explain its presence at Ao-Day 0 (Fig. 6.2A) (276).

An effective coronary stent would be one that promotes regeneration of the arterial endothelium after injury. Past studies have revealed complete regeneration of the

endothelial layer to have the potential of inhibiting intimal thickening because ECs are capable of secreting SMC proliferation inhibiting factors (e.g. nitric oxide, endothelin-1) (10, 255, 280). Additionally, the ideal coronary stent needs to support good EC proliferation while at the same time preventing SMC proliferation in order to avoid restenosis. In the present chapter, histological and immunohistochemistry analysis revealed Gr and GO coated stents to have no significant influence on the thickness of neointima and growth/integrity of ECs.

6.5 Limitations

One of the main limitations of this study, was the removal of the stent after fixing and prior to tissue processing for paraffin embedding. The removal may have caused some surface structural damage, particularly between the tissue/stent junction. This is because sectioning would not have been possible with the stent secured onto the coronary artery or aortic tissue specimens (due to metallic nature of the stent). *E*x-vivo organ culture lacks the incorporation of blood components, systemic inflammatory responses and the effect of shear stress caused by blood flow. Even though blood components are essential in the responding outcome of the vessel wall, these require to be investigated *in vivo.* However, for the purpose of investigating presence/absence of neointima and endothelium, our model provided useful information and also preserved animal use at this early stage. In addition, there was reduced source of endothelial cells after injury, except the remaining adherent cells, though *in vivo* it is believed that the source of endothelial cells for regeneration are either from distal/proximal areas of the unstented region of a vessel or most likely from endothelial progenitor cells within the blood stream (281, 282).

6.6 Conclusion

To date, these are the first *ex vivo* data presenting the possible effects of graphene and graphene oxide coating on coronary artery stents, and particularly in terms of neointimal thickness.

Overall, Gr and GO coating had no effect on intimal thickening, EC integrity and regrowth. The main objective of this chapter was to study effect of Gr or GO on neointima formation. This objective was addressed by *ex vivo* organ culture and the resulting outcome was that there was no influence from either Gr or GO coating on neointima

formation. This is the first investigation where influence of Gr and GO coatings versus stainless steel bare metal stent on porcine coronary or aortic tissue was investigated.

In the ex vivo settings, neointimal thickening occurs as a result of cellular/tissue interaction without systemic inflammatory or blood electrolyte/molecule involvement. In this setting, there is only the interaction of the components within the vessel with each other and with the stented cultures. The absence of neointima in the Ao-EES group confirm that neointima formation is due to SMC proliferation (EES elute drugs inhibiting SMA proliferation). As has been described, factors released from the endothelium modulate SMC migration and proliferation and thus in the *ex vivo* settings, it is potentially the response of the SMC in response to the factors released from the remaining (un-denudated) endothelial cells or the absence/drop of the factors that are normally released by the endothelium on the luminal surface of the tissue due to de-endothelialisation (10). The data suggest the neointima formed was not as a response to the stents because a similar degree of neointima is also formed on unstented aortic tissue as Ao-GAZELLE (Fig. 6.4).

6.7 Key findings

- Graphene or graphene oxide appears to have no effect on neointimal thickness in an *ex vivo* porcine aortic organ culture model.
- No influence on endothelial preservation or regeneration was identified on the Graphene or graphene oxide coated bare metal stents.

CHAPTER 7

General discussion

7.1 Study Rationale

Despite the existence of drug eluting stents, which are much more effective than bare metal stents in maintaining the open state of a stenosed coronary artery, stent associated complications remain an issue. DES delay re-endothelialisation and thus pose an added risk of stent thrombosis, that may be overcome by improving the efficacy of BMS in reducing restenosis. Thus, there is a definite advantage to improving the effectiveness of BMS, if the prospect exists, since it could also eliminate the need for long-term anti-platelet therapy, which too can add to the complication rate.

Since graphene has been reported to be impermeable to gases, including even Helium, studies have proved graphene coating to significantly improve corrosion at non-medical settings (165, 200). This may translate to the inhibition of metal leaching from the implant, that may thus lead to reduced inflammatory response and smoother implant surface (168, 201). In addition, there are reports that graphene possesses antibacterial and biocompatible properties that may be exploited for biomedical use (196, 199).

7.2 Summary of results

Objective 1

In this project, two different types of water based graphene and graphene oxide dispersions were prepared. The initial project aim was to manufacture pristine graphene and graphene oxide in dispersion using the LPE method with PS1 and modified Hummer's method, respectively. This achieved 1 $mgmL^{-1}$ concentration of both dispersions and also produced high pristine yield Gr and GO. This is another example of the advantage of LPE producing high yield graphene based materials in solution that enables various applications, including coating methods.

Objective 2

Spray coating was selected as the technique to coat LPE graphene based materials onto bare metal stents. The technique was optimised in order to achieve uniform, thin and maximal stent coverage. Spraying was performed for a duration of 60-80 minutes from a

distance of 10 cm using 400 µL of 0.4mgmL^{-1}LPE Gr or GO onto a pre-plasma cleaned bare metal stent, positioned on a 75 ˚C hotplate.

Objective 3

Significantly increased human coronary artery endothelial cell number was observed after seven days of *in vitro* cell culture, indicating an enhance proliferative affinity of the endothelial cells on the graphene coated bare metal stent compared to the uncoated BMS.

Objective 4

Neointima thickness was unaffected by either graphene or graphene oxide coating of the bare metal stents in organ culture of porcine aorta (and coronary artery although small sample size). Neointima of aortic tissue was similar in thickness when cultured with Gr and GO coated BMS as well as uncoated BMS, supporting biocompatibility of the graphene and graphene oxide coating further. No enhanced growth of endothelial cells on the graphene or graphene oxide coated stent was observed compared with uncoated BMS.

7.3 Limitations

The absence of physiological flow may have an influence on the behaviour of endothelial cells (264, 283). ECs have been documented to have enhanced migration capability under flow when compared to disturbed or absence of flow as well as a reduced EC turnover under static conditions (283). The main limitation of this project was the flow dynamic in the *ex vivo* investigations that eliminated any influence from shear stress, endogenous blood metabolites.

The porcine model enables use of the human medical devices and has previously been described as the model representative of human healing (284). However, this is still an animal model and thus natural differences exist, therefore the results attained from this *ex vivo* porcine model organ culture, may still not be replicable or translatable to the response in humans.

7.4 Overall Conclusion

This is the first time a coating method describing a technique to coat coronary artery bare metal stainless steel stents with LPE graphene and graphene oxide has been reported.

This approach of coating coronary artery stents is a simple method to utilise in the laboratory setting but is also highly scalable allowing control of thickness via standardisation of the parameters. This technique is also applicable to graphene coating of any medical implant. Of course, for large scale production of coated implants, the opportunity to include advanced technology to prepare even better coating quality exists. Examples include the incorporation of ultra-sonication simultaneous to spray-coating that would produce improved flake distribution and dispersibility (285, 286). The first step to producing Gr and GO coated stents has been described in this study, that can also be applied to orthopaedic implants, where potential improvements could be acquired from the highly robust and anti-wear qualities of graphene coating.

The application of graphene as a coating has been reported by others in literature (196, 197), and this study further confirms these findings. However, this study provides the first reporting of LPE graphene as well as graphene oxide coating of medical implants by spray coating. In agreement with data provided in literature about the biocompatibility of graphene in supporting cell survival and enhanced cell proliferation, this project provides further data in support of this. Enhanced human coronary artery endothelial cell growth on graphene coated stainless steel BMS has been reported in this study as well as equivalent growth of HCAECs on GO coated BMS in comparison to the uncoated BMS.

This project provides the first reporting of *ex vivo* data investigating the effect of graphene or graphene oxide coating on porcine coronary artery and aortic tissue. In terms of neointima formation, both graphene and graphene oxide coated stents demonstrated equivalent formation of neointima compared with the uncoated or the unstented tissues although significantly increased neointimal thickness versus EES. This implicates Gr and GO coated stents as comparable to uncoated stents and thus biocompatible with the surrounding tissue qualifying further investigations within a physiologically relevant environment, where stents would be acting as scaffolds against the vessel, under pressure with blood flow as well as the influence of inflammatory and corrosion-inducing electrolytes in the blood (164).

Due to the significant limitations of *ex vivo* investigations; inadequate source of endothelial cells for proliferation (from un-denudated areas of vessel segment only), ambiguity still lies in the performance of Gr and GO coated stents in supporting

endothelial cell growth *in vivo*, and thus its effect on re-endothelialisation. It is clear that compared to EES, Gr and GO are non-inferior in relation to EC proliferation in *ex vivo* organ culture.

The efficacy of a graphene coated coronary artery stent would eliminate the need for a polymer, which not only often adds to the cost of stent production but also adds to the complication risk. In comparison to developing and innovative coronary artery stent designs, which mainly employ a polymer base coating onto the BMS to act as a carrier for drugs or genes, graphene coating would save a lot of resources and cost, acting as a cheaper yet effective alternative to the currently popular DES and also developing stents.

In conclusion, this project demonstrated biocompatibility of graphene coated BMS but failed to demonstrate a reduced neointima thickness *ex vivo* when compared to currently available drug eluting stents.

7.5 Future directions

A clear future direction of this pre-clinical trial is to conduct porcine *in vivo* experiments to precisely delineate the degree of in-stent restenosis following implantation of Gr coated stents. The trial groups should be as outlined in Table 2.2, where EES is involved as the superior efficacy stent as comparison. The *in vivo* study should ideally be performed in the porcine model due to their similarity in inflammatory, structural and size profiles, particularly as human medical devices can be utilised for the investigations (259). Porcine circulation has been described similar to that of humans (255) and the response to vessel injury from stents is documented to be in a similar manner to human coronary arteries, with porcine neointima identical to human neointima achieved within a month of stent deployment (287). Their response to the coronary artery stents under investigation, even though not entirely representative of humans, provide a much reliable model for pre-clinical settings (260).

In vivo, optical coherence tomography could be utilised to determine stent patency and restenosis real time. Subsequently post-euthanasia, *ex vivo* examination of the stented vessel could be performed by slicing of the fixed stent-vessels (stent remaining in situ to vessel) using diamond blades (288). There remains additional and broad data that is yet to be attained from investigations performed under *in vivo* conditions, where exposure to

physiological processes including shear stress, inflammatory response and blood electrolyte influence on the in-situ coronary artery stents, will add to our knowledge of graphene based coronary artery stents.

REFERENCES

1. Wasilewski J, Niedziela J, Osadnik T, Duszańska A, Sraga W, Desperak P, et al. Predominant location of coronary artery atherosclerosis in the left anterior descending artery. The impact of septal perforators and the myocardial bridging effect. Kardiochirurgia i torakochirurgia polska = Polish journal of cardio-thoracic surgery. 2015;12(4):379-85.

2. Rajendran P, Rengarajan T, Thangavel J, Nishigaki Y, Sakthisekaran D, Sethi G, et al. The vascular endothelium and human diseases. Int J Biol Sci. 2013;9(10):1057-69.

3. Gutiérrez E, Flammer AJ, Lerman LO, Elízaga J, Lerman A, Fernández-Avilés F. Endothelial dysfunction over the course of coronary artery disease. European heart journal. 2013;34(41):3175-81.

4. DeVile MPJ, Foëx P. Antiplatelet drugs, coronary stents, and non-cardiac surgery. Continuing Education in Anaesthesia Critical Care & Pain. 2010;10(6):187-91.

5. Wang DH, Rätsep M, Chapman A, Boyd R. Adventitial fibroblasts in vascular structure and function: The role of oxidative stress and beyond2010. 177-86 p.

6. BHF BHF. CVD Statistics- BHF UK Factsheet. 2018.

7. WHO WHO. Fact sheet: Cardiovascular diseases (CVDs). In: WHO, editor. 2017.

8. Townsend N, Williams J, Bhatnagar P, Wickramasinghe K, Rayner M. Cardiovascular Disease Statistics 2014. London: British Heart Foundation; 2014. 126 p.

9. Roberts WC. Atherosclerotic risk factors — are there ten, or is there only one? Atherosclerosis. 1992;97:S5-S9.

10. Lusis AJ. Atherosclerosis. Nature. 2000;407:233.

11. Grundy SM, Bilheimer D, Chait A, et al. Summary of the second report of the national cholesterol education program (ncep) expert panel on detection, evaluation, and treatment of high blood cholesterol in adults (adult treatment panel ii). JAMA. 1993;269(23):3015-23.

12. Mudau M, Genis A, Lochner A, Strijdom H. Endothelial dysfunction: the early predictor of atherosclerosis. Cardiovasc J Afr. 2012;23(4):222-31.

13. Urowitz MB, Gladman D, Ibañez D, Fortin P, Sanchez-guerrero J, Bae S, et al. Accumulation of coronary artery disease risk factors over three years: Data from an international inception cohort. Arthritis Care & Research. 2008;59(2):176-80.

14. Lieb W, Jansen H, Loley C, Pencina MJ, Nelson CP, Newton-Cheh C, et al. Genetic Predisposition to Higher Blood Pressure Increases Coronary Artery Disease Risk. Hypertension. 2013;61(5):995-1001.

15. Booth HP, Prevost AT, Gulliford MC. Severity of obesity and management of hypertension, hypercholesterolaemia and smoking in primary care: population-based cohort study. J Hum Hypertens. 2015.

16. Tuzcu EM, Kapadia SR, Tutar E, Ziada KM, Hobbs RE, McCarthy PM, et al. High Prevalence of Coronary Atherosclerosis in Asymptomatic Teenagers and Young Adults: Evidence From Intravascular Ultrasound. Circulation. 2001;103(22):2705-10.

17. Adams CWM. Arteriosclerosis in man, other mammals and birds. Biological Reviews. 1964;39(3):372-423.

18. Poole JCF, Florey HW. Changes in the endothelium of the aorta and the behaviour of macrophages in experimental atheroma of rabbits. The Journal of Pathology and Bacteriology. 1958;75(2):245-51.

19. Insull W, Jr. The Pathology of Atherosclerosis: Plaque Development and Plaque Responses to Medical Treatment. The American Journal of Medicine. 2009;122(1):S3-S14.

20. Navab M, Fogelman AM, Berliner JA, Territo MC, Demer LL, Frank JS, et al. Pathogenesis of atherosclerosis. Am J Cardiol. 1995;76(9):18c-23c.

21. Ross R, Glomset JA. Atherosclerosis and the arterial smooth muscle cell: Proliferation of smooth muscle is a key event in the genesis of the lesions of atherosclerosis. Science. 1973;180(4093):1332-9.

22. Ludmer PL, Selwyn AP, Shook TL, Wayne RR, Mudge GH, Alexander RW, et al. Paradoxical vasoconstriction induced by acetylcholine in atherosclerotic coronary arteries. N Engl J Med. 1986;315(17):1046-51.

23. Libby P, Ridker PM, Hansson GK. Progress and challenges in translating the biology of atherosclerosis. Nature. 2011;473:317.

24. Stary HC, Chandler AB, Glagov S, Guyton JR, Insull W, Rosenfeld ME, et al. A definition of initial, fatty streak, and intermediate lesions of atherosclerosis. A report from the Committee on Vascular Lesions of the Council on Arteriosclerosis, American Heart Association. Circulation. 1994;89(5):2462-78.

25. Glagov S, Weisenberg E, Zarins CK, Stankunavicius R, Kolettis GJ. Compensatory enlargement of human atherosclerotic coronary arteries. N Engl J Med. 1987;316(22):1371-5.

26. Zarins CK, Weisenberg E, Kolettis G, Stankunavicius R, Glagov S. Differential enlargement of artery segments in response to enlarging atherosclerotic plaques. J Vasc Surg. 1988;7(3):386-94.

27. Falk E, Shah PK, Fuster V. Coronary Plaque Disruption. Circulation. 1995;92(3):657-71.

28. Moore Kathryn J, Tabas I. Macrophages in the Pathogenesis of Atherosclerosis. Cell. 2011;145(3):341-55.

29. Falk EE. Atherothrombosis and thrombosis-prone plaques. Hurst's the Heart. 2004:1123-39.

30. Hallow K, Taylor WR, Rachev A, Vito R. Markers of inflammation collocate with increased wall stress in human coronary arterial plaque. Biomechanics and Modeling in Mechanobiology. 2009;8(6):473-86.

31. Farb A, Burke AP, Tang AL, Liang TY, Mannan P, Smialek J, et al. Coronary plaque erosion without rupture into a lipid core. A frequent cause of coronary thrombosis in sudden coronary death. Circulation. 1996;93(7):1354-63.

32. Campbell IC, Suever JD, Timmins LH, Veneziani A, Vito RP, Virmani R, et al. Biomechanics and Inflammation in Atherosclerotic Plaque Erosion and Plaque Rupture: Implications for Cardiovascular Events in Women. PLoS ONE. 2014;9(11):e111785.

33. Chandran S, Watkins J, Abdul-Aziz A, Shafat M, Calvert PA, Bowles KM, et al. Inflammatory Differences in Plaque Erosion and Rupture in Patients With ST-Segment Elevation Myocardial Infarction. Journal of the American Heart Association. 2017;6(5):e005868.

34. Libby P. Superficial erosion and the precision management of acute coronary syndromes: not one-size-fits-all. European Heart Journal. 2017;38(11):801-3.

35. Jafarzadeh F. An introduction to graphene coating stents. Manchester: University of Manchester; 2015.

36. Ridker PM, Everett BM, Thuren T, MacFadyen JG, Chang WH, Ballantyne C, et al. Antiinflammatory Therapy with Canakinumab for Atherosclerotic Disease. New England Journal of Medicine. 2017;377(12):1119-31.

37. Fraker TD, Fihn SD, Writing on behalf of the Chronic Stable Angina Writing C, Writing Committee M, Gibbons RJ, Abrams J, et al. 2007 Chronic Angina Focused Update of the ACC/AHA 2002 Guidelines for the Management of Patients With Chronic Stable Angina: A Report of the American College of Cardiology/American Heart Association Task Force on Practice Guidelines Writing Group to Develop the Focused Update of the 2002 Guidelines for the Management of Patients With Chronic Stable Angina. Circulation. 2007;116(23):2762-72.

38. Goetz RHR, M.Haller, J. D.Dee, R.Rosenak, S. S. Internal mammary-coronary artery anastomosis. A nonsuture method employing tantalum rings. J Thorac Cardiovasc Surg. 1961;41:378-86.

39. Murray G, Porcheron R, Hilario J, Roschlau W. Anastomosis of systemic artery to the coronary. Canadian Medical Association journal. 1954;71(6):594.

40. Carrel A. Experimental operations on the sigmoid valves of the pulmonary artery. The Journal of experimental medicine. 1914;20(1):9.

41. Bravata DM, Gienger AL, McDonald KM, Sundaram V, Perez MV, Varghese R, et al. Systematic review: the comparative effectiveness of percutaneous coronary interventions and coronary artery bypass graft surgery. Annals of internal medicine. 2007;147(10):703.

42. Hlatky MA, Boothroyd DB, Bravata DM, Boersma E, Booth J, Brooks MM, et al. Coronary artery bypass surgery compared with percutaneous coronary interventions for multivessel disease: a collaborative analysis of individual patient data from ten randomised trials. The Lancet. 2009;373(9670):1190-7.

43. Goldman S, Zadina K, Moritz T, Ovitt T, Sethi G, Copeland JG, et al. Long-term patency of saphenous vein and left internal mammary artery grafts after coronary artery bypass surgery: Results from a Department of Veterans Affairs Cooperative Study. Journal of the American College of Cardiology. 2004;44(11):2149-56.

44. Otsuka F, Yahagi K, Sakakura K, Virmani R. Why is the mammary artery so special and what protects it from atherosclerosis? Annals of Cardiothoracic Surgery; Vol 2, No 4 (July 2013): Total arterial revascularization. 2013.

45. Mayo Clinic M. Coronary bypass surgery. https://wwwmayoclinicorg/tests-procedures/coronary-bypass-surgery/about/pac-20384589.

46. Grüntzig A. Transluminal dilatation of coronary-artery stenosis. The Lancet. 1978;311(8058):263.

47. Fischman DL, Leon MB, Baim DS, Schatz RA, Savage MP, Penn I, et al. A Randomized Comparison of Coronary-Stent Placement and Balloon Angioplasty in the Treatment of Coronary Artery Disease. New England Journal of Medicine. 1994;331(8):496-501.

48. Waller BF, Pinkerton CA, Orr CM, Slack JD, VanTassel JW, Peters T. Restenosis 1 to 24 months after clinically successful coronary balloon angioplasty: A necropsy study of 20 patients. Journal of the American College of Cardiology. 1991;17(6s2):58-70.

49. Hamid H, Coltart J. 'Miracle stents'--a future without restenosis. Mcgill J Med. 2007;10(2):105-11.

50. Post MJ, Borst C, Kuntz RE. The relative importance of arterial remodeling compared with intimal hyperplasia in lumen renarrowing after balloon angioplasty. A study in the normal rabbit and the hypercholesterolemic Yucatan micropig. Circulation. 1994;89(6):2816-21.

51. Koh AS, Choi LM, Sim LL, Tan JW, Khin LW, Chua TS, et al. Comparing the use of cobalt chromium stents to stainless steel stents in primary percutaneous coronary intervention for acute myocardial infarction: a prospective registry. Acute Card Care. 2011;13(4):219-22.

52. Fujiu K, Manabe I, Sasaki M, Inoue M, Iwata H, Hasumi E, et al. Nickel-free stainless steel avoids neointima formation following coronary stent implantation. Science and technology of advanced materials. 2012;13(6):064218-.

53. Sigwart U, Puel J, Mirkovitch V, Joffre F, Kappenberger L. Intravascular stents to prevent occlusion and restenosis after transluminal angioplasty. N Engl J Med. 1987;316(12):701-6.

54. Serruys PW, de Jaegere P, Kiemeneij F, Macaya C, Rutsch W, Heyndrickx G, et al. A Comparison of Balloon-Expandable-Stent Implantation with Balloon Angioplasty in Patients with Coronary Artery Disease. New England Journal of Medicine. 1994;331(8):489-95.

55. Torrado J, Buckley L, Duran A, Trujillo P, Toldo S, Valle Raleigh J, et al. Restenosis, Stent Thrombosis, and Bleeding Complications: Navigating Between Scylla and Charybdis. J Am Coll Cardiol. 2018;71(15):1676-95.

56. Agostoni P, Biondi-Zoccai GG, Gasparini GL, Anselmi M, Morando G, Turri M, et al. Is bare-metal stenting superior to balloon angioplasty for small vessel coronary artery disease? Evidence from a meta-analysis of randomized trials. Eur Heart J. 2005;26(9):881-9.

57. Agostoni P, Valgimigli M, Biondi-Zoccai GGL, Abbate A, Garcia Garcia HM, Anselmi M, et al. Clinical effectiveness of bare-metal stenting compared with balloon angioplasty in total coronary occlusions: Insights from a systematic overview of randomized trials in light of the drug-eluting stent era. American Heart Journal. 2006;151(3):682-9.

58. Kornowski R, Hong MK, Tio FO, Bramwell O, Wu H, Leon MB. In-Stent Restenosis: Contributions of Inflammatory Responses and Arterial Injury to Neointimal Hyperplasia. Journal of the American College of Cardiology. 1998;31(1):224-30.

59. Farb A, Sangiorgi G, Carter AJ, Walley VM, Edwards WD, Schwartz RS, et al. Pathology of Acute and Chronic Coronary Stenting in Humans. Circulation. 1999;99(1):44-52.

60. Svilaas T, van der Horst ICC, Zijlstra F. A quantitative estimate of bare-metal stenting compared with balloon angioplasty in patients with acute myocardial infarction: angiographic measures in relation to clinical outcome. Heart. 2007;93(7):792-800.

61. Douglas G, Van Kampen E, Hale AB, McNeill E, Patel J, Crabtree MJ, et al. Endothelial cell repopulation after stenting determines in-stent neointima formation: effects of bare-metal vs. drug-eluting stents and genetic endothelial cell modification. Eur Heart J. 2013;34(43):3378-88.

62. Misra SK, Ostadhossein F, Babu R, Kus J, Tankasala D, Sutrisno A, et al. 3D-Printed Multidrug-Eluting Stent from Graphene-Nanoplatelet-Doped Biodegradable Polymer Composite. Advanced Healthcare Materials. 2017;6(11):1700008.

63. Cassese S, Byrne RA, Tada T, Pinieck S, Joner M, Ibrahim T, et al. Incidence and predictors of restenosis after coronary stenting in 10 004 patients with surveillance angiography. Heart. 2014;100(2):153-9.

64. Garg S, Serruys PW. Coronary stents: current status. J Am Coll Cardiol. 2010;56(10 Suppl):S1-42.

65. Grube E, Silber S, Hauptmann KE, Mueller R, Buellesfeld L, Gerckens U, et al. TAXUS I: Six- and Twelve-Month Results From a Randomized, Double-Blind Trial on a Slow-Release Paclitaxel-Eluting Stent for De Novo Coronary Lesions. Circulation. 2003;107(1):38-42.

66. Moses JW, Leon MB, Popma JJ, Fitzgerald PJ, Holmes DR, O'Shaughnessy C, et al. Sirolimus-Eluting Stents versus Standard Stents in Patients with Stenosis in a Native Coronary Artery. New England Journal of Medicine. 2003;349(14):1315-23.

67. Marx SO, Marks AR. Bench to bedside: the development of rapamycin and its application to stent restenosis. Circulation. 2001;104(8):852-5.

68. Bennett MR. In-stent stenosis: pathology and implications for the development of drug eluting stents. Heart. 2003;89(2):218-24.

69. Yin R-X, Yang D-Z, Wu J-Z. Nanoparticle drug- and gene-eluting stents for the prevention and treatment of coronary restenosis. Theranostics. 2014;4(2):175-200.

70. Giannakakou P, Robey R, Fojo T, Blagosklonny MV. Low concentrations of paclitaxel induce cell type-dependent p53, p21 and G1/G2 arrest instead of mitotic arrest: molecular determinants of paclitaxel-induced cytotoxicity. Oncogene. 2001;20(29):3806-13.

71. Jordan MA, Toso RJ, Thrower D, Wilson L. Mechanism of mitotic block and inhibition of cell proliferation by taxol at low concentrations. Proceedings of the National Academy of Sciences. 1993;90(20):9552-6.

72. Axel DI, Kunert W, Göggelmann C, Oberhoff M, Herdeg C, Küttner A, et al. Paclitaxel Inhibits Arterial Smooth Muscle Cell Proliferation and Migration In Vitro and In Vivo Using Local Drug Delivery. Circulation. 1997;96(2):636-45.

73. Sousa JE, Costa MA, Abizaid A, Abizaid AS, Feres F, Pinto IMF, et al. Lack of Neointimal Proliferation After Implantation of Sirolimus-Coated Stents in Human Coronary Arteries: A

Quantitative Coronary Angiography and Three-Dimensional Intravascular Ultrasound Study. Circulation. 2001;103(2):192-5.

74. Morice M-C, Serruys PW, Sousa JE, Fajadet J, Ban Hayashi E, Perin M, et al. A Randomized Comparison of a Sirolimus-Eluting Stent with a Standard Stent for Coronary Revascularization. New England Journal of Medicine. 2002;346(23):1773-80.

75. De Luca G, Dirksen MT, Spaulding C, Kelbaek H, Schalij M, Thuesen L, et al. Drug-eluting vs bare-metal stents in primary angioplasty: a pooled patient-level meta-analysis of randomized trials. Arch Intern Med. 2012;172(8):611-21; discussion 21-2.

76. Spertus JA, Kettelkamp R, Vance C, Decker C, Jones PG, Rumsfeld JS, et al. Prevalence, predictors, and outcomes of premature discontinuation of thienopyridine therapy after drug-eluting stent placement: results from the PREMIER registry. Circulation. 2006;113(24):2803-9.

77. Windecker S, Meier B. Late Coronary Stent Thrombosis. Circulation. 2007;116(17):1952-65.

78. Nakazawa G, Otsuka F, Nakano M, Vorpahl M, Yazdani SK, Ladich E, et al. The pathology of neoatherosclerosis in human coronary implants bare-metal and drug-eluting stents. J Am Coll Cardiol. 2011;57(11):1314-22.

79. Konishi T, Yamamoto T, Funayama N, Yamaguchi B, Sakurai S, Nishihara H, et al. Stent thrombosis caused by metal allergy complicated by protein S deficiency and heparin-induced thrombocytopenia: a case report and review of the literature. Thrombosis journal. 2015;13:25-.

80. Costa MA, Sabaté M, van der Giessen WJ, Kay IP, Cervinka P, Ligthart JMR, et al. Late Coronary Occlusion After Intracoronary Brachytherapy. Circulation. 1999;100(8):789-92.

81. Liistro F, Colombo A. Late acute thrombosis after paclitaxel eluting stent implantation. Heart. 2001;86(3):262-4.

82. Albiero R, Nishida T, Adamian M, Amato A, Vaghetti M, Corvaja N, et al. Edge Restenosis After Implantation of High Activity 32P Radioactive β-Emitting Stents. Circulation. 2000;101(21):2454-7.

83. Mehta SR, Yusuf S, Peters RJG, Bertrand ME, Lewis BS, Natarajan MK, et al. Effects of pretreatment with clopidogrel and aspirin followed by long-term therapy in patients undergoing percutaneous coronary intervention: the PCI-CURE study. The Lancet. 2001;358(9281):527-33.

84. Bertrand ME, Legrand V, Boland J, Fleck E, Bonnier J, Emmanuelson H, et al. Randomized Multicenter Comparison of Conventional Anticoagulation Versus Antiplatelet Therapy in Unplanned and Elective Coronary Stenting: The Full Anticoagulation Versus Aspirin and Ticlopidine (FANTASTIC) Study. Circulation. 1998;98(16):1597-603.

85. Pfisterer M, Brunner-La Rocca HP, Buser PT, Rickenbacher P, Hunziker P, Mueller C, et al. Late Clinical Events After Clopidogrel Discontinuation May Limit the Benefit of Drug-Eluting StentsAn Observational Study of Drug-Eluting Versus Bare-Metal Stents. Journal of the American College of Cardiology. 2006;48(12):2584-91.

86. Kiran U, Makhija N. Patient with Recent Coronary Artery Stent Requiring Major Non Cardiac Surgery. Indian Journal of Anaesthesia. 2009;53(5):582-91.

87. Navarese EP, Kowalewski M, Kandzari D, Lansky A, Górny B, Kołtowski L, et al. First-generation versus second-generation drug-eluting stents in current clinical practice: updated evidence from a comprehensive meta-analysis of randomised clinical trials comprising 31 379 patients. Open Heart. 2014;1(1):e000064.

88. Alfonso F, Fernandez C. Second-Generation Drug-Eluting Stents. Journal of the American College of Cardiology. 2011;58(1):26-9.

89. Gada H, Kirtane AJ, Newman W, Sanz M, Hermiller JB, Mahaffey KW, et al. 5-Year Results of a Randomized Comparison of XIENCE V Everolimus-Eluting and TAXUS Paclitaxel-Eluting Stents: Final Results From the SPIRIT III Trial (Clinical Evaluation of the XIENCE V Everolimus Eluting Coronary Stent System in the Treatment of Patients With De Novo Native Coronary Artery Lesions). JACC: Cardiovascular Interventions. 2013;6(12):1263-6.

90. Serruys PW, Ruygrok P, Neuzner J, Piek JJ, Seth A, Schofer JJ, et al. A randomised comparison of an everolimus-eluting coronary stent with a paclitaxel-eluting coronary stent:the SPIRIT II trial. EuroIntervention. 2006;2(3):286-94.

91. Serruys PW, Ong AT, Piek JJ, Neumann FJ, van der Giessen WJ, Wiemer M, et al. A randomized comparison of a durable polymer Everolimus-eluting stent with a bare metal coronary stent: The SPIRIT first trial. EuroIntervention. 2005;1(1):58-65.

92. Joner M, Nakazawa G, Finn AV, Quee SC, Coleman L, Acampado E, et al. Endothelial Cell Recovery Between Comparator Polymer-Based Drug-Eluting Stents. Journal of the American College of Cardiology. 2008;52(5):333-42.

93. Pilgrim T, Piccolo R, Heg D, Roffi M, Tüller D, Muller O, et al. Ultrathin-strut, biodegradable-polymer, sirolimus-eluting stents versus thin-strut, durable-polymer, everolimus-eluting stents for percutaneous coronary revascularisation: 5-year outcomes of the BIOSCIENCE randomised trial. The Lancet. 2018;392(10149):737-46.

94. Levine GN, Bates ER, Bittl JA, Brindis RG, Fihn SD, Fleisher LA, et al. 2016 ACC/AHA Guideline Focused Update on Duration of Dual Antiplatelet Therapy in Patients With Coronary Artery Disease: A Report of the American College of Cardiology/American Heart Association Task Force on Clinical Practice Guidelines: An Update of the 2011 ACCF/AHA/SCAI Guideline for Percutaneous Coronary Intervention, 2011 ACCF/AHA Guideline for Coronary Artery Bypass Graft Surgery, 2012 ACC/AHA/ACP/AATS/PCNA/SCAI/STS Guideline for the Diagnosis and Management of Patients With Stable Ischemic Heart Disease, 2013 ACCF/AHA Guideline for the Management of ST-Elevation Myocardial Infarction, 2014 AHA/ACC Guideline for the Management of Patients With Non-ST-Elevation Acute Coronary Syndromes, and 2014 ACC/AHA Guideline on Perioperative Cardiovascular Evaluation and Management of Patients Undergoing Noncardiac Surgery. Circulation. 2016;134(10):e123-55.

95. Investigators B. The Final 10-Year Follow-Up Results From the BARI Randomized Trial. Journal of the American College of Cardiology. 2007;49(15):1600-6.

96. Grewe PH, Deneke T, Machraoui A, Barmeyer J, Müller K-M. Acute and chronic tissue response to coronary stent implantation: pathologic findings in human specimen. Journal of the American College of Cardiology. 2000;35(1):157-63.

97. Gomes WJ, Buffolo E. Coronary stenting and inflammation: implications for further surgical and medical treatment. Ann Thorac Surg. 2006;81(5):1918-25.

98. Weintraub WS. The Pathophysiology and Burden of Restenosis. The American Journal of Cardiology. 2007;100(5, Supplement):S3-S9.

99. Rajagopal V, Rockson SG. Coronary restenosis: a review of mechanisms and management. The American Journal of Medicine. 2003;115(7):547-53.

100. Cutlip DE, Chauhan MS, Baim DS, Ho KK, Popma JJ, Carrozza JP, et al. Clinical restenosis after coronary stenting: perspectives from multicenter clinical trials. J Am Coll Cardiol. 2002;40(12):2082-9.

101. Chen C-H, Kirtane AJ. Stents, Restenosis, and Stent Thrombosis. In: Kern MJ, Sorajja P, Lim MJ, editors. The Interventional Cardiac Catheterization Handbook (Fourth Edition): Elsevier; 2018. p. 179-99.

102. Mori H, Kutys R, Romero M, Virmani R, Finn AV. Metallic Coronary Stents: Is There a Relationship Between Stent Fracture and Hypersensitivity? JACC Cardiovasc Interv. 2017;10(11):1175-7.

103. Alfonso F, Byrne RA, Rivero F, Kastrati A. Current treatment of in-stent restenosis. J Am Coll Cardiol. 2014;63(24):2659-73.

104. Dangas GD, Claessen BE, Caixeta A, Sanidas EA, Mintz GS, Mehran R. In-Stent Restenosis in the Drug-Eluting Stent Era. Journal of the American College of Cardiology. 2010;56(23):1897-907.

105. Vanags LZ, Tan JTM, Galougahi KK, Schaefer A, Wise SG, Murphy A, et al. Apolipoprotein A-I Reduces In-Stent Restenosis and Platelet Activation and Alters Neointimal Cellular Phenotype. JACC Basic to translational science. 2018;3(2):200-9.

106. Kereiakes DJ, Choo JK, Young JJ, Broderick TM. Thrombosis and drug-eluting stents: a critical appraisal. Reviews in cardiovascular medicine. 2004;5(1):9-15.

107. Takayama T, Hiro T, Hirayama A. Stent thrombosis and drug-eluting stents. Journal of Cardiology. 2011;58(2):92-8.

108. Hannan EL, Racz MJ, Walford G, Jones RH, Ryan TJ, Bennett E, et al. Long-Term Outcomes of Coronary-Artery Bypass Grafting versus Stent Implantation. New England Journal of Medicine. 2005;352(21):2174-83.

109. Weintraub WS, Grau-Sepulveda MV, Weiss JM, O'Brien SM, Peterson ED, Kolm P, et al. Comparative Effectiveness of Revascularization Strategies. New England Journal of Medicine. 2012;366(16):1467-76.

110. Zhang Z, Kolm P, Grau-Sepulveda MV, Ponirakis A, O'Brien SM, Klein LW, et al. Cost-effectiveness of revascularization strategies: the ASCERT study. J Am Coll Cardiol. 2015;65(1):1-11.

111. Mohr FW, Morice MC, Kappetein AP, Feldman TE, Stahle E, Colombo A, et al. Coronary artery bypass graft surgery versus percutaneous coronary intervention in patients with three-vessel disease and left main coronary disease: 5-year follow-up of the randomised, clinical SYNTAX trial. Lancet. 2013;381(9867):629-38.

112. Hoffman SN, TenBrook JA, Wolf MP, Pauker SG, Salem DN, Wong JB. A meta-analysis of randomized controlled trials comparing coronary artery bypass graft with percutaneous

transluminal coronary angioplasty: One- to eight-year outcomes. Journal of the American College of Cardiology. 2003;41(8):1293-304.

113. Serruys PW, Ong ATL, van Herwerden LA, Sousa JE, Jatene A, Bonnier JJRM, et al. Five-Year Outcomes After Coronary Stenting Versus Bypass Surgery for the Treatment of Multivessel Disease: The Final Analysis of the Arterial Revascularization Therapies Study (ARTS) Randomized Trial. Journal of the American College of Cardiology. 2005;46(4):575-81.

114. Gaziano T, Reddy K, Paccaud F, Horton S, Chaturvedi V. Cardiovascular Disease. In: Jamison D, JG, Measham A, editors. Disease Control Priorities in Developing Countries. 2nd edition ed. Washington, DC, USA: World Bank; 2006.

115. Weintraub WS, Mahoney EM, Zhang Z, Chu H, Hutton J, Buxton M, et al. One year comparison of costs of coronary surgery versus percutaneous coronary intervention in the stent or surgery trial. Heart. 2004;90(7):782-8.

116. Alfonso F, Perez-Vizcayno MJ, Garcia Del Blanco B, Garcia-Touchard A, Lopez-Minguez JR, Masotti M, et al. Everolimus-Eluting Stents in Patients With Bare-Metal and Drug-Eluting In-Stent Restenosis: Results From a Patient-Level Pooled Analysis of the RIBS IV and V Trials. Circ Cardiovasc Interv. 2016;9(7):e003479.

117. Brener SJ, Lytle BW, Casserly IP, Schneider JP, Topol EJ, Lauer MS. Propensity Analysis of Long-Term Survival After Surgical or Percutaneous Revascularization in Patients With Multivessel Coronary Artery Disease and High-Risk Features. Circulation. 2004;109(19):2290-5.

118. Erbel R, Di Mario C, Bartunek J, Bonnier J, de Bruyne B, Eberli FR, et al. Temporary scaffolding of coronary arteries with bioabsorbable magnesium stents: a prospective, non-randomised multicentre trial. Lancet. 2007;369(9576):1869-75.

119. Peuster M, Wohlsein P, Brügmann M, Ehlerding M, Seidler K, Fink C, et al. A novel approach to temporary stenting: degradable cardiovascular stents produced from corrodible metal—results 6–18 months after implantation into New Zealand white rabbits. Heart. 2001;86(5):563-9.

120. Waksman R, Pakala R, Kuchulakanti PK, Baffour R, Hellinga D, Seabron R, et al. Safety and efficacy of bioabsorbable magnesium alloy stents in porcine coronary arteries. Catheter Cardiovasc Interv. 2006;68(4):607-17; discussion 18-9.

121. Bosiers M, Peeters P, D'Archambeau O, Hendriks J, Pilger E, Duber C, et al. AMS INSIGHT--absorbable metal stent implantation for treatment of below-the-knee critical limb ischemia: 6-month analysis. Cardiovasc Intervent Radiol. 2009;32(3):424-35.

122. Moravej M, Mantovani D. Biodegradable metals for cardiovascular stent application: interests and new opportunities. International journal of molecular sciences. 2011;12(7):4250-70.

123. Elgendy IY, Mahmoud AN, Anderson RD. First generation bioresorbable vascular scaffolds: do they hold the promise? Journal of Thoracic Disease. 2017;9(8):2293-5.

124. Tamai H, Igaki K, Kyo E, Kosuga K, Kawashima A, Matsui S, et al. Initial and 6-Month Results of Biodegradable Poly-l-Lactic Acid Coronary Stents in Humans. Circulation. 2000;102(4):399-404.

125. Nishio S, Kosuga K, Igaki K, Okada M, Kyo E, Tsuji T, et al. Long-Term (>10 Years) clinical outcomes of first-in-human biodegradable poly-l-lactic acid coronary stents: Igaki-Tamai stents. Circulation. 2012;125(19):2343-53.

126. Onuma Y, Serruys PW. Bioresorbable Scaffold: The Advent of a New Era in Percutaneous Coronary and Peripheral Revascularization? Circulation. 2011;123(7):779-97.

127. O'Riordan M, editor Long-term Absorb BVS Data Continue to Disappoint. TCT; 2017; Denver, CO.

128. Puricel S, Arroyo D, Corpataux N, Baeriswyl G, Lehmann S, Kallinikou Z, et al. Comparison of Everolimus- and Biolimus-Eluting Coronary Stents With Everolimus-Eluting Bioresorbable Vascular Scaffolds. Journal of the American College of Cardiology. 2015;65(8):791-801.

129. Serruys PW, Farooq V, Kalesan B, de Vries T, Buszman P, Linke A, et al. Improved Safety and Reduction in Stent Thrombosis Associated With Biodegradable Polymer-Based Biolimus-Eluting Stents Versus Durable Polymer-Based Sirolimus-Eluting Stents in Patients With Coronary Artery DiseaseFinal 5-Year Report of the LEADERS (Limus Eluted From A Durable Versus ERodable Stent Coating) Randomized, Noninferiority Trial. JACC: Cardiovascular Interventions. 2013;6(8):777-89.

130. Kereiakes DJ, Ellis SG, Metzger C, Caputo RP, Rizik DG, Teirstein PS, et al. 3-Year Clinical Outcomes With Everolimus-Eluting Bioresorbable Coronary Scaffolds: The ABSORB III Trial. Journal of the American College of Cardiology. 2017;70(23):2852-62.

131. Tada N, Virmani R, Grant G, Bartlett L, Black A, Clavijo C, et al. Polymer-Free Biolimus A9-Coated Stent Demonstrates More Sustained Intimal Inhibition, Improved Healing, and Reduced Inflammation Compared With a Polymer-Coated Sirolimus-Eluting Cypher Stent in a Porcine Model. Circulation: Cardiovascular Interventions. 2010;3(2):174-83.

132. Garot P, Morice MC, Tresukosol D, Pocock SJ, Meredith IT, Abizaid A, et al. 2-Year Outcomes of High Bleeding Risk Patients After Polymer-Free Drug-Coated Stents. J Am Coll Cardiol. 2017;69(2):162-71.

133. Jensen L, Maeng M, Raungaard B, editors. A randomized trial comparing a polymer-free coronary drug-eluting stent with an ultra-thin strut bioresorbable polymer-based drug-eluting stent in an allcomers patient population: SORT OUT IX. TCT; 2018; San Diego, CA: News-Interventional.

134. Lekshmi KM, Che H-L, Cho C-S, Park I-K. Drug- and Gene-eluting Stents for Preventing Coronary Restenosis. Chonnam Medical Journal. 2017;53(1):14-27.

135. Klugherz BD, Song C, DeFelice S, Cui X, Lu Z, Connolly J, et al. Gene delivery to pig coronary arteries from stents carrying antibody-tethered adenovirus. Hum Gene Ther. 2002;13(3):443-54.

136. Walter DH, Cejna M, Diaz-Sandoval L, Willis S, Kirkwood L, Stratford PW, et al. Local gene transfer of phVEGF-2 plasmid by gene-eluting stents: an alternative strategy for inhibition of restenosis. Circulation. 2004;110(1):36-45.

137. Che HL, Bae IH, Lim KS, Uthaman S, Song IT, Lee H, et al. Novel Fabrication of MicroRNA Nanoparticle-Coated Coronary Stent for Prevention of Post-Angioplasty Restenosis. Korean Circ J. 2016;46(1):23-32.

138. Che HL, Bae IH, Lim KS, Song IT, Lee H, Lee D, et al. Therapeutic Effect of Akt1 siRNA Nanoparticle Eluting Coronary Stent on Suppression of Post-Angioplasty Restenosis. J Biomed Nanotechnol. 2016;12(6):1211-22.

139. Allen M, Myer B, Rushton N. In vitro and in vivo investigations into the biocompatibility of diamond-like carbon (DLC) coatings for orthopedic applications. Journal of Biomedical Materials Research. 2001;58(3):319-28.

140. Roy RK, Lee Kr. Biomedical applications of diamond-like carbon coatings: A review. Journal of Biomedical Materials Research Part B: Applied Biomaterials. 2007;83(1):72-84.

141. Nakatani T, Okamoto K, Omura I, Yamashita S. Application of Diamond-Like-Carbon Coating to a Coronary Artery Drug-Eluting Stent. Journal of Photopolymer Science and Technology. 2007;20(2):221-8.

142. Airoldi F, Colombo A, Tavano D, Stankovic G, Klugmann S, Paolillo V, et al. Comparison of diamond-like carbon-coated stents versus uncoated stainless steel stents in coronary artery disease. Am J Cardiol. 2004;93(4):474-7.

143. Kesavan S, Strange JW, Johnson TW, Flohr-Roese S, Baumbach A. First-in-man evaluation of the MOMO cobalt-chromium carbon-coated stent. EuroIntervention. 2013;8(9):1012-8.

144. Ando K, Ishii K, Tada E, Kataoka K, Hirohata A, Goto K, et al. Prospective multi-center registry to evaluate efficacy and safety of the newly developed diamond-like carbon-coated cobalt–chromium coronary stent system. Cardiovascular Intervention and Therapeutics. 2017;32(3):225-32.

145. Takazawa K, Ishikawa N, Miyagawa H, Yamamoto T, Hariya A, Dohi S. Metal allergy to stainless steel wire after coronary artery bypass grafting. J Artif Organs. 2003;6(1):71-2.

146. Eliades T, Pratsinis H, Kletsas D, Eliades G, Makou M. Characterization and cytotoxicity of ions released from stainless steel and nickel-titanium orthodontic alloys. American Journal of Orthodontics and Dentofacial Orthopedics. 2004;125(1):24-9.

147. Guerra A, Kirkwood M. Severe generalized dermatitis in a nickel-allergic patient with a popliteal artery nitinol stent. Journal of vascular surgery cases and innovative techniques. 2017;3(1):23-5.

148. Ruff CA, Belsito DV. The impact of various patient factors on contact allergy to nickel, cobalt, and chromate. Journal of the American Academy of Dermatology. 2006;55(1):32-9.

149. Yang K, Ren Y. Nickel-free austenitic stainless steels for medical applications. Science and technology of advanced materials. 2010;11(1):014105-.

150. Sheth S, Litvack F, Dev V, Fishbein MC, Forrester JS, Eigler N. Subacute thrombosis and vascular injury resulting from slotted-tube nitinol and stainless steel stents in a rabbit carotid artery model. Circulation. 1996;94(7):1733-40.

151. Sakamoto A, Jinnouchi H, Torii S, Virmani R, Finn AV. Understanding the Impact of Stent and Scaffold Material and Strut Design on Coronary Artery Thrombosis from the Basic and Clinical Points of View. Bioengineering (Basel). 2018;5(3).

152. Novoselov KS, Geim A, Morozov SV, Jiang D, Zhang Y, Dubonos SV, et al. Electric field effect in atomically thin carbon films. Science. 2004;306(5696):666-9.

153. Novoselov KS, Jiang D, Schedin F, Booth TJ, Khotkevich VV, Morozov SV, et al. Two-dimensional atomic crystals. Proceedings of the National Academy of Sciences of the United States of America. 2005;102(30):10451-3.

154. Kumar K, Chee Huei. Synthesis and Biomedical Applications of Graphene: Present and Future Trends. 2013.

155. Partoens B, Peeters FM. From graphene to graphite: Electronic structure around the K point. Physical Review B. 2006;74(7):075404.

156. Timp GL. Nanotechnology. Timp GL, editor. New York: Springer-Verlag New York; 1999. 700 p.

157. Lee C, Wei X, Kysar JW, Hone J. Measurement of the Elastic Properties and Intrinsic Strength of Monolayer Graphene. Science. 2008;321(5887):385.

158. Novoselov KS, Falko VI, Colombo L, Gellert PR, Schwab MG, Kim K. A roadmap for graphene. Nature. 2012;490(7419):192-200.

159. Das S, Gulotty R, Sumant AV, Roelofs A. All Two-Dimensional, Flexible, Transparent, and Thinnest Thin Film Transistor. Nano Letters. 2014;14(5):2861-6.

160. Berry V. Impermeability of graphene and its applications. Carbon. 2013;62:1-10.

161. Georgakilas V, Otyepka M, Bourlinos AB, Chandra V, Kim N, Kemp KC, et al. Functionalization of graphene: covalent and non-covalent approaches, derivatives and applications. Chemical reviews. 2012;112(11):6156.

162. Schneider GF, Xu Q, Hage S, Luik S, Spoor JNH, Malladi S, et al. Tailoring the hydrophobicity of graphene for its use as nanopores for DNA translocation. Nat Commun. 2013;4.

163. Xu Z, Ao Z, Chu D, Younis A, Li CM, Li S. Reversible Hydrophobic to Hydrophilic Transition in Graphene via Water Splitting Induced by UV Irradiation. Sci Rep. 2014;4.

164. Paprottka KJ, Paprottka PM, Reiser MF, Waggershauser T. Comparative study of the corrosion behavior of peripheral stents in an accelerated corrosion model: experimental in vitro study of 28 metallic vascular endoprostheses. Diagnostic and interventional radiology (Ankara, Turkey). 2015;21(5):403-9.

165. Nine MJ, Cole MA, Tran DNH, Losic D. Graphene: a multipurpose material for protective coatings. Journal of Materials Chemistry A. 2015;3(24):12580-602.

166. Barbolina I, Woods CR, Lozano N, Kostarelos K, Novoselov KS, Roberts IS. Purity of graphene oxide determines its antibacterial activity. 2D Materials. 2016;3(2):025025.

167. Cote Laura J, Kim J, Tung Vincent C, Luo J, Kim F, Huang J. Graphene oxide as surfactant sheets. Pure and Applied Chemistry2010. p. 95.

168. Ali-Boucetta H, Bitounis D, Raveendran-Nair R, Servant A, Van den Bossche J, Kostarelos K. Purified graphene oxide dispersions lack in vitro cytotoxicity and in vivo pathogenicity. Adv Healthc Mater. 2013;2(3):433-41.

169. Nurunnabi M, Parvez K, Nafiujjaman M, Revuri V, Khan HA, Feng X, et al. Bioapplication of graphene oxide derivatives: drug/gene delivery, imaging, polymeric modification, toxicology, therapeutics and challenges. RSC Advances. 2015;5(52):42141-61.

170. Hernandez Y, Nicolosi V, Lotya M, Blighe FM, Sun Z, De S, et al. High-yield production of graphene by liquid-phase exfoliation of graphite. Nat Nano. 2008;3(9):563-8.

171. Li X, Cai W, An J, Kim S, Nah J, Yang D, et al. Large-area synthesis of high-quality and uniform graphene films on copper foils. Science. 2009;324(5932):1312-4.

172. Bae S, Kim H, Lee Y, Xu X, Park JS, Zheng Y, et al. Roll-to-roll production of 30-inch graphene films for transparent electrodes. Nat Nanotechnol. 2010;5(8):574-8.

173. Emtsev KV, Bostwick A, Horn K, Jobst J, Kellogg GL, Ley L, et al. Towards wafer-size graphene layers by atmospheric pressure graphitization of silicon carbide. Nat Mater. 2009;8(3):203-7.

174. Wang H, Wang X, Li X, Dai H. Chemical self-assembly of graphene sheets. Nano Research. 2009;2(4):336-42.

175. Tour JM. Top-Down versus Bottom-Up Fabrication of Graphene-Based Electronics. Chemistry of Materials. 2014;26(1):163-71.

176. Xu J, Dang DK, Tran VT, Liu X, Chung JS, Hur SH, et al. Liquid-phase exfoliation of graphene in organic solvents with addition of naphthalene. Journal of Colloid And Interface Science. 2014;418:37-42.

177. Ou E, Xie Y, Peng C, Song Y, Peng H, Xiong Y, et al. High concentration and stable few-layer graphene dispersions prepared by the exfoliation of graphite in different organic solvents. RSC Advances. 2013;3(24):9490-9.

178. Bonaccorso F, Lombardo A, Hasan T, Sun Z, Colombo L, Ferrari AC. Production and processing of graphene and 2d crystals. Materials Today. 2012;15(12):564-89.

179. Feng L, Liu Y-W, Tang X-Y, Piao Y, Chen S-F, Deng S-L, et al. Propagative Exfoliation of High Quality Graphene. Chemistry of Materials. 2013;25(22):4487-96.

180. Tu Z, Liu Z, Li Y, Yang F, Zhang L, Zhao Z, et al. Controllable growth of 1–7 layers of graphene by chemical vapour deposition. Carbon. 2014;73:252-8.

181. Aristov VY, Urbanik G, Kummer K, Vyalikh DV, Molodtsova OV, Preobrajenski AB, et al. Graphene Synthesis on Cubic SiC/Si Wafers. Perspectives for Mass Production of Graphene-Based Electronic Devices. Nano Letters. 2010;10(3):992-5.

182. Narayan R, Kim SO. Surfactant mediated liquid phase exfoliation of graphene. Nano Convergence. 2015;2(1):1-19.

183. Yang H, Hernandez Y, Schlierf A, Felten A, Eckmann A, Johal S, et al. A simple method for graphene production based on exfoliation of graphite in water using 1-pyrenesulfonic acid sodium salt. Carbon. 2013;53(0):357-65.

184. Brodie BC. On the atomic weight of graphite. Philosophical Transactions of the Royal Society of London. 1859;149:249-59.

185. Staudenmaier L. Verfahren zur Darstellung der Graphitsäure. Berichte der deutschen chemischen Gesellschaft. 1898;31(2):1481-7.

186. Hummers WS, Offeman RE. Preparation of Graphitic Oxide. Journal of the American Chemical Society. 1958;80(6):1339-.

187. Rourke JP, Pandey PA, Moore JJ, Bates M, Kinloch IA, Young RJ, et al. The Real Graphene Oxide Revealed: Stripping the Oxidative Debris from the Graphene-like Sheets. Angewandte Chemie. 2011;123(14):3231-5.

188. Stankovich S, Dikin DA, Piner RD, Kohlhaas KA, Kleinhammes A, Jia Y, et al. Synthesis of graphene-based nanosheets via chemical reduction of exfoliated graphite oxide. Carbon. 2007;45(7):1558-65.

189. Paredes JI, Villar-Rodil S, Martínez-Alonso A, Tascón JMD. Graphene Oxide Dispersions in Organic Solvents. Langmuir. 2008;24(19):10560-4.

190. Wang Y, Wu S, Zhao X, Su Z, Du L, Sui A. In vitro toxicity evaluation of graphene oxide on human RPMI 8226 cells. Biomed Mater Eng. 2014;24(6):2007-13.

191. Wu S, Zhao X, Cui Z, Zhao C, Wang Y, Du L, et al. Cytotoxicity of graphene oxide and graphene oxide loaded with doxorubicin on human multiple myeloma cells. International Journal of Nanomedicine. 2014;9:1413-21.

192. Bressan E, Ferroni L, Gardin C, Sbricoli L, Gobbato L, Ludovichetti FS, et al. Graphene based scaffolds effects on stem cells commitment. Journal of Translational Medicine. 2014;12(1).

193. Bussy C, Ali-Boucetta H, Kostarelos K. Safety considerations for graphene: lessons learnt from carbon nanotubes. Acc Chem Res. 2013;46(3):692-701.

194. Aryaei A, Jayatissa AH, Jayasuriya AC. The effect of graphene substrate on osteoblast cell adhesion and proliferation. Journal of Biomedical Materials Research Part A. 2014;102(9):3282-90.

195. Podila R, Moore T, Alexis F, Rao A. Graphene coatings for biomedical implants. J Vis Exp. 2013(73):e50276.

196. Podila R, Moore T, Alexis F, Rao AM. Graphene coatings for enhanced hemo-compatibility of nitinol stents. RSC Advances. 2013;3(6):1660-5.

197. Wawrzyńska M, Bil-Lula I, Krzywonos-Zawadzka A, Arkowski J, Łukaszewicz M, Hreniak D, et al. Biocompatible Carbon-Based Coating as Potential Endovascular Material for Stent Surface. BioMed research international. 2018;2018:2758347-.

198. Wang L-J, Li L, Yu J, Wu Y, He H, Ouyang X, et al. Large-area graphene coating via superhydrophilic-assisted electro-hydrodynamic spraying deposition. Carbon. 2014;79:294-301.

199. Zhao C, Pandit S, Fu Y, Mijakovic I, Jesorka A, Liu J. Graphene oxide based coatings on nitinol for biomedical implant applications: effectively promote mammalian cell growth but kill bacteria. RSC Advances. 2016;6(44):38124-34.

200. Pu N-W, Shi G-N, Liu Y-M, Sun X, Chang J-K, Sun C-L, et al. Graphene grown on stainless steel as a high-performance and ecofriendly anti-corrosion coating for polymer electrolyte membrane fuel cell bipolar plates. Journal of Power Sources. 2015;282:248-56.

201. Zhou K, Motamed S, Thouas GA, Bernard CC, Li D, Parkington HC, et al. Graphene Functionalized Scaffolds Reduce the Inflammatory Response and Supports Endogenous Neuroblast Migration when Implanted in the Adult Brain. PLoS ONE. 2016;11(3):e0151589.

202. Bonaccorso F, Sun Z. Solution processing of graphene, topological insulators and other 2d crystals for ultrafast photonics. Optical Materials Express. 2014;4(1):63-78.

203. Sommer L. Analytical absorption spectrophotometry in the visible and ultraviolet : the principles. Amsterdam ;: Elsevier; 1989.

204. Khan MZH, Shahed SMF, Yuta N, Komeda T. Deposition of an Ultraflat Graphene Oxide Nanosheet on Atomically Flat Substrates. Journal of Electronic Materials. 2017;46(7):4160-5.

205. Jiao K, Zhang D, Chen Y. Efficient and cost-effective graphene on silicon solar cells prepared by spray coating. 2014;4.

206. Belkind A, Gershman S. Plasma Cleaning of Surfaces. In: Jinghong Vaccum Thin Film (Shenzhen) Co. L, editor. Vacuum Technology & Coating2008.

207. Withers S, B. Elucidating the mechanism of apoptosis following the dysregulation of c-Myb. Manchester, UK: University of Manchester; 2005.

208. Bigelow J. Chapter 11 - Bioanalytical Tools for Drug Analysis. In: Hacker M, Messer W, Bachmann K, editors. Pharmacology. San Diego: Academic Press; 2009. p. 279-302.

209. Cheng Z-L, Cao B-C, Wu P-R, Ma L, Liu Z. Templated synthesis of graphene nanosheets within curling layered nanostructure of halloysite nanotubes. Materials Letters. 2017;202:62-5.

210. Raman CV, Krishnan KS. A new type of secondary radiation. Nature. 1928;121:501-2.

211. Khandpur RS. Raman Spectrometer. 2006. In: Handbook of Analytical Instruments, Second Edition [Internet]. McGraw Hill Professional, Access Engineering. Available from: https://www.accessengineeringlibrary.com:443/browse/handbook-of-analytical-instruments-second-edition/c9780070604605ch07.

212. Haar S, El Gemayel M, Shin Y, Melinte G, A. Squillaci M, Ersen O, et al. Enhancing the Liquid-Phase Exfoliation of Graphene in Organic Solvents upon Addition of n-Octylbenzene. Scientific Reports. 2015;5.

213. Ferrari AC, Basko DM. Raman spectroscopy as a versatile tool for studying the properties of graphene. Nat Nano. 2013;8(4):235-46.

214. Coleman JN. Liquid exfoliation of defect-free graphene. Acc Chem Res. 2013;46(1):14-22.

215. Eckmann A, Park J, Yang H, Elias D, Mayorov AS, Yu G, et al. Raman Fingerprint of Aligned Graphene/h-BN Superlattices. Nano Letters. 2013;13(11):5242-6.

216. Trusovas R, Račiukaitis G, Niaura G, Barkauskas J, Valušis G, Pauliukaite R. Recent Advances in Laser Utilization in the Chemical Modification of Graphene Oxide and Its Applications. Advanced Optical Materials. 2015;4(1):37-65.

217. Shearer CJ, Slattery AD, Stapleton AJ, Shapter JG, Gibson CT. Accurate thickness measurement of graphene. Nanotechnology. 2016;27(12):125704.

218. Geisse NA. AFM and combined optical techniques. Materials Today. 2009;12(7):40-5.

219. Shin Y, Prestat E, Zhou K-G, Gorgojo P, Althumayri K, Harrison W, et al. Synthesis and characterization of composite membranes made of graphene and polymers of intrinsic microporosity. Carbon. 2016;102:357-66.

220. Jasim DA, Lozano N, Kostarelos K. Synthesis of few-layered, high-purity graphene oxide sheets from different graphite sources for biology. 2D Materials. 2016;3(1):014006.

221. Casiraghi C, Pisana S, Novoselov KS, Geim AK, Ferrari AC. Raman fingerprint of charged impurities in graphene. 2007.

222. Oliveros A, Coletti C, Saddow SE. Chapter 12 - Carbon Based Materials on SiC for Advanced Biomedical Applications. In: Saddow SE, editor. Silicon Carbide Biotechnology. Oxford: Elsevier; 2012. p. 431-58.

223. Ma J, Liu R, Wang X, Liu Q, Chen Y, Valle RP, et al. Crucial Role of Lateral Size for Graphene Oxide in Activating Macrophages and Stimulating Pro-inflammatory Responses in Cells and Animals. ACS Nano. 2015;9(10):10498-515.

224. King AAK, Davies BR, Noorbehesht N, Newman P, Church TL, Harris AT, et al. A New Raman Metric for the Characterisation of Graphene oxide and its Derivatives. Scientific Reports. 2016;6:19491.

225. Jeon M-H, Choi H-K, Hwang S-H, Kim H-k, inventorsMethod for producing counter electrode based on electrophoretic deposition of graphene, counter electrode produced by the method and dye-sensitized solar cell including the counter electrode2013 2013-9-19.

226. Lin L, Wu H, Green SJ, Crompton J, Zhang S, Horsell DW. Formation of tunable graphene oxide coating with high adhesion. Physical Chemistry Chemical Physics. 2016;18(7):5086-90.

227. ElMaraghy H, Luangkularb S, Prombanpong S, Tangwarodomnukun V. Variety Management in ManufacturingMaterial Consumption and Dry Film Thickness in Spray Coating Process. Procedia CIRP. 2014;17:789-94.

228. O'Kane DF, Mittal KL. Plasma cleaning of metal surfaces. Journal of Vacuum Science and Technology. 1974;11(3):567-9.

229. Zhao J, Chir D. Plasma Processing For Enhanced Underfill2004.

230. Lian H, Qi L, Luo J, Hu K. Experimental study and mechanism analysis on the effect of substrate wettability on graphene sheets distribution morphology within uniform printing droplets. Journal of Physics: Condensed Matter. 2018;30(33):335001.

231. Li W, Liang Y, Yu D, Peng L, Pernstich KP, Shen T, et al. Ultraviolet/ozone treatment to reduce metal-graphene contact resistance. Applied Physics Letters. 2013;102(18):183110.

232. Tong Y, Bohmb S, Song M. Graphene based materials and their composites as coatings. Austin J Nanomed Nanotechnol. 2014;1(1).

233. Getty JD. How Plasma-Enhanced Surface Modification Improves the Production of Microelectronics and Optoelectronics. Chip Scale Review. 2002(January-February):72-5.

234. Bose S, Keller SS, Alstrom TS, Boisen A, Almdal K. Process optimization of ultrasonic spray coating of polymer films. Langmuir. 2013;29(23):6911-9.

235. Perfetti G, Alphazan T, van Hee P, Wildeboer WJ, Meesters GM. Relation between surface roughness of free films and process parameters in spray coating. Eur J Pharm Sci. 2011;42(3):262-72.

236. Bunch JS, Verbridge SS, Alden JS, van der Zande AM, Parpia JM, Craighead HG, et al. Impermeable atomic membranes from graphene sheets. Nano Lett. 2008;8(8):2458-62.

237. Zhang W, Lee S, McNear KL, Chung TF, Lee S, Lee K, et al. Use of graphene as protection film in biological environments. Sci Rep. 2014;4.

238. Mulyana Y, Uenuma M, Ishikawa Y, Uraoka Y. Reversible Oxidation of Graphene Through Ultraviolet/Ozone Treatment and Its Nonthermal Reduction through Ultraviolet Irradiation. The Journal of Physical Chemistry C. 2014;118(47):27372-81.

239. Gu M, Lv L, Du F, Niu T, Chen T, Xia D, et al. Effects of thermal treatment on the adhesion strength and osteoinductive activity of single-layer graphene sheets on titanium substrates. Scientific Reports. 2018;8(1):8141.

240. Berman D, Erdemir A, Zinovev AV, Sumant AV. Nanoscale friction properties of graphene and graphene oxide. Diamond and Related Materials. 2015;54:91-6.

241. Matsuzawa Y, Lerman A. Endothelial dysfunction and coronary artery disease: assessment, prognosis, and treatment. Coronary artery disease. 2014;25(8):713-24.

242. Frohlich E. The role of surface charge in cellular uptake and cytotoxicity of medical nanoparticles. Int J Nanomedicine. 2012;7:5577-91.

243. Li N, Zhang X, Song Q, Su R, Zhang Q, Kong T, et al. The promotion of neurite sprouting and outgrowth of mouse hippocampal cells in culture by graphene substrates. Biomaterials. 2011;32(35):9374-82.

244. Khalili AA, Ahmad MR. A Review of Cell Adhesion Studies for Biomedical and Biological Applications. International journal of molecular sciences. 2015;16(8):18149-84.

245. Bosworth LA, Rathbone SR, Cartmell SH. Optimizing Attachment of Human Mesenchymal Stem Cells on Poly(ε-caprolactone) Electrospun Yarns. Journal of visualized experiments : JoVE. 2015(98):52135.

246. Hong SW, Lee JH, Kang SH, Hwang EY, Hwang YS, Lee MH, et al. Enhanced neural cell adhesion and neurite outgrowth on graphene-based biomimetic substrates. Biomed Res Int. 2014;2014:212149.

247. Ruiz ON, Fernando KAS, Wang B, Brown NA, Luo PG, McNamara ND, et al. Graphene Oxide: A Nonspecific Enhancer of Cellular Growth. ACS Nano. 2011;5(10):8100-7.

248. Wang K, Ruan J, Song H, Zhang J, Wo Y, Guo S, et al. Biocompatibility of Graphene Oxide. Nanoscale Res Lett. 2011;6(1):1-8.

249. Xu M, Zhu J, Wang F, Xiong Y, Wu Y, Wang Q, et al. Improved In Vitro and In Vivo Biocompatibility of Graphene Oxide through Surface Modification: Poly(Acrylic Acid)-Functionalization is Superior to PEGylation. ACS Nano. 2016;10(3):3267-81.

250. Fadini GP, Avogaro A. Cell-based methods for ex vivo evaluation of human endothelial biology. Cardiovascular Research. 2010;87(1):12-21.

251. Koo EW, Gotlieb AI. Endothelial stimulation of intimal cell proliferation in a porcine aortic organ culture. Am J Pathol. 1989;134(3):497-503.

252. Fishman JA, Ryan GB, Karnovsky MJ. Endothelial regeneration in the rat carotid artery and the significance of endothelial denudation in the pathogenesis of myointimal thickening. Lab Invest. 1975;32(3):339-51.

253. Guber S, Ebrahimian T, Heidari M, Eliopoulos N, Lehoux S. Endothelial nitric oxide synthase overexpressing human early outgrowth cells inhibit coronary artery smooth muscle cell migration through paracrine functions. Scientific reports. 2018;8(1):877-.

254. Kipshidze N, Dangas G, Tsapenko M, Moses J, Leon MB, Kutryk M, et al. Role of the endothelium in modulating neointimal formation: Vasculoprotective approaches to attenuate restenosis after percutaneous coronary interventions. Journal of the American College of Cardiology. 2004;44(4):733-9.

255. Carere RG, Koo EWY, Liu PP, Gotlieb AI. Porcine coronary artery organ culture: A model for the study of angioplasty injury. Cardiovascular Pathology. 1992;1(2):107-15.

256. Wilson GJ, Polovick JE, Huibregtse BA, Poff BC. Overlapping paclitaxel-eluting stents: long-term effects in a porcine coronary artery model. Cardiovasc Res. 2007;76(2):361-72.

257. Kim D-E, Oh K-H, Yang J-H, Kwon S-K, Cho T-J, Lee S-B, et al. The Porcine Aortic Tissue Culture System in vitro for Stem Cell Research. International Journal of Stem Cells. 2011;4(2):116-22.

258. Gotlieb AI, Boden P. Porcine aortic organ culture: a model to study the cellular response to vascular injury. In Vitro. 1984;20(7):535-42.

259. Weaver ME, Pantely GA, Bristow JD, Ladley HD. A quantitative study of the anatomy and distribution of coronary arteries in swine in comparison with other animals and man. Cardiovasc Res. 1986;20(12):907-17.

260. Suzuki Y, Yeung AC, Ikeno F. The representative porcine model for human cardiovascular disease. Journal of biomedicine & biotechnology. 2011;2011:195483-.

261. Wilson DP, Saward L, Zahradka P, Kee Cheung P. Angiotensin II receptor antagonists prevent neointimal proliferation in a porcine coronary artery organ culture model. Cardiovascular Research. 1999;42(3):761-72.

262. Lee YU, Luo J, Sprague E, Han HC. Comparison of artery organ culture and co-culture models for studying endothelial cell migration and its effect on smooth muscle cell proliferation and migration. Ann Biomed Eng. 2010;38(3):801-12.

263. Holt CM, Francis SE, Newby AC, Rogers S, Gadsdon PA, Taylor T, et al. Comparison of response to injury in organ culture of human saphenous vein and internal mammary artery. Ann Thorac Surg. 1993;55(6):1522-8.

264. Kural MH, Dai G, Niklason LE, Gui L. An Ex Vivo Vessel Injury Model to Study Remodeling. Cell transplantation. 2018;27(9):1375-89.

265. Townsend JC, Rideout P, Steinberg DH. Everolimus-eluting stents in interventional cardiology. Vascular Health and Risk Management. 2012;8:393-405.

266. Mahmoud AN, Shah NH, Elgendy IY, Agarwal N, Elgendy AY, Mentias A, et al. Safety and efficacy of second-generation drug-eluting stents compared with bare-metal stents: An updated meta-analysis and regression of 9 randomized clinical trials. Clinical Cardiology. 2018;41(1):151-8.

267. Valgimigli M, Sabaté M, Kaiser C, Brugaletta S, de La Torre Hernandez JM, Galatius S, et al. Effects of cobalt-chromium everolimus eluting stents or bare metal stent on fatal and non-fatal cardiovascular events: patient level meta-analysis. BMJ : British Medical Journal. 2014;349(nov04 12).

268. Sabate M, Cequier A, Iniguez A, Serra A, Hernandez-Antolin R, Mainar V, et al. Everolimus-eluting stent versus bare-metal stent in ST-segment elevation myocardial infarction (EXAMINATION): 1 year results of a randomised controlled trial. Lancet. 2012;380(9852):1482-90.

269. De Meyer GR, Bult H. Mechanisms of neointima formation--lessons from experimental models. Vasc Med. 1997;2(3):179-89.

270. Charron T, Nili N, Strauss BH. The cell cycle: a critical therapeutic target to prevent vascular proliferative disease. The Canadian journal of cardiology. 2006;22 Suppl B(Suppl B):41B-55B.

271. Fejes Z, Czimmerer Z, Szük T, Póliska S, Horváth A, Balogh E, et al. Endothelial cell activation is attenuated by everolimus via transcriptional and post-transcriptional regulatory mechanisms after drug-eluting coronary stenting. PloS one. 2018;13(6):e0197890-e.

272. Reidy MA, Clowes AW, Schwartz SM. Endothelial regeneration. V. Inhibition of endothelial regrowth in arteries of rat and rabbit. Lab Invest. 1983;49(5):569-75.

273. Forte A, Della Corte A, De Feo M, Cerasuolo F, Cipollaro M. Role of myofibroblasts in vascular remodelling: focus on restenosis and aneurysm. Cardiovasc Res. 2010;88(3):395-405.

274. Grenier S, Sandig M, Holdsworth DW, Mequanint K. Interactions of coronary artery smooth muscle cells with 3D porous polyurethane scaffolds. Journal of Biomedical Materials Research Part A. 2008;89A(2):293-303.

275. Thakar RG, Cheng Q, Patel S, Chu J, Nasir M, Liepmann D, et al. Cell-shape regulation of smooth muscle cell proliferation. Biophysical journal. 2009;96(8):3423-32.

276. Pasta S, Phillippi JA, Gleason TG, Vorp DA. Effect of aneurysm on the mechanical dissection properties of the human ascending thoracic aorta. The Journal of Thoracic and Cardiovascular Surgery. 2012;143(2):460-7.

277. Farand P, Garon A, Plante GE. Structure of large arteries: Orientation of elastin in rabbit aortic internal elastic lamina and in the elastic lamellae of aortic media. Microvascular Research. 2007;73(2):95-9.

278. Conte MS, VanMeter GA, Akst LM, Clemons T, Kashgarian M, Bender JR. Endothelial cell seeding influences lesion development following arterial injury in the cholesterol-fed rabbit. Cardiovascular Research. 2002;53(2):502-11.

279. Niimi M, Keyamura Y, Nozako M, Koyama T, Kohashi M, Yasufuku R, et al. Probucol Inhibits the Initiation of Atherosclerosis in Cholesterol-Fed Rabbits2013. 166 p.

280. Eguchi H, Okadome K, Mii S, Yukizane T, Sugimachi K. Significance of the endothelial lining in prevention of intimal thickening of autogenous vein grafts in dogs. Journal of Surgical Research. 1991;50(2):179-87.

281. Tahir H, Bona-Casas C, Narracott AJ, Iqbal J, Gunn J, Lawford P, et al. Endothelial repair process and its relevance to longitudinal neointimal tissue patterns: comparing histology with in silico modelling. J R Soc Interface. 2014;11(94):20140022.

282. Gijsen FJH, Wentzel JJ, Van der Heiden K, Narracott A, Gunn J, Hsiao S, et al. The effects of stenting on shear stress: relevance to endothelial injury and repair. Cardiovascular Research. 2013;99(2):269-75.

283. Chiu J-J, Chien S. Effects of disturbed flow on vascular endothelium: pathophysiological basis and clinical perspectives. Physiological reviews. 2011;91(1):327-87.

284. Dixon JA, Spinale FG. Large animal models of heart failure: a critical link in the translation of basic science to clinical practice. Circ Heart Fail. 2009;2(3):262-71.

285. Slegers S, Linzas M, Drijkoningen J, D'Haen J, Reddy KN, Deferme W. Surface Roughness Reduction of Additive Manufactured Products by Applying a Functional Coating Using Ultrasonic Spray Coating. Coatings. 2017;7(12).

286. Modesto L, Miettinen M, Riikonen J, Torvela T, Pfüller C, Lehto V-P, et al. Films of Graphene Nanomaterials Formed by Ultrasonic Spraying of Their Stable Suspensions2015. 45-56 p.

287. Suzuki Y, Yeung AC, Ikeno F. The Pre-Clinical Animal Model in the Translational Research of Interventional Cardiology. JACC: Cardiovascular Interventions. 2009;2(5):373-83.

288. Malik N, Gunn J, Holt CM, Shepherd L, Francis SE, Newman CM, et al. Intravascular stents: a new technique for tissue processing for histology, immunohistochemistry, and transmission electron microscopy. Heart. 1998;80(5):509-16.

APPENDIX I

MATLAB script for Raman peak analysis of LPE Graphene

```
%read data
i=50;% number of files
%check data range and change x1d, y1d, x1g, y1g, x22d, y22d range
%according to appropriate range for fitting

resultarray = zeros (i,16); %create zero array of i by 16

%start looping for each file
for n = 1:i
    namedata = sprintf ('p%d.txt',n);  %data file name variation
    namegraphG = sprintf ('G_graph_p%d',n);    %graph file name
variation
    ...for later saving to jpeg file
    namegraph2d = sprintf ('2D_graph_p%d',n);    %graph file name
variation
    ...for later saving to jpeg file
    Data = dlmread (namedata);    %reading in the spectra data
into array A

    x1 = Data(:,1); %variable x for g-peak area
    y1 = Data(:,2); %variable y for g-peak area
    x2 = Data(:,3);
    y2 = Data(:,4);

    if Data(1,1) <= 2179.49289
        x1 = Data(1:928,1);
        y1 = Data(1:928,2);
        x1d = x1(600:820);
        y1d = y1(600:820);
        x1g = x1(401:620);
        y1g = y1(401:620);
    else
        x1d = x1(684:904);
        y1d = y1(684:904);
        x1g = x1(485:704);
        y1g = y1(485:704);
    end

    x22d = x2(326:680);
    y22d = y2(326:680);

    figure %open figure window

    plot (x1,y1,'k')
    ymin = min(y1);
    ymax = max(y1);
    ymin = 0.9*ymin;
    ymax = ymax*1.1;
    axis([1200,1750,ymin,ymax])%axis range
    xlabel('Raman Shift (cm^-^1)','FontSize',12)
    ylabel('Counts (a.u.)','FontSize',12)
```

```
    %D-peak fitting
    f = ezfit (x1d,y1d,'y(x)=(2*A/pi)*(w/(4*(x-
x_c)^2+w^2))+c',[300000 500 30 1350]);
    showfit (f,'fitcolor', 'red','boxlocation',[0.80 0.99 0.01
0.01]);
    r2 = f.r^2;
    h = (2*A)/(pi*w);
    resultarray(n,1) = n;
    resultarray(n,2) = x_c;
    resultarray(n,3) = r2;
    resultarray(n,4) = w;
    resultarray(n,5) = h;
    resultarray(n,6) = A;

    clear A; clear h; clear r2; clear w;clear x_c;

    %G-peak fitting
    f = ezfit (x1g,y1g,'y(x)=(2*A/pi)*(w/(4*(x-
x_c)^2+w^2))+c',[200000 500 30 1600]);
    showfit (f,'fitcolor', 'blue','boxlocation',[0.80 0.75 0.01
0.01]);
    r2 = f.r^2;
    h = (2*A)/(pi*w);
    resultarray(n,7) = x_c;
    resultarray(n,8) = r2;
    resultarray(n,9) = w;
    resultarray(n,10) = h;
    resultarray(n,11) = A;

    saveas(gcf,namegraphG,'jpg') %Save G-peak graph file

    clear ym*; clear c; clear f; clear h; clear r2; clear w; clear
x_c;
    clear x1*; clear y1*;
    close

    figure %open figure window

    %2D-peak fitting
    plot (x2,y2,'k')
    ymin = min(y22d);
    ymax = max(y22d);
    ymin = 0.9*ymin;
    ymax = ymax*1.1;
    axis([2400,3000,ymin,ymax])%axis range
    xlabel('Raman Shift (cm^-^1)','FontSize',12)
    ylabel('Counts (a.u.)','FontSize',12)
    f = ezfit (x22d,y22d,'y(x)=(2*A/pi)*(w/(4*(x-
x_c)^2+w^2))+c',[500000 500 70 2700]);
    showfit (f,'fitcolor', 'red','boxlocation',[0.80 0.99 0.01
0.01]);

    r2 = f.r^2;
    h = (2*A)/(pi*w);

    saveas(gcf,namegraph2d,'jpg') %Save 2D-peak graph file
```

```
    resultarray(n,12) = x_c;
    resultarray(n,13) = r2;
    resultarray(n,14) = w;
    resultarray(n,15) = h;
    resultarray(n,16) = A;

    clear ym*; clear Data; clear name*; clear A; clear c; clear f;
    clear h; clear r2; clear h; clear w; clear x2; clear y2; clear
x_c;
    close
end

result = array2table(resultarray,'VariableNames',{'point'
'Pos_D'...
    'R2_D' 'w_D' 'h_D' 'a_D' 'Pos_G' 'R2_G' 'w_G' 'h_G' 'a_G'...
    'Pos_2D' 'R2_2D' 'w_2D' 'h_2D' 'a_2D'});
writetable (result, 'result_2.txt','Delimiter','tab');

clear;
```